

THE SEPARATION OF HEXANE FROM POLYBUTADIENE

by

Timothy George Peter Gutowski

B.S., University of Wisconsin, 1967
M.S., University of Illinois, 1968

Submitted in Partial Fulfillment
of the Requirements of the
Degree of

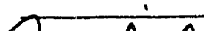
Doctor of Philosophy

at the

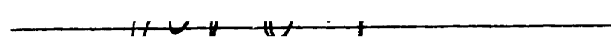
Massachusetts Institute of Technology

April 1981

Signature of Author

 Department of Mechanical Engineering
April 29, 1981

Certified by

 Thesis Supervisor

Accepted by

Chairman, Department Committee on Graduate Students

Archives

MASSACHUSETTS INSTITUTE
OF TECHNOLOGY

JUL 31 1981

LIBRARIES

THE SEPARATION OF HEXANE FROM POLYBUTADIENE

by

TIMOTHY GEORGE PETER GUTOWSKI

Submitted to the Department of Mechanical Engineering on April 29, 1981 in partial fulfillment of the requirements for the Degree of Doctor of Philosophy

ABSTRACT

Solvent separation is an energy intensive process. The separation of hexane from polybutadiene (PBD) after solution polymerization requires approximately 5000 BTU's per pound of rubber. This represents about 10% of the final product cost. The theoretical lower bound on the other hand, is only 5 BTU/lb rubber. The goal of this thesis was to reduce the separation energy. In view of the large quantity of solution polymerized synthetic rubbers consumed and produced in the United States (10^8 lbs of PBD consumed in 1977), even a small improvement in this area could have an enormous impact on the industry.

Energy reduction schemes under three broad categories were investigated; 1) solvent reduction, 2) efficiency improvement by means of a heat pump cycle, and 3) separation techniques that avoided the liquid-vapor transition. The most attractive scenario is based upon a high temperature phase transition. By this method 70% of the solvent can be separated for only 300 BTU/lb-rubber. To show the feasibility of this method required resolving three major issues; 1) the determination of the phase diagram, 2) the determination of the recycle-ability of the dilute phase, and 3) the physical separation of the phases. Each of these issues is addressed in detail in this thesis. The determination of the phase diagram is straightforward but complicated by the broad molecular weight of the polymer, and the mixed nature of the solvent. The recycling of the dilute phase with terminator does not affect the reaction if the dilute phase is properly dried. By far the most difficult problem, however, is the physical separation of the phases. Under most circumstances the dilute phase nucleates, yielding a very unfavorable arrangement for gravity settlement. This problem can be resolved by properly entering the unstable region of the phase diagram, called the spinodal decomposition regime. Several practical methods for accomplishing this are described and supported by experimental evidence. The final proposed low energy separation scenario would require only 610 BTU/lb-rubber (assuming perfect efficiency).

Thesis Supervisor: Nam P. Suh

Title: Professor of Mechanical Engineering

ACKNOWLEDGEMENTS

First off, I would like to thank Professor Nam P. Suh, my advisor and mentor for the trust, and stimulation he provided me. Professor Suh has the exceptional skill of being able to help people to achieve their own best performance. I feel I have gained immeasurably by my association with him. I would also like to thank the other members of my thesis committee, Professors Robert Armstrong, Peter Griffith, and Joseph Smith, Jr. for their contributions to this thesis and to my education.

This research was sponsored by the MIT-Industry Polymer Processing Program. The sponsors of this program include AMP Inc., Boeing Commercial Airplane Company, E.I. duPont de Nemours and Company, Eastman Kodak Company, General Motors Corporation, Goodyear Tire and Rubber Company, Instrumentation Laboratories, Inc., ITT Corporation, Rogers Corporation, and Xerox Corporation. I would like to thank all of the members of this program for their technical support, encouragement, and criticism throughout this project. My association with this program has been very fruitful and rewarding for me. In particular, I would like to thank, Mr. Robert Workman, Mr. Robert Stachowiak, and Mr. Donald Schoneman from Goodyear for their judicious application of experience and criticism to this work. The project reviews provided by Mr. Stachowiak were exceptionally helpful. (He's the one who reminded me, just before takeoff, to design the landing gear.) I would

also like to thank Mr. Tony Puccio of Goodyear for his friendly and enthusiastic experimental work on sometimes not-so-rewarding experiments.

I was extremely fortunate to be part of a laboratory staffed by many exceptional and talented people. Much of the work done in this thesis depended heavily on their assistance. Fred Anderson, Ralph Whittemore, Bob Kane, John Ford, Fred Cote, Margie McDonald, and last, but far from least, Alice Markunas helped me with everything from machining to filling out a purchase order.

Special thanks goes to Charles (Chip) Cangialose. In addition to the many useful experiments he diligently performed, he contributed significantly to this research project by his inquisitiveness and his amiability.

I would also like to thank my many student friends, colleagues and past officemates, especially, Ken Smith, Richard Okine, Luu Nguyen, Kim Stelson, and past students, Dr. Dave Wilson and Dr. Alan Kirkpatrick. In addition to our many useful technical discussions they did much to dispel my original and incorrect impression that M.I.T. was a cold, unfriendly place. In fact, it is a place where many lasting friendships are formed.

It takes more than technical input to do research. In fact, in many ways, it is the nontechnical aspects that are more important in influencing one's performance. I am grateful to my many friends and my family who encouraged me, stimulated me, and comforted me

through this process.

I would like to thank Dr. Jane Snyder for her understanding, wisdom, common sense and love throughout this project (and hopefully beyond it). Many of my friends have also been through the thesis ritual and have been very kind in helping me through mine. Thank you Dr. Rick Michael, Dr. Jean Whitehouse; my past roommate and cousin, Dr. Rob Klueppel, and many thanks to my brother, Dr. Tom Gutowski.

My parents, Mr. and Mrs. Chester Gutowski, told me when I was young, "get a good education, no one can take it away from you." Well, you're right. Thank you both very much for your good advice and your encouragement and your love.

Finally, I'd like to thank the people who helped me put this thesis together, Diane Leonard-Senge did an excellent job on all the illustrations in this thesis. Liz Manzi typed much of this thesis, and Theresa Gautreau helped. A special thanks goes to Rosalie Allen for her "emergency" effort help with typing the appendices and figures.

TABLE OF CONTENTS

	PAGE
Title Page	1
Abstract	2
Acknowledgements	3
Table of Contents	6
List of Figures	9
List of Tables	15
CHAPTER	
1. Introduction and Summary	16
References for Chapter 1	22
2. Polybutadiene and Its Production	23
References for Chapter 2	32
3. Separation Processes	33
3.1 Bulk Polymerization	33
3.2 Improved Heat Transfer in the Reactor Vessel	36
3.3 Heat Pump Cycle	38
3.4 Reverse Osmosis	44
3.5 Liquid-Liquid Phase Separation	51
3.5.1 Energy Consumption	54
3.5.2 Physical Separation	56
3.5.3 Dilute Phase Recycle	57
References for Chapter 3	59

	PAGE
4 Chemical Thermodynamics of Polymer-Solvent Systems	60
4.1 The Thermodynamics of Mixing	60
4.2 The Thermodynamics of Separation	69
4.3 Mechanisms of Liquid-Liquid Phase Separation	75
4.4 Flory-Huggins Theory	86
4.5 Limitations of the Flory-Huggins Theory	100
References for Chapter 4	104
5 Equilibrium Thermodynamic Data for Hexane and Polybutadiene	106
5.1 Quasi-binary Solutions	106
5.2 Cloud Point Curves	108
5.3 Polymers with Broad Molecular Weight Distributions	112
5.4 Mixed Solvents	125
5.5 Pressure Effects	129
References for Chapter 5	135
6. Gravity Settlement Behavior	136
6.1 Gravity Settlement Model	136
6.2 Gravity Settlement Observations	143
References for Chapter 6	168
7 Spinodal Decomposition	169
7.1 Estimate of the Spinodal	171
7.2 Pressure Drop Method	176
References for Chapter 7	187

	PAGE
8 The Low Energy Separation Scenario and Conclusions	188
8.1 The Low Energy Separation Scenario	188
8.2 Conclusions	195
8.3 Future Work	197
APPENDIX	
A Vortex Reactor Vessel	199
A.1 Fluid Mechanics	199
A.2 Heat Transfer	203
A.3 Mathematical Model	206
A.4 Experimental Results	210
References for Appendix A.	219
B Free Volume Theories	221
References for Appendix B	233
C Experimental Determination of the Coexistence Curves	234
References for Appendix C	240
D Rapid Evaporation Separation Scheme	241
References for Appendix D	244
BIOGRAPHICAL NOTE	245

LIST OF FIGURES

Figure Number	PAGE
1.1 Energy scale for hexane-polybutadiene separation.	18
2.1 Repeating units for polybutadiene and polyisoprene.	23
2.2 Polymerization of diene monomers.	24
2.3 Possible polymerization sequences.	25
2.4 Conformation of the monomer.	27
2.5 Effect of lithium catalyst on monomer conformation.	27
2.6 Schematic of polymerization process.	30
3.1 Vortex reactor vessel.	37
3.2 Schematic of "heat pump" separation cycle.	39
3.3 Typical idealized heat pump cycle.	41
3.4 Low temperature cycle.	43
3.5 High temperature cycle.	45
3.6 Reverse osmosis.	47
3.7 Solvent flux rates vs. applied pressure.	50
3.8 Phase diagram for high temperature separation of binary polymer-solvent system.	53
3.9 Separation scenario based upon high temperature phase separation.	55
4.1a Total immiscibility.	66
4.1b Total miscibility.	66
4.1c Partial miscibility.	66

	PAGE
4.2a Phase diagram for polymer-solvent system.	67
4.2b Details of liquid-liquid phase separation at T_2 .	67
4.3 Partially miscible system, C_0 will separate into C' and C'' .	73
4.4 The phase diagram, Gibbs free energy, and chemical potential for a partially miscible system.	76
4.5 A stable solution.	78
4.6 An unstable solution.	79
4.7 Two phase structure (50:50) resulting from spinodal decomposition, from Cahn [4-10].	82
4.8a How do the new solutions C' and C'' form from C_0 ?	84
4.8B Migration of a polymer molecule to form C'' .	84
4.8c Migration of a solvent molecule to form C' .	84
4.9 Phase diagram for a binary system, showing separation mechanisms and their relationship to the chemical potential.	87
4.10 Polymer molecule represented as connected solvent-sized segments on a liquid lattice.	89
4.11 Cloud point curves for solutions of the same polymer but different molecular weights, $M_1 > M_2 > M_3$.	98
4.12 Variation of the interaction parameter g as a function of temperature T .	101
5.1 Cloud point curves for monodisperse samples of polybutadiene in a n-hexane.	110
5.2 Exploded view of sight bomb used for cloud point determination.	111
5.3 Cloud points for broad molecular weight cis PBD in commercial grade hexane.	113

	PAGE
5.4 Comparison of cloud point curves, X is 50:50 mixture of 5.5K and 43K.	114
5.5 Constant temperature plane for three dimensional phase diagram.	116
5.6 Three dimensional phase diagram for two polymer-solvent system.	117
5.7 Constant temperature plane ($T = T_1$) through three dimensional phase diagram.	118
5.8 Projections of cloud point curve and coexistence curves on T-O-X plane.	120
5.9 Cloud point curves and coexistence curves for broad molecular weight cis PBD in commercial grade hexane.	121
5.10 Specific volume curves for hexane-PBD solutions.	123
5.11 Volume ratio vs. temperature for $C_0 = .079$ and $C_0 = .123$.	124
5.12 Comparison of cis and trans conformations on cloud point curves for PBD in n-hexane.	126
5.13 Cloud point curves for PBD in different solvents.	130
5.14 Effect of pressure on cloud point curves for polystyrene-diethyl ether [5-10].	132
6.1a Case I, lower bound hindered settlement.	140
6.1b Case II, upper bound hindered settlement.	140
6.2 Comparison of Case I and Case II type hindered settling.	144
6.3 Comparison of settling times for different initial values of β .	145
6.4 Thick walled glass tube in stainless steel housing for gravity settlement observations.	146

	PAGE	
6.5	Orderly gravity settlement of 7.9% Wt. PBD solution.	148
6.6	Unstable gravity settlement of 7.9% Wt. PBD solution.	149
6.7	Gravity settlement and temperature history for 7.9% Wt. PBD solution.	150
6.8	Comparison of upper bound settlement model with data.	152
6.9	Hot stage set-up.	155
6.10	Nucleation and growth sequence.	156
6.11	Nucleation and growth sequence.	157
6.12	Nucleation and growth sequence.	158
6.13	Nucleation and growth sequence.	159
6.14	Nucleation and growth sequence.	160
6.15	Resulting two phase structure after nucleation and growth of the dilute phase.	161
6.16	Comparison of gravity settlement for two different concentrations, with the temperature history for $C_0 = .123$.	162
6.17	Viscosity of polybutadiene in hexane at 24°C.	164
6.18	Separation behavior of polybutadiene in hexane solution (12.3% Wt.).	165
6.19a	Rapid heating into the spinodal decomposition regime.	167
6.19b	Rapid pressure drop into the spinodal decomposition regime.	167
7.1	Comparison of several ways to approximate the interaction parameter g .	175
7.2	Estimated spinodal with cloud point curve for hexane-PBD solution.	177

	PAGE
7.3 Estimated cloud point boundary and vessel pressure used to avoid phase transition.	179
7.4 Schematic of pressure drop over time Δt .	180
7.5 High pressure apparatus.	181
7.6 Gravity settlement data for pressure drop experiment.	183
7.7 Weight ratio of solvent lost during pressure drop.	184
8.1 "The 7.9% solution".	192
8.2 Low energy separation scenario using pressure drop method to enter spinodal regime.	194
A.1 Laminar motion of a fluid of kinematic viscosity ν in a gap between two concentric cylinders.	201
A.2 Vortex instability between concentric cylinders.	202
A.3 Comparison of heat transfer across-the-gap results for different fluids [A-5].	205
A.4 Real case, and idealized case for mathematical model.	207
A.5 Range of Re_{axial} and Ta for experiments.	212
A.6 Heat transfer results for vortex reactor.	213
A.7 Heat transfer results for 13% Wt. PBD solution in the vortex reactor.	215
A.8 Viscous heating effect for vortex reactor (13% Wt. PBD solution).	217
B.1 Potential interaction function.	224
B.2 Reduced volume as a function of reduced temperature.	227
B.3 Reduced Gibbs free energy as a function of the reduced temperature.	228
B.4 $-U$ vs. T for hexane.	231

	PAGE
C.1 Photograph of physical separation of phases in centrifuge.	235
C.2 Time history of dilute phase-mixed phase interface for 12.3% Wt. solution originally at 160°C in centrifuge.	236
C.3 Temperature profiles for solution in centrifuge.	237
D.1 Rapid evaporation separation scheme.	243

LIST OF TABLES

Table Number	PAGE
1.1 Energy Reduction Methods	20
2.1 Effect of Solvent on Stereochemistry	28
2.2 Composition of Commercial Grade Hexane in Weight Percent	31
3.1 Low Temperature Heat Pump Cycle for Hexane	44
5.1 Suppliers Specifications; for Commercial Grade Hexane	125
5.2 Solvent Properties	128
5.3 Rank Ordering of the Solvents in Commercial Grade Hexane.	128
5.4 The Effect of Pressure on the LCST	133
6.1 Calculation of Particle Sizes for Two Different Phase Arrangements	154
7.1 Estimated Length Scale λ_m for PBD-hexane	170
7.2 Data Used to Estimate Temperature Dependence of g	173
8.1 Bottle Polymerization Results	196

CHAPTER 1

INTRODUCTION AND SUMMARY

Many important polymer manufacturing processes are done in a polymer-solvent solution. Adding solvent to the polymer greatly reduces its viscosity and, in general, improves all of the transport properties. Polybutadiene, as well as other important synthetic polymers, are made in a solution by a process called solution polymerization. By this process alone can a very high quality, elastic polybutadiene suitable for the sidewall and tread material of tires be made. After polymerization, the polymer and solvent are separated into pure components. The solvent, in this case, isomers of hexane, is recycled for continued use. The polybutadiene is baled, and sent to a tire making plant where it is subjected to further processing before it is formed into a tire carcass and vulcanized (crosslinked).

The separation process usually involves, in one way or another, the evaporation of the solvent. Sometimes this process is aided by an intermediate agent such as hot water or steam which effectively heats the solution and supplies the necessary latent heat of evaporation of the solvent. In general these separation processes were designed 20 years ago when energy costs were low. Consequently, a typical separation process for a hexane-12% wt. polybutadiene solution requires 5000 BTU's per pound of rubber. This is comparable to the energy necessary to mix carbon black into rubber [1-1]* and is one of the most energy intensive steps in the production of

*References, given in brackets, are listed at the end of each chapter.

solution polymerized rubbers. In some cases the separation process may account for 10-15% of the final product cost.

The goal of this project has been to reduce the energy necessary to separate hexane and polybutadiene. The limits of this problem are shown in Fig. 1.1. The upper limit is set by the present commercially employed processes. Next to this is the latent heat of evaporation of hexane. Since many commercial processes are based upon evaporation, they must have an overall efficiency of about 0.2. The lower bound set in Fig. 1.1 is the negative of the Gibbs free energy of mixing. In general, we can see that there is a three order of magnitude improvement theoretically possible. In view of the large amount of polybutadiene produced and consumed yearly in the United States (see Ch. 2) even a small improvement over the present method could represent millions of dollars in savings.

In general, three different approaches to this problem were tried. The first was to identify the solvent requirements, and look for ways to reduce the needed solvent. Since the energy of separation is directly related to the amount of solvent to be separated, less solvent means less energy. The second approach was to live with the original quantity of solvent, but employ a heat pump cycle between the evaporation and condensation of the hexane. The third approach was to concentrate the original solution using some method that avoided the liquid-vapor-liquid phase changes for the solvent. In this approach we tried to take advantage of certain obvious physical and chemical differences between the two components. Energy

BTU/lb-rubber

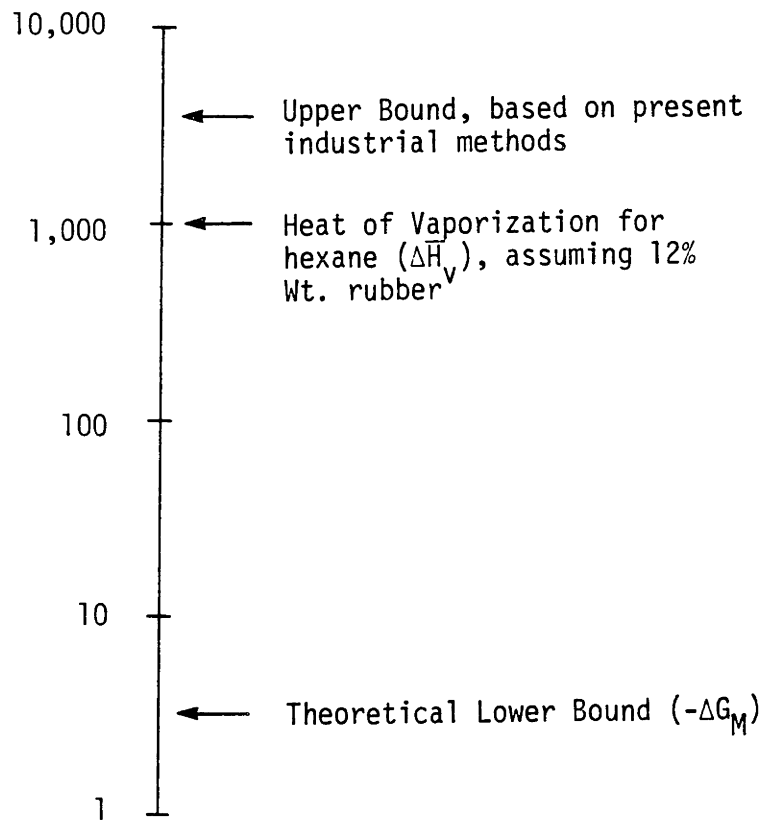


Fig. 1.1 Energy scale for hexane-polybutadiene separation.

reduction methods that employed waste heat, or even the heat of polymerization, were not considered. Such methods could be employed to augment our proposed "low energy separation scenario."

A brief list of the energy reduction methods that were considered is given in Table 1.1.

These methods are discussed in some detail in Chapter 3. The bulk of this thesis however is devoted to a discussion of a separation scenario based upon a high temperature liquid-liquid phase transition.

Freeman and Rowlinson [1-2] discovered in 1960 that, upon heating, a polymer-solvent solution would break up into two component solutions, one more concentrated than the original solution, and the other more dilute. This was recognized by Anolick and Goffinet [1-3] as a potential means for concentrating polymer solutions. A possible separation scenario based on this phenomenon would involve, heating, physically separating the phases, cleaning and recycling the dilute phase, and removing the remaining solvent from the concentrated phase. The key problems involved in employing such a scenario are:

- i. determining the phase diagram -- too high a temperature or too little concentrating could make the process unfeasible,
2. physically separating the two liquid phases -- this is a key problem; to be economical, reactors must operate at fairly high concentrations, at these high concentrations the liquid phases do not readily separate by gravity -- additional measures are necessary.

TABLE 1-1

Energy Reduction Methods

<u>Method</u>	<u>Comment</u>
Bulk Polymerization	limited by heat transfer
Improved heat transfer in reactor vessel	limited by viscous shaft work
Heat pump cycle	promising, but mechanically complex
Two solvent system	now solvents must be separated
Reverse osmosis	limited by low mass flux rates
Liquid-liquid phase separation	very promising, basis for "low energy separation scenario"

In general continuous centrifuging is not a realistic method to handle the very high viscosity concentrated solution; and

3. recycling the dilute phase -- polybutadiene requires a terminator to stop its reaction, recycling the dilute phase with the terminator could stop polymerization, recycling without the terminator means that polymerization was taking place during the high temperature heating -- with a probable dramatic change in kinetics, molecular wt. and physical properties.

This thesis is about solving these problems. Removal of the remaining solvent from the concentrated solution can be done in a straightforward way -- using a vented barrel extruder for example. The final result is something we call the Low Energy Separation Scenario. At perfect efficiency it will require only 12% of the energy of the present separation methods, and even at an efficiency of 0.2 it will only require 64% of the energy of present methods.

An outline of this thesis is given in the Table of Contents. The basic results and conclusions concerning the proposed Low Energy Separation Scenario are given in Chapter 8. A basic description of this method is given in Section 3.5 of Chapter 3. The rest of the thesis is support material. The key problem concerning the implementation of the proposed separation method is the physical separation of the two phases. This is discussed in detail in Chapters 6 and 7. Chapter 3 gives a small amount of detail concerning several alternative methods that were considered. A detailed development of the thermodynamics of separation is given in Chapter 4. Such a development was not found in the literature.

References, Chapter 1

- 1-1 C.A. Rotz, "Methods of Pulverization for Reducing the Energy Consumption of Elastomer Mixing Process," Ph.D. thesis, Department of Mechanical Engineering, M.I.T. (1978).
- 1-2 P.I. Freeman and J.S. Rowlinson, "Lower Critical Points in Polymer Solutions," Polymer 1, p. 20 (1960).
- 1-3 C. Anolick and E.P. Goffinet, Jr.; U.S. Patent No. 3, 553, 156 (Jan. 5, 1971).

POLYBUTADIENE AND ITS PRODUCTION

Polybutadiene (PBD) is an important synthetic rubber that is used primarily in tires. In the "cis" conformation it is a very elastic rubber, with low hysteresis.* This leads to low heat build-up in the constantly flexing sidewalls of tires, and therefore improved tire life. PBD was first discovered in the early 1930's. Mass production, which required certain improvements in the polymerization technique, began in the 1960's. Now polybutadiene occupies the number two position among synthetic rubbers, second only to emulsion-polymerized styrenebutadiene rubber (SBR). In 1977 U.S. tire firms consumed 6.1×10^8 lbs. of polybutadiene [1-1].

Polybutadiene is similar in structure to natural rubber (polyisoprene). The repeating units for PBD and polyisoprene are shown in Fig. 2.1.

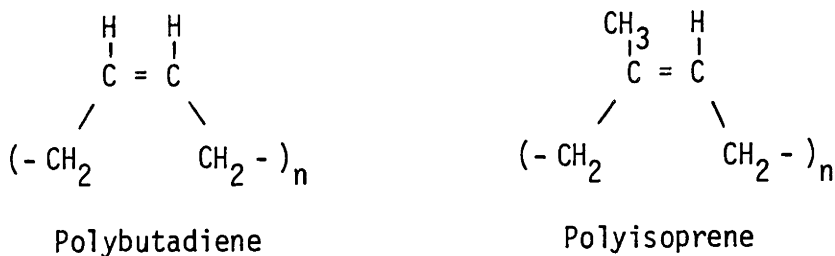
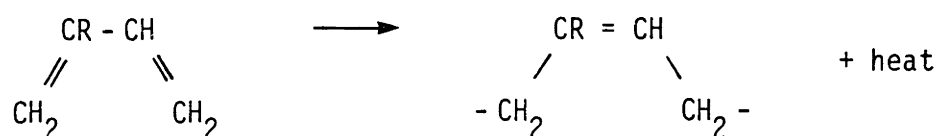


Fig. 2.1 Repeating units for polybutadiene and polyisoprene

*Incidentally, the "superballs" that children play with are made of polybutadiene.

The only difference between the two is the CH₃ (methyl) group that replaces the hydrogen on the second carbon atom. The development of PBD rubber was very much dependent upon the break-throughs necessary to synthesize natural rubber. The polymerization of the two is represented in Fig. 2.2.



where R = H for polybutadiene, or
R = CH₃ for polyisoprene

Fig. 2.2 Polymerization of diene monomers

The breaking of two carbon-carbon double bonds and formation of a single double bond results in the liberation of heat. The important detail of the natural process that was difficult to reproduce in the laboratory was how the double bond in the polymer chain was formed. There are at least three different possible end results of polymerization. These are shown in Fig. 2.3.

The cis and trans molecules are restricted in their rotation by the carbon-carbon double bond in their backbone structure. These two distinct types of rubber yield very different mechanical

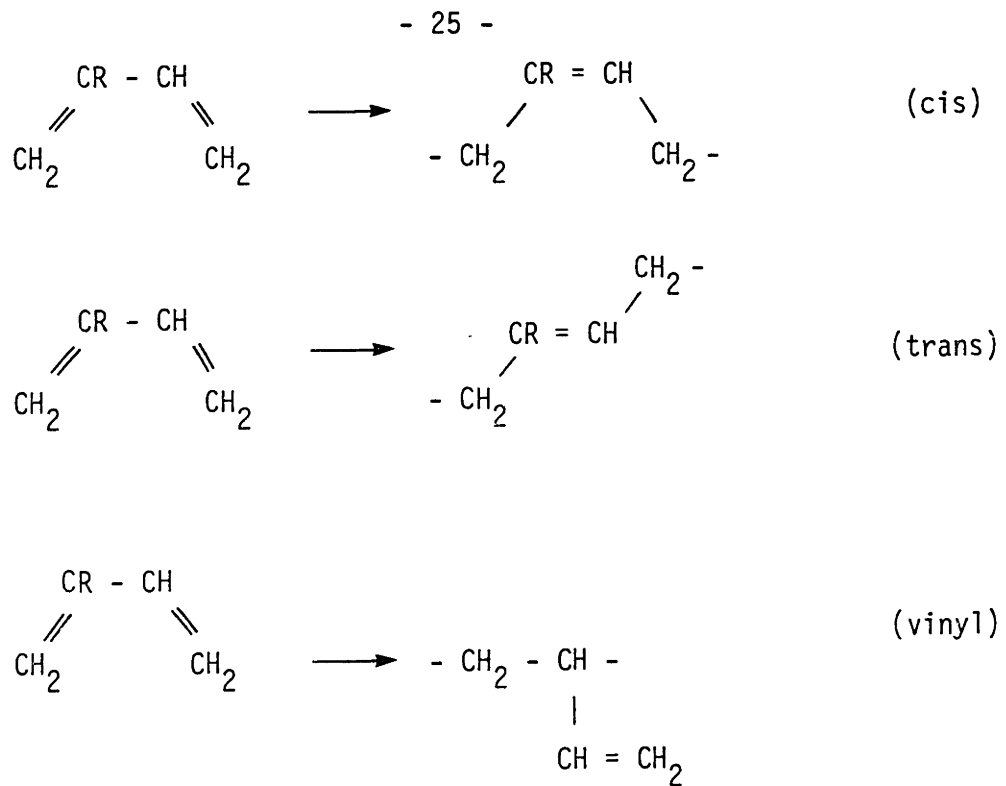


Fig. 2.3 Possible polymerization sequences

properties. Since the elastic nature of rubbers is due to the coiling of the long chain molecules, one can see that the more extended trans molecule will be stiffer than the cis. Similarly the extended trans molecules will be more likely to crystallize. In the case of polyisoprene, the cis conformation yields "natural rubber," where as the trans conformation yields a very stiff material called Gutta-Percha. In the case of PBD it is the high cis type rubber that we

are interested in. In natural rubber, the cis conformation is catalyzed by certain enzymes. In the laboratory, all attempts to produce cis polyisoprene failed until the 1950's when Karl Ziegler in Germany and Giulio Natta in Italy performed extensive research on new types of catalysts. For their work in understanding the synthesis of natural rubber Ziegler and Natta received the Nobel Prize for Chemistry in 1963.

This work also opened the way for the production of high cis polybutadiene. Polybutadiene can be made in several ways. According to Morton [2-1] and referring to Fig. 2.3, we can say in general that, emulsion polymerization leads to a high trans structure, Na and K catalysts lead to a high vinyl structure, and solution polymerization can yield a high cis structure. It is the purpose of this thesis to analyze the end product of solution polymerization.

Polybutadiene rubber with a high cis content can be made by polymerizing in a nonpolar solvent using a special ionic catalyst. The solvent must be nonpolar so as not to interfere with the ionic coordination of the incoming monomer unit. This is shown in Fig. 2.4.

The single carbon-carbon bond in the center of the monomer allows rotation (although a rotational energy barrier may favor the trans conformation). The role of the ionic catalyst is to coordinate the incoming unit. For the case of a lithium catalyst this is shown in Fig. 2.5 [2-3].

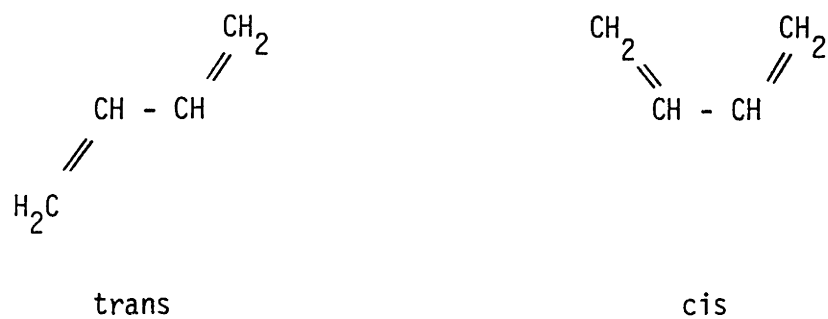


Fig. 2.4 Conformation of the monomer

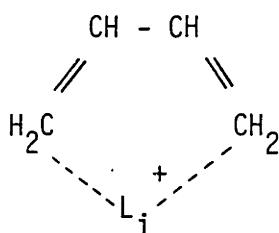


Fig. 2.5 Effect of lithium catalyst on monomer conformation

Once coordinated, polymerization will proceed to predominantly the cis conformation. The important role of the nonpolar solvent can not be over-emphasized. Even small amounts of polar contaminants (like water) can kill the reaction or change the conformation. Odian shows the results of polymerizing isoprene in pentane or in a slightly polar, or very polar solvent on the polymer structure [2-3].

TABLE 2-1

<u>Catalyst</u>	<u>Solvent</u>	<u>Structure of Polymer (%)</u>		
		<u>cis, 1-4</u>	<u>trans, 1-4</u>	<u>vinyl</u>
C ₄ H ₉ Li	100% Pentane	93	---	7
C ₄ H ₉ Li	90% Pentane/ 10% Tetrahydrofuran	---	26	74
C ₄ H ₉ Li	100% Tetrahydrofuran	---	---	100

The 10% tetrahydrofuran, a polar solvent, completely changes the polymerization from predominantly cis, to predominantly vinyl.

As mentioned earlier, this reaction is exothermic, with an enthalpy of polymerization of $\Delta H = -17.4$ K cal/mole. Since the molecular wt. of the monomer is 54 and its heat capacity is about .5 cal/gr °C, this heat of polymerization would lead to an adiabatic temperature rise of 644°C. Such a temperature rise is completely unacceptable. Removal of this heat therefore limits the rate of reaction. Also as the reaction proceeds the polymer chains grow,

which greatly increases the solution viscosity. So in addition to providing a polymerization medium, the solvent is needed to aid in heat transfer. It does this by reducing the solution viscosity and allowing convective heat transfer against the cooler walls of the reactor vessel. In some cases the solvent is also allowed to boil off, removing heat in the phase change. The effect of reducing viscosity also improves mixing and reduces shaft work. The output of the reactor vessel is a viscous solution not very different from rubber cement. The polymerization process is shown schematically in Fig. 2.6. The viscosity of the resulting "cement" depends strongly on concentration, and less so on temperature. For a solution of 12% wt PBD in commercial grade hexane the viscosity at room temperature is about 5000 cps. At a concentration of 30% the viscosity increases to 5×10^5 cps, where 1 cps = 100 gr/cm-sec.

The system we are considering here is made up of a broad molecular weight polymer and a mixed solvent. Typical values for the number average, weight average, and z-average molecular wts are $M_n = 10^5$, $M_w = 4 \times 10^5$, $M_z = 1.7 \times 10^6$. For a monodisperse polymer all of these averages would be identical. The solvent is made up of a variety of hexane isomers, but predominantly n-hexane, Table 2-2 shows the composition, by weight percent, of the commercial grade hexane used in the work reported in this thesis.

After exiting the polymerization vessel the reaction is terminated. This can, in principle, be done by almost any polar substance, including water or some alcohols. Antioxidants and oil

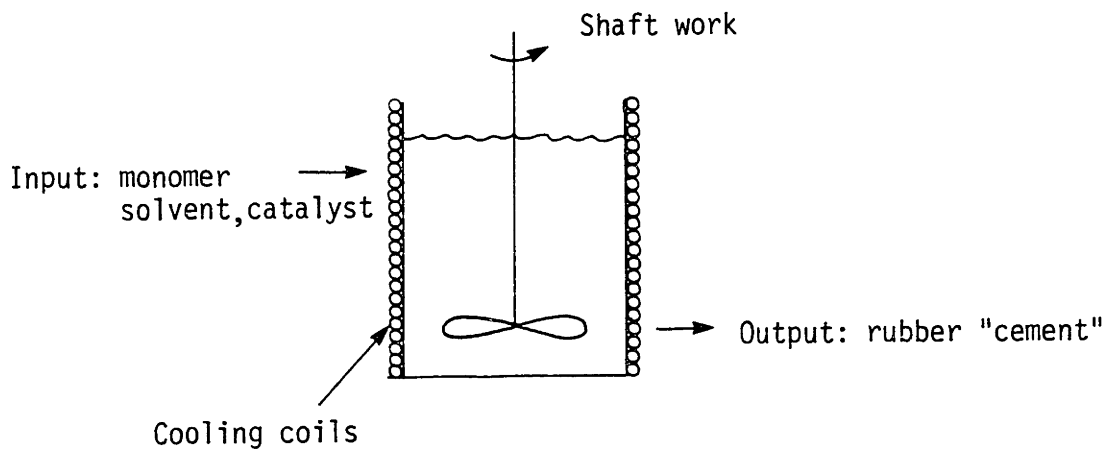


Fig. 2.6 Schematic of polymerization process.

TABLE 2-2

Composition of commercial grade Hexane
in weight percent

n-hexane	64.4
methylcyclopentane	20.1
3 methylpentane	7.6
2 methylpentane and 2,3 dimethylbutane	4.9
other isomers	3.0
	<hr/>
	100.0

extenders are added and the solvent is then separated from the rubber. After separation, the rubber is baled and then sent to a tire manufacturing plant.

In summary then, the solvent is used as a passive medium in which the ionic polymerization of polybutadiene can take place. Any variation in the nonpolar nature of the solvent may strongly effect the final polymer conformation. Perhaps the main reason for the presence of the solvent, however, is to improve heat transfer. This is, to maintain adequate control over the kinetics of polymerization. In addition, the solvent aids in mixing the monomer, catalyst and polymer, and reduces the shaft work.

References, Chapter 2

- 2-1 Chemicalweek 126, 19, May, 1980.
- 2-2 Maurice Morton (ed.) Rubber Technology, Van Nostrand Reinhold Co., 1973.
- 2-3 George Odian, Principles of Polymerization, McGraw-Hill, 1970.

CHAPTER 3

SEPARATION PROCESSES

This chapter is intended to give a brief glimpse at some separation process improvements that, by and large, won't work. This discussion is intended to clarify the limits on these processes, because under some circumstances they may be quite applicable. There are two notable exceptions to the "won't work" list however. The heat pump cycle looks very promising but is mechanically quite complex. In addition, some clever evaporation scheme must be worked out to implement this idea. One possible evaporation mechanism, based upon spinodal decomposition of the solution is discussed in Chapter 7. The other promising separation improvement is based upon liquid-liquid phase separation. It is discussed in the last section of this chapter, and throughout the remainder of this thesis.

3.1 Bulk Polymerization

If solvent removal is a problem, the obvious first question to ask is, why not polymerize without a solvent, i.e., in bulk? In fact some polymers can be made this way. Polymethyl methacrylate (PMMA) can be polymerized in bulk by casting it into sheets, or by stirring it in its own monomer, and then removing the polymer before 100% conversion. In either case the key problem is heat transfer. High heat buildup will accelerate the reaction which in turn will generate more heat. Such an unstable condition

(called autoacceleration or the Tromsdorff effect) can lead to an undesirable molecular weight distribution, degradation of the polymer, and in some cases a violent explosion. In this respect, the fact that PMMA has a much lower heat of polymerization than PBD is of considerable advantage. It should also be pointed out that hexane, and butadiene (a gas at room temperature and pressure) are extremely flammable, and in some cases the catalysts are pyroforic. So safety, as well as the control of the reaction, are issues here.

One way of solving this problem would be to cast polybutadiene in continuous sheets, thin enough to allow heat diffusion. For a sheet cooled on both sides and subjected to a constant temperature, the appropriate terms of the energy equation, and the boundary conditions are [3-1].

$$\frac{d^2T}{dx^2} = - \frac{\dot{W}_{poly}}{k} \quad (3.1)$$

and $\frac{dT}{dx} = 0$ at $x = 0$

$$T = T_0 \quad \text{at } x = x_0$$

where k is thermal diffusivity, \dot{W}_{poly} is the heat of polymerization rate, and the sheet is of thickness $2x_0$. This results in a parabolic temperature distribution in the sheet.

Now to maintain adequate control over the molecular weight distribution it is necessary to restrict the temperature gradient in the sheet to $\Delta T \leq 10^\circ\text{C}$.

The solution of equation (3.1) yields

$$x_0^2 = \frac{2k\Delta T}{\dot{W}_{\text{poly}}} \quad (3.2)$$

Substituting $k = 5 \times 10^{-4} \frac{\text{cal}}{\text{sec-cm-}^\circ\text{C}}$, $\dot{W}_{\text{poly}} = 17.4 \text{ kcal/mole}$, and a reaction time (t_r) of 1 hr. yields,

$$x_0 \cong .5 \text{ cm} \quad .$$

So other problems aside, if we go to thin enough sheets, ($2x_0 \leq 1 \text{ cm}$) this method should allow adequate heat transfer. However, for large producers, the combination of thin sheets and fairly long reaction times will lead to enormous area requirements and consequently large capital investments. For example if a producer can make 10^6 tons/year they must devote more than 8 football fields in area to this operation. One possible way around this is to shorten the reaction time. Note, however, that this will increase \dot{W}_{poly} , since \dot{W}_{poly} is fixed and $x_0 \sim 1/\sqrt{\dot{W}_{\text{poly}}}$ so, $\text{Area} \sim \sqrt{t_r}$ and a large change in t_r is needed.

$$\text{Area} = \frac{\text{Volume production rate}}{\text{thickness} (\sim \sqrt{t_r})} \times \text{reaction time} (=t_r)$$

3.2 Improved Heat Transfer in the Reactor Vessel

A second approach to this problem, which also recognizes that heat transfer is the number one reason for the solvent, would be to improve heat transfer in the reactor vessel. Then the reaction could occur at a higher polymer concentration. This also means, however, a higher viscosity. So this approach would involve a tradeoff between heat transfer and viscous shaft work. Heat transfer in a reactor vessel can be characterized by the convective term of the energy equation [3-1].

$$V_x \frac{\partial T}{\partial x}$$

The idea is to generate flow in the direction of the temperature gradient in order to improve heat transfer. Viscous shaft work is characterized by the term

$$\dot{W} \sim \mu V^2 .$$

One needs to maximize one term and minimize the other, but both velocities V_x and V are related to the shafts rotational rate ω and so the equations are coupled. Consequently, a large improvement by this approach is not foreseeable.

One other approach to this problem, which is generically similar, would be to increase the heat transfer area in the reactor vessel. This is often tried by inserting cooling pipes or tubes into the

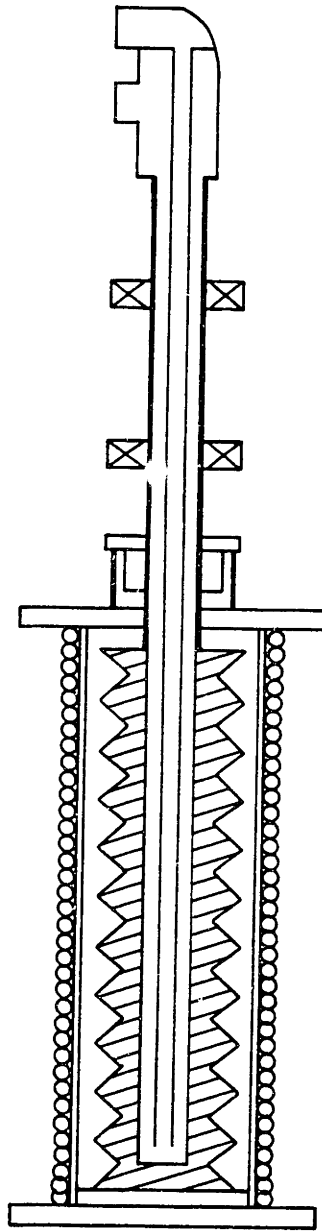


Fig. 3.1 Vortex reactor vessel. Grooved, rotating, inner core generates vortex motion in annulus. Coils on outside wall, and core can be cooled or heated.

reactor vessel. Alternatively, one could design a vessel with a cooled core, such as the one shown in Fig. 3.1. In this vessel, the grooved core generates vortex pairs which provide convective currents between the cooled core and the cooled wall. A vessel like this one was evaluated in some detail and is presented in Appendix A. In general it suffers from the problem of high viscous work at high heat transfer rates and so is probably much better suited to heating rather than cooling applications.

3.3 Heat Pump Cycle

Heat pumps make it possible to transfer heat from a low temperature to a high temperature with the application of some work. This is exactly what is needed if the separation process being considered includes the evaporation, and then recondensation of hexane. In fact, the hexane could be used as the working fluid for the heat pump cycle. In such a scheme, the hexane would be evaporated, compressed, and then condensed at a higher temperature. This would allow us to use the latent heat of condensation to supply some of the needed latent heat of evaporation. A schematic of this basic idea is shown in Fig. 3.2. The steps involved would be,

- 0-1 evaporation of the hexane at constant temperature and pressure,
- 1-2 adiabatic compression of the hexane vapor,
- 2-3 constant pressure condensation, and
- 3-4 constant enthalpy expansion.

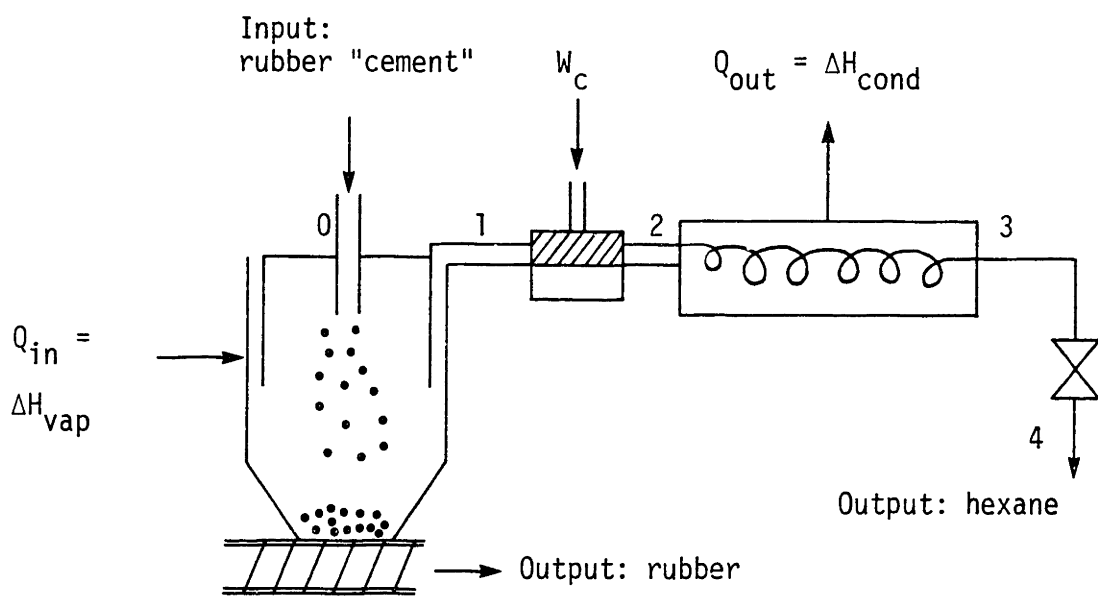


Fig. 3.2 Schematic of "heat pump" separation cycle.

By some means then, Q_{out} at T_H would be used to supply some of Q_{in} at T_L , where $T_H > T_L$, and $\Delta T = T_H - T_L$. The temperature-entropy diagram for this process is shown in Fig. 3.3 [3-2]. The coefficient of performance η , for the heat pump cycle, 0-1-2-3-4, is given as,

$$\eta = \frac{Q_{out}}{W_c} \quad , \quad (3.3)$$

where $Q_{out} = \Delta H_{condensation}$, and $W_c =$ the compressor work. For purposes of this discussion, it is convenient to consider an approximate cycle A-1-B-3. Then η can be given as

$$\eta_{A1B3} = \frac{T_H}{\Delta T} \quad (3.4)$$

Now it is clear how the efficiency of this cycle depends on ΔT . This same ΔT is needed, however, to transfer Q_{out} to supply ΔH_{vapor} . The heat transfer rate using some over-all surface heat transfer coefficient U , and area A would be [3-1],

$$\dot{Q}_{in} = AU\Delta T. \quad (3.5)$$

It is clear then, by equations (3.4) and (3.5) that rate and efficiency are coupled. This is a reoccurring theme for all separation processes.

Implementation of this proposed heat pump cycle would require

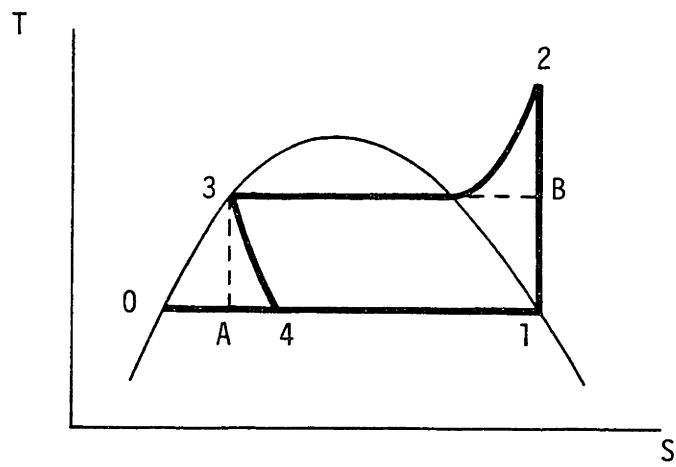


Fig. 3.3 Typical idealized heat pump cycle

optimizing ΔT , which in turn will depend upon the method of heat transfer. As the idea is shown in Fig. 3.2, the rubber cement is spray dried in a large chamber. Heating coils on the parameter of such a large vessel would probably be ineffective. Heat transfer to the drying particles in the container would require some carrier gas, which would then be compressed with the hexane, increasing compressor work, and reducing heat transfer efficiency in the condensor. Alternatively, the cement could be preheated, and then adiabatically evaporated. This would require a preheating of $\Delta T = 170^\circ\text{C}$ which is out of the question for two reasons; it would degrade the polymer, and require an enormous compressor. Furthermore, and more importantly the auto ignition temperature of hexane is about 260°C ; with a reactor temperature up to 130°C a possibility, any leaks to the atmosphere would be catastrophic.

A more realistic process, would probably use some combination of preheating and heat transfer during evaporation, perhaps taking place on a scraped drum. Spinodal decomposition could be used to aid in the rapid evaporation of hexane from the thin layers of cement (see Chapter 7).

In spite of the mechanical complexities inherent in any heat pump cycle separation scheme, however, the energy requirement does make the method look attractive. Fig. 3.4 shows a possible cycle running between 120°C and 150°C , $\Delta T = 30^\circ\text{C}$. The various steps, and enthalpy changes for this process are given in Table 3.1.

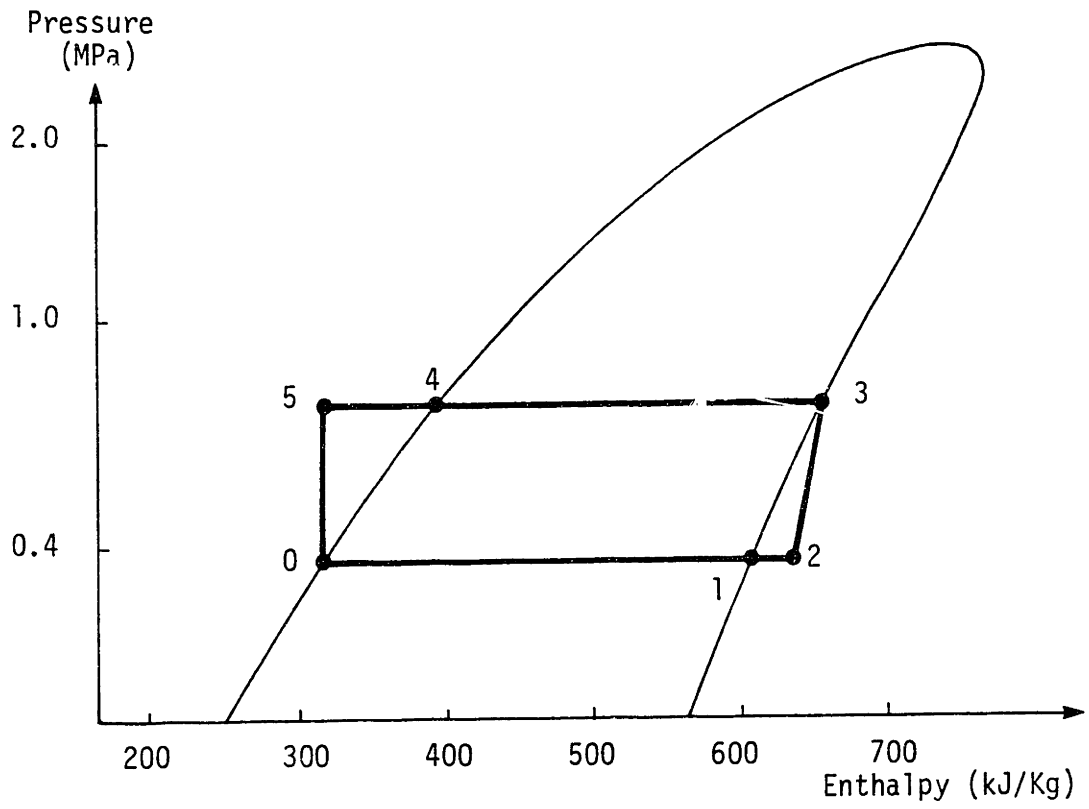


Fig. 3.4 Low temperature cycle.

TABLE 3.1

Low Temperature Heat Pump Cycle for Hexane

0-1	evaporation, $P = \text{const.}$	$\Delta h = 69.0 \text{ cal/g}$
1-2	heating, $P = \text{const.}$	$\Delta h = 8.8 \text{ cal/g}$
2-3	compression, $dQ = 0$	$\Delta h = 7.9 \text{ cal/g}$
3-4	condensation, $P = \text{const.}$	$\Delta h = 62.8 \text{ cal/g}$
4-5	cooling, $P = \text{const.}$	$\Delta h = 21.5 \text{ cal/g}$
5-0	expansion, $H = \text{const.}$	$\Delta h = 0 \text{ cal/g}$

The energy required then is

$$69 + 8.8 + 7.9 + 21.5 - 62.8 = 44.4 \text{ cal/g}$$

If 1000 BTU/lb-rubber are required for evaporation, this process only requires 640 BTU/lb-rubber. This is a considerable reduction, and there are several possible ways to improve upon this cycle. Increasing the temperature to $T_H = 190^\circ\text{C}$ and $T_L = 160^\circ$ will not improve the energy situation however, contrary to what might be implied by equation (3.4). A high temperature cycle is shown in Fig. 3.5. This process would require 810 BTU/lb-rubber not including the heat necessary to bring the reactor output up to 160°C .

3.4 Reverse Osmosis

The next group of separation process improvements considered, all deal with the separation process explicitly. The energy scale shown in Chapter 1 suggests that processes that avoid the

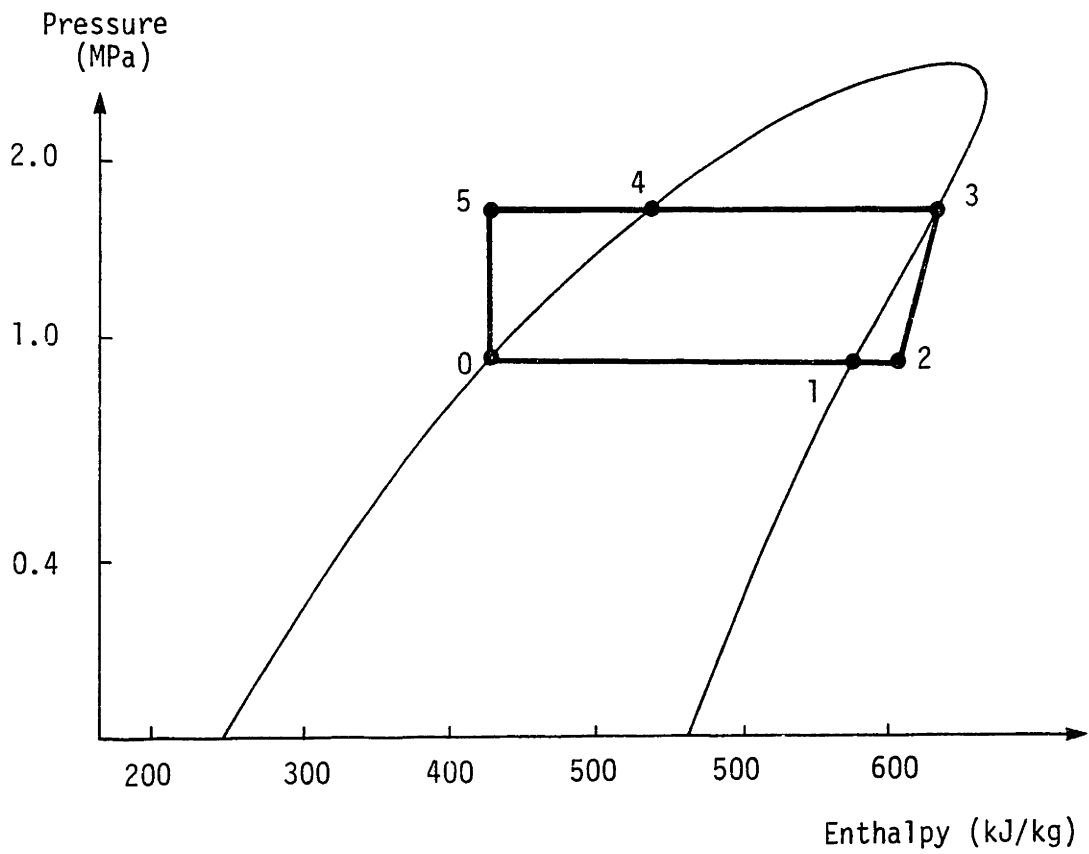


Fig. 3.5 High temperature cycle.

liquid-vapor-liquid phase transitions for hexane have the potential of greatly reducing the energy required. One of these processes, reverse osmosis, has the potential of operating near the theoretical energy minimum.

Reverse osmosis is a process by which only certain chemical species are allowed to pass through a special filter called a semi-permeable membrane. Essentially the process involves squeezing the hexane out of solution. Fig. 3.6 shows the main features of reverse osmosis. We start with pure solvent, and a solution separated by a semipermeable membrane which allows only solvent molecules to pass. This is shown on top. On the right, the pure solvent will have a higher chemical potential causing the solvent molecules to migrate from right to left through the membrane. At some point the added pressure caused by the influx of solvent molecules will balance the chemical potentials and the system will be in equilibrium. In Fig. 3.6, the added pressure, called the osmotic pressure π , is shown as a hydrostatic head, $\pi = \rho gh$. If we now insert a piston on the left hand side and exceed the osmotic pressure, we can cause the solvent molecules to flow from left to right. This process, called reverse osmosis (R.O.), will have the effect of concentrating the solution on the left hand side of Fig. 3.6. Methods like this one can be used to generate pure water from salt water [3.3], and can concentrate some polymer solutions.

If for the moment, we ignore the issue of membrane design, there are two important problems concerning reverse osmosis. In the

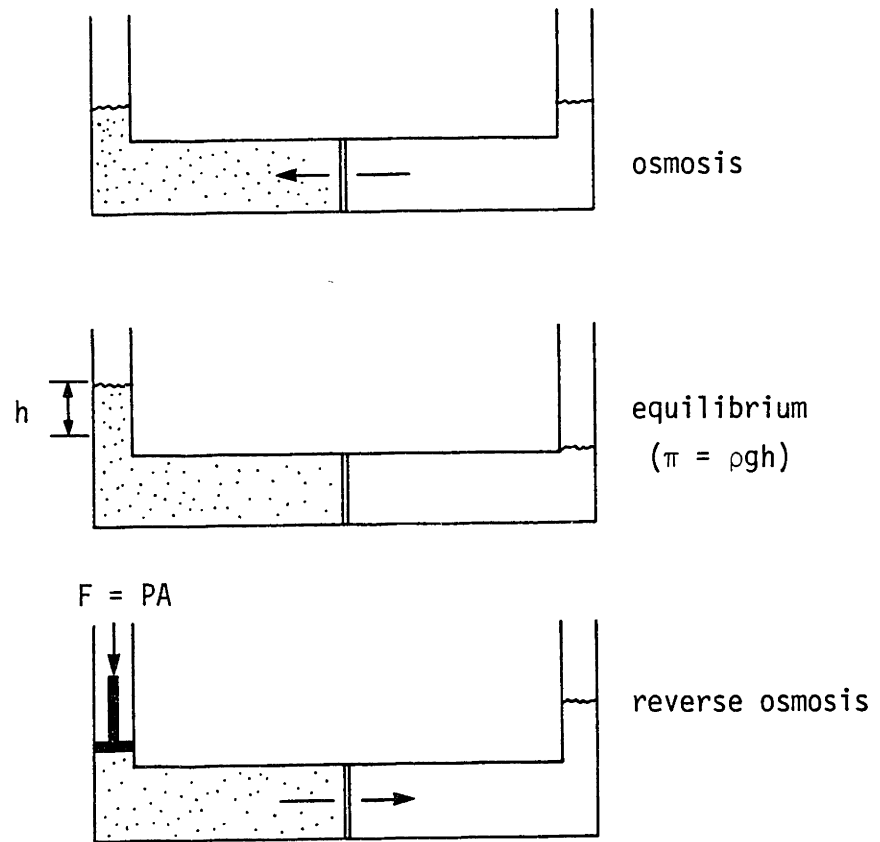


Fig. 3.6 Reverse Osmosis.

first place, the osmotic pressure increases with concentration in a logarithmic manner, and so the method rapidly becomes impractical at high concentrations. For a 12% wt. solution of PBD in hexane the osmotic pressure was measured at room temperature, after eight days, to be about .07 atm (1 psi). At a concentration of 50% wt. the estimated osmotic pressure would be about 5.4 atm (80 psi). Such high pressures would require some kind of mechanical support for the membrane, which would greatly limit the possible filter geometries. This is particularly important because the characteristically low solvent flux rates for R.O. require very large filter areas.

The second problem is called concentration polarization. As the solvent exits the solution, it leaves behind a solute rich layer on the solution side of the membrane. For further concentrating, the remaining solvent must now diffuse through this layer before joining the pure solvent. The result is that the solvent flux is diffusion limited, and in general decreases with time. To minimize this problem, the solution can be stirred, or the membrane scraped, but the effect is difficult to eliminate.

The mass flux, and energy consumption for reverse osmosis can be characterized by two simple approximations. The energy E required for the process can be given as

$$E = \int (P - \pi) Q dt \quad (3.6)$$

where P is the applied pressure, π is the osmotic pressure, Q is the volume flux rate, and t is time. The solvent flux can be approximated

as,
$$Q = \frac{1}{R} A(P-\pi) \quad (3.7)$$

where R is the flow resistance, and A the flow area. These equations are coupled, and imply that some trade-off is needed. The osmotic pressure effect is shown in the term $P - \pi$, since only $P > \pi$ will cause reverse osmosis. The concentration polarization effect is accounted for in the resistance R. To obtain adequate flux rates, to make a process commercially viable, involves minimizing R, and maximizing A and P. In practical terms, the issues are,

1. reducing the concentration polarization effect, and/or improving upon the design of the membrane,
2. increasing filter area and, consequently, the capital investment, and
3. increasing the pressure, which requires providing adequate mechanical support for the filters, and consequently results in increasing the energy consumption.

The order of magnitude for R for a 10,000 molecular weight cut off, polysulfone Millipore filter can be estimated from Fig. 3.7.

Assuming that equation (3.7) is approximately correct, at least locally, the slope of the lines in Fig. 3.7 correspond to $1/R$.

The reverse osmosis value applies to the flux from a quiescent reservoir from time equals zero to 1000 sec. In general this value will decrease with time.

The pure solvent curve gives an upper bound flux rate, or lower bound resistance. It represents the total elimination of the

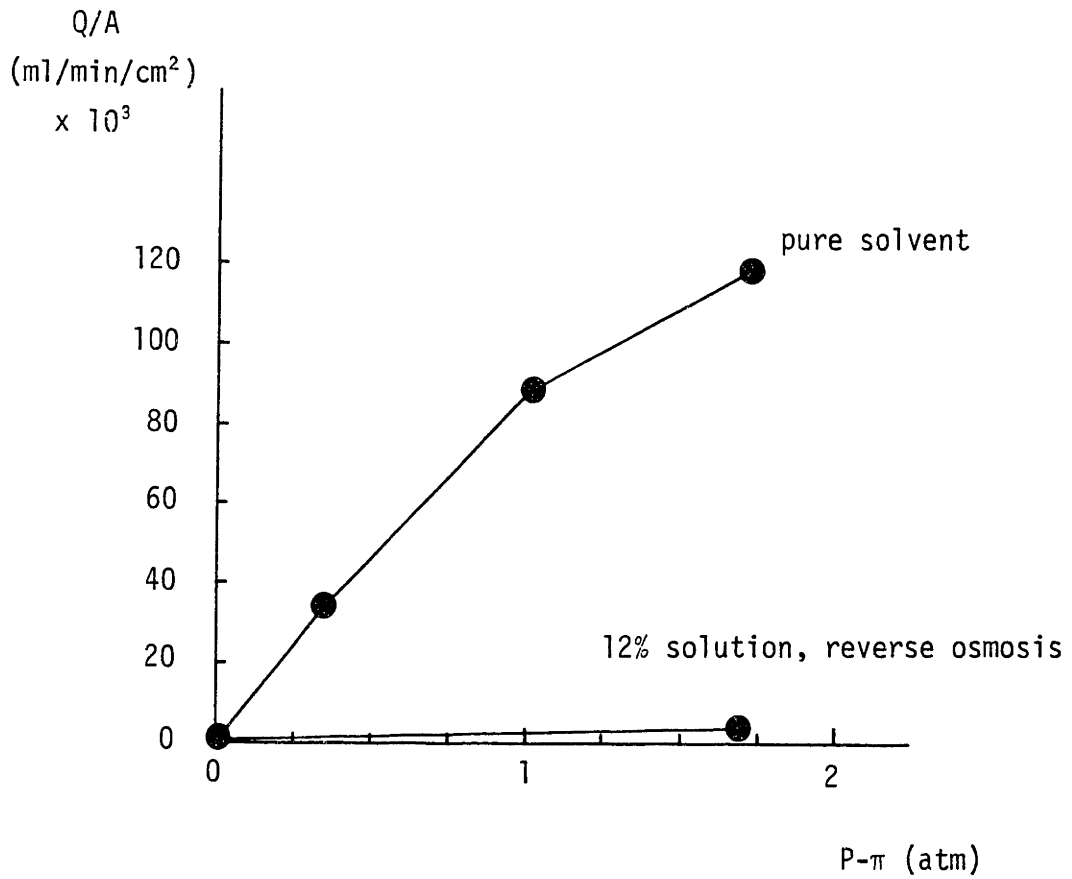


Fig. 3.7 Solvent flux rates vs. applied pressure

concentration polarization effect. Unfortunately even these flux rates are extremely low. Water flux rates through semipermeable filters, for example, can be six times greater or more [3-4]. In fact, these values are so low, and in view of the other problems involved, that reverse osmosis does not appear to be a practical method for separating solvents from solutions in the concentration range we are considering.

Improvements in the filter that reduce the concentrations polarization effects might be possible. Due to the slightly polar nature of PBD, and the nonpolar solvent, a nonpolar membrane, perhaps out of polyethylene might discourage the polymer build-up. Increasing the filter pore size won't help due to the broad molecular weight distribution of the rubber. Even the 10,000 molecular weight cut off filter we used allowed some low molecular weight PBD species through. In short a large improvement in the filter design is not foreseeable.

3.5 Liquid-liquid phase separation

In general, polymer solutions will phase separate if subjected to sufficient heating or cooling [3-5]. As mentioned earlier, this phenomenon could be used in principle to concentrate polymer solutions. In either the heating, or cooling case, a solution at an original concentration of C_0 , will separate into two new solutions, one more dilute $C' < C_0$, and one more concentrated $C'' > C_0$. Consequently these separations are between liquid phases. The amount of separation will depend upon the amount of heating or cooling beyond the phase separation temperature. For a 12% wt. solution of

PBD in commercial grade hexane, the high and low phase separation temperatures are 133°C and -10°C (see Chapter 5 for more details). Since the reactor can operate between 70°C and 120°C depending upon the details of the particular polymerization process, we can readily see that it is the high temperature phase separation phenomenon in which we are interested. The phase diagram for the high temperature separation of a simple binary mixture (a polymer of a single molecular weight, and a single solvent) is shown in Fig. 3.8. This shows all of the essential features of the phenomenon. If a single phase (1 ϕ) solution of concentration C_0 is heated to T , it will break up into two phases (2 ϕ) at concentrations C' and C'' . Physically, the solution becomes cloudy at the phase boundary due to the difference in the refractive indices of the two solutions. The phase diagram is a little more complicated for a broad molecular weight polymer, so a discussion of these details is deferred until Chapter 5.

In general the dilute phase C' is quite dilute, in many cases around 1 to 2% wt. The concentrated phase C'' , on the other hand, can in principle, be made as concentrated as desired simply by raising the temperature. The ratio of the weight of dilute phase W' to the concentrated phase W'' can be determined from the tie lines joining C' , C_0 and C'' ,

$$\frac{W'}{W''} = \beta_W = \frac{C'' - C_0}{C_0 - C'} \quad (3.8)$$

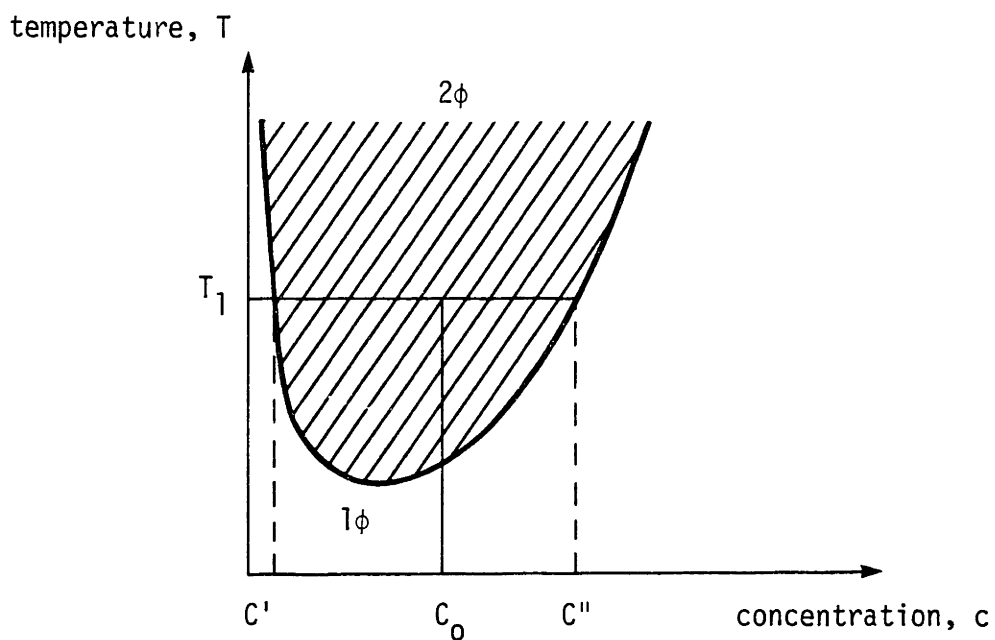


Fig. 3.8 Phase diagram for high temperature separation of binary polymer-solvent system.

where $W' + W'' = W_0$, W_0 is the original mass or weight of solution C_0 . So as the solution C_0 is heated, β_W increases, and more and more dilute phase is generated. Now if the dilute phase could be recycled as "solvent" to the reactor, the high temperature phase separation phenomenon could be used as a method to concentrate polymer solutions. The steps of this method would be,

1. Heat the solution above the phase separation temperature,
2. Physically separate the dilute and concentrated phases,
3. Recycle the dilute phase, to the reactor, and
4. Remove the remaining hexane from the concentrated phase.

A schematic of this method is shown in Fig. 3.9. The major issues that have to be addressed to show even preliminary feasibility for such a method are energy consumption, physical separation, and dilute phase "recycle-ability."

3.5.1 Energy consumption

The energy consumed by this method will involve two major terms, one to account for the heating required, and the other to account for the removal of the remaining hexane from the concentrated phase. Because the solution becomes more concentrated at higher temperatures, there is less hexane to remove. So the second term decreases with increasing temperature, and the first term increases. An optimum value can be calculated, once the phase diagram is known in detail, this is done in Chapter 8. It turns out that the optimum occurs at 170°C, and the energy consumed is 610 BTU/lb-rubber. This is only 12% of the energy required for the commercial separation process. Also the concentrated phase is of sufficient viscosity to

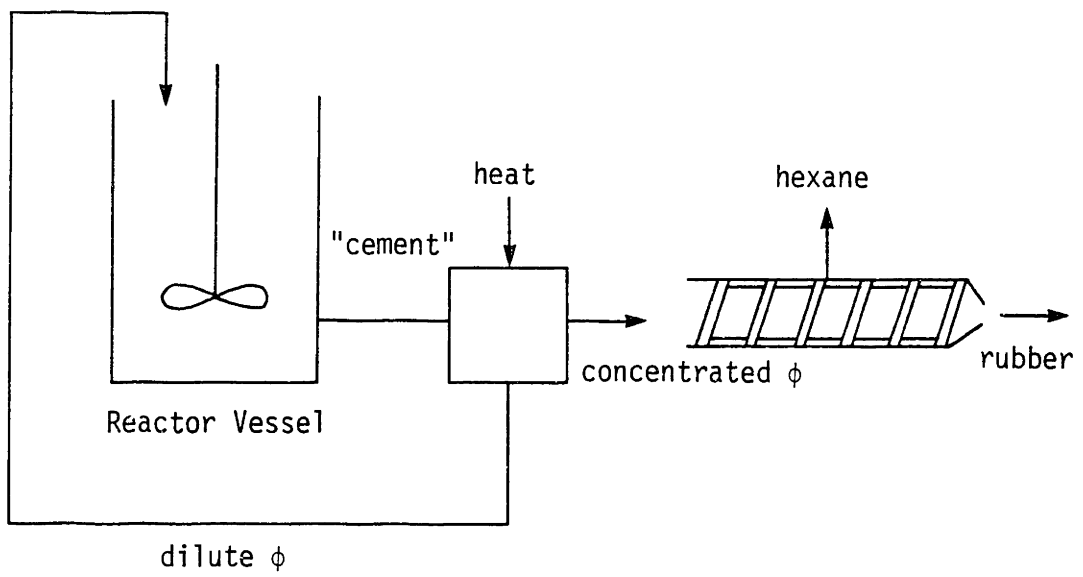


Fig. 3.9 Separation scenario based upon high temperature phase separation.

be handled in a vented barrel extruder.

The amount of solvent removed this way can be calculated as follows, at 170°C and $C_0 = .123$, the resulting solutions are $C' = .015$ and $C'' = .30$, so

$$\frac{W'}{W''} = 1.64$$

Using $W' + W'' = W_0 = 1$, and $C' = \frac{w'}{w' + s'}$ where w' = the weight of rubber in the dilute phase and s' = the weight of solvent in the dilute phase, and $W' = w' + s'$, you can then calculate the amount of solvent in the dilute phase s' and the amount of original solvent s_0 as

$$\frac{s'}{s_0} = \frac{.612}{.877} = .697 \quad .$$

So 70% of the original solvent is removed by the phase separation method, and 30% is removed in the vented extruder

3.5.2 Physical separation

As already mentioned in Chapter 1, to be economical, reactors must operate at fairly high concentrations, and at these high concentrations the liquid phases, obtained after phase separation, do not readily separate by gravity. This is due to the arrangement of the two phases. With $\beta_W = 1.64$, there is considerable dilute phase. Unfortunately however, it is often arranged as bubbles surrounded by the viscous concentrated phase. This situation is

hopeless. On the other hand, if the arrangement of the phases were reversed, settlement by gravity would be quite rapid. The exact arrangement of the phases depends on where you are in the phase diagram, and how you got there. In general, there are two different phase separation mechanisms that we must consider here, nucleation and growth, and spinodal decomposition. For the range of concentrations that we are interested in, the key to rapid settlement is to get into the spinodal decomposition regime as rapidly as possible. This can be done in several ways,

1. heat rapidly
2. heat at high pressure and then drop pressure rapidly,
3. mix in more solvent, or a non-solvent rapidly.

For polymer solutions of characteristically low thermal conductivity, heating rapidly usually won't work, but the other methods do. In fact these techniques can change settlement times by six orders of magnitude or more. In short, practical separations-by-gravity methods can be designed. These are discussed in Chapters 6 and 7.

3.5.3 Dilute phase recycle

Polybutadiene requires a terminator to stop its reaction, so there are two options concerning the heating of the solution. One is to heat before adding the terminator, and the other is to heat after adding the terminator. In the first case, the reaction will proceed into the heating stage, this should make it easier to recycle the reacting dilute phase, but it should also greatly accelerate the reaction. The result maybe a reaction that is very

difficult to control, and perhaps a marked change in the molecular weight of the resulting polymer. In the second case, the terminator travelling with the dilute phase, may degrade the reaction in the reactor vessel once it is recycled.

The second method, terminating and then heating, is the simpler of the two and in fact it works. At Goodyear a series of bottle polymerizations were run with various percentages of recycled dilute phase (up to 20%) added to their standard premix. For comparison, similar portions of pure hexane were added to the premix and polymerized also. The results are that the monomer conversion and catalyst usage were the same. (See Table 8.1 in Chapter 8)

References, Chapter 3

- 3-1 W.M. Rohsenow and H. Choi; Heat, Mass, and Momentum Transfer, Prentice-Hall (1961).
- 3-2 G.J. Van Wylen and R.E. Sonntag; Fundamentals of Classical Thermodynamics, 2nd ed. Wiley (1978).
- 3-3 U. Merten, ed.; Desalination by Reverse Osmosis, M.I.T. Press (1966).
- 3-4 Millipore Ultrafiltration Membranes and Systems Catalog (1977).
- 3-5 F.W. Billmeyer, Jr; Textbook of Polymer Science, Wiley-Interscience 2nd ed. (1971).

CHAPTER 4

CHEMICAL THERMODYNAMICS OF POLYMER-SOLVENT SYSTEMS

The goal of this chapter is to develop the background material necessary to discuss liquid-liquid phase separations in polymer-solvent systems. Much of the information contained here will be used in later sections of this thesis to explain and analyze thermodynamic data and certain observed phenomenological results. By and large this chapter is a literature review drawing heavily from the works of others. First, I will review the thermodynamics of mixing and separation for any general liquid-liquid system. In the later part of this chapter, the discussion will turn to theories which are specific to long chain molecules mixed with smaller solvent molecules.

4.1 The Thermodynamics of Mixing

Two components will mix if the resulting solution has a lower Gibbs free energy than the sum of the individual components. This can be expressed in terms of the Gibbs free energy of mixing ΔG_M [4-1, 2].

$$G_M = G_{12}(T, P, n_1, n_2) - G_1^0(T, P, n_1) - G_2^0(T, P, n_2) \quad (4.1)$$

Here, G_{12} = the Gibbs free energy of the solution
 G^0 = the Gibbs free energy of a pure component
 n = the number of molecules of a particular species
 1 = solvent
 2 = polymer
 T = temperature, and
 P = pressure.

For convenience, it is always assumed that the pure and mixed components are taken at the same temperature and pressure. Since G is an extensive property, there is a mass balance implied among the terms in equation (4.1). This can be shown explicitly by using some intensive form of Gibbs free energy. Mass fractions, site fractions, and mole fractions are commonly used. Using intensive quantities,

$$\Delta g_M = g_{12} - X_1 g_1^0 - X_2 g_2^0 \quad (4.2)$$

where $X_1 + X_2 = 1$ and the g 's are in the appropriate units, and the temperature and pressure dependencies are implied. If g is the Gibbs free energy per unit mass of solution, then $X_1 = 1 - C$ and $X_2 = C$, where C is the concentration (weight fraction) of component 2.

Applying the definition $G = H - TS$, where H = enthalpy, and S = entropy, ΔG_M can be written at constant temperature and pressure as [4-1, 2, 3],

$$\Delta G_M = \Delta H_M - T\Delta S_M \quad (4.3)$$

or
$$\Delta g_m = \Delta h_m - T\Delta s_m \quad (4.4)$$

when $\Delta G_M < 0$, or $\Delta g_m < 0$, spontaneous mixing is implied. This is the well known criterion for thermodynamic mixing. If $\Delta G_M = 0$, the pure and mixed components are in equilibrium.

ΔH_M and ΔS_M are also mixing functions, and can be expressed individually in forms similar to equations (4.1 or 4.2). Their signs and magnitudes will determine mixing behavior. In general, at low temperatures, the second term, $T\Delta S_M$, becomes less important and mixing behavior is dominated by enthalpic considerations. At high temperatures the details of the entropy term become important.

The enthalpy of mixing ΔH_M is the heat of mixing at constant pressure. For polymer-solvent systems, it is associated with the making and breaking of intermolecular bonds. Several types of mixing behavior are possible.

$\Delta H_M > 0$ implies endothermal mixing

$\Delta H_M = 0$ implies althermal mixing, and

$\Delta H_M < 0$ implies exothermal mixing.

In practice, all of these are observed. At temperatures around room temperature and for reasonably nonpolar molecules, and in the absence of hydrogen bonding, ΔH_M is positive and can be estimated from the solubility parameters δ [4-3],

$$\Delta h_M = \phi_1 \phi_2 (\delta_1 - \delta_2)^2 \quad (4.5)$$

where ϕ is the volume fraction, and the subscripts 1 and 2 refer to the solvent and polymer, respectively. For n-hexane $\delta_1 = 7.24$ $(\text{cal}/\text{cm}^3)^{1/2}$ [4-3] and for polybutadiene $\delta_2 = 8.6$ $(\text{cal}/\text{cm}^3)^{1/2}$ [4-4]. Δh_M then depends on the concentration, with typical values $\phi_1 = .9$ and $\phi_2 = .1$,

$$\Delta h_M = (.9 \times .1)(7.24 - 8.6)^2 = .17 \text{ cal}/\text{cm}^3 \quad .$$

Since hexane and polybutadiene do mix at room temperature, it must be that $T\Delta S_M > 0$ and is sufficiently large to overcome this bond energy barrier. Mixing is then entropy driven. The entropy of mixing ΔS_M has two contributions. The first is due to the geometrical rearrangement of the mixing molecules. It is called the combinatorial entropy ΔS_{comb} . The second term accounts for the entropy of the individual molecules in their specific environment. It is called the noncombinatorial entropy ΔS_{nc} . These two terms are additive,

$$\Delta S_M = \Delta S_{\text{comb}} + \Delta S_{\text{nc}} \quad , \quad (4.6)$$

and can be expressed individually in a form similar to equation (4.1).

The combinatorial entropy term ΔS_{comb} recognizes that the unmixed state is a very ordered state, and therefore, in terms of

geometrical arrangements, very improbable. The mixed state, on the other hand, is quite probable. This idea is expressed in Boltzmann's equation

$$\Delta S = k \ln \Omega + \text{constant} \quad (4.7)$$

where k = Boltzmann's constant, and Ω = the probability that a given state will exist. Since $\Omega_{\text{MIXED}} \gg \Omega_{\text{UNMIXED}} \geq 1$ it is always true that $\Delta S_{\text{comb}} > 0$. ΔS_{nc} is affected by the intermolecular contacts, and by volume changes upon mixing. Both of these could act to restrict (or amplify) the available vibrational states of the molecules and thereby reduce (or increase) the noncombinatorial entropy. ΔS_{nc} becomes very important for polymer-solvent systems at high temperatures, where it makes a large negative contribution to the entropy of mixing. This behavior is directly related to a negative volume change upon mixing which restricts the available vibrational states of the solvent molecules.

In general then,

$$\Delta G_{\text{M}} = \Delta H_{\text{M}} - T(\Delta S_{\text{comb}} + \Delta S_{\text{nc}}) \quad (4.8)$$

and two possible simplifications for polymer-solvent systems arise. At low temperatures, $\Delta H_{\text{M}} > 0$ dominates the mixing behavior. At high temperatures the relative magnitudes of $\Delta S_{\text{comb}} > 0$ and $\Delta S_{\text{nc}} < 0$ are important.

Examples of possible plots of ΔG_M (or Δg_M) versus the concentration of component 2 are shown in Fig. 4.1. By definition $\Delta G_M = \Delta g_M = 0$ at $c = 0$ and $c = 1$. Fig. 4.1a shows a system that does not mix, that is, it is totally immiscible in all proportions. Fig. 4.1b shows total miscibility, and Fig. 4.1c shows a system that mixes ($\Delta g_M < 0$) but not at all concentrations. It is only partially miscible. In principle, a system may exhibit all of these behaviors by varying certain parameters, such as temperature or pressure. In practice, only the situations shown in Figs. 4.1b and c can be obtained for the hexane and polybutadiene system with which we are concerned.

A typical (temperature-composition) phase diagram for a simple two component polymer-solvent system is shown in Fig. 4.2a. At temperatures around T_1 the solution would exist as a single phase (1ϕ) and its Gibbs free energy of mixing plot would look like Fig. 4.1b. At temperatures around T_2 , only solutions at the extremes of concentration could exist as a single phase. In the central region a solution would tend to separate into two solutions or phases (2ϕ). One would be more dilute than the original phase and one would be more concentrated. This is the region of partial miscibility. Fig. 4.2b shows the details of this region. If a solution originally at concentration C_0 were heated to T_2 it would separate into two new solutions C' and C'' . The line joining C' and C'' is called the tie line and the ratio of distances along this line will give the mass balance between component phases. That is

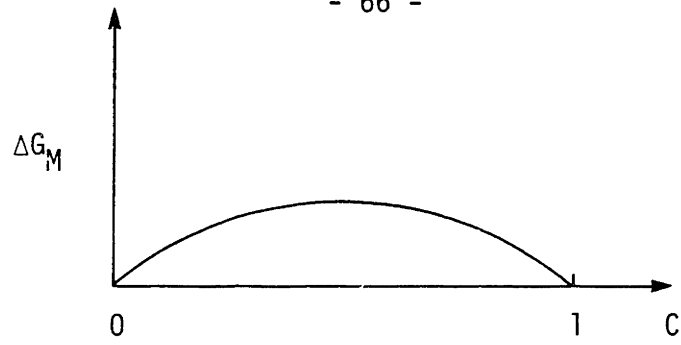


Fig. 4.1a Total immiscibility.

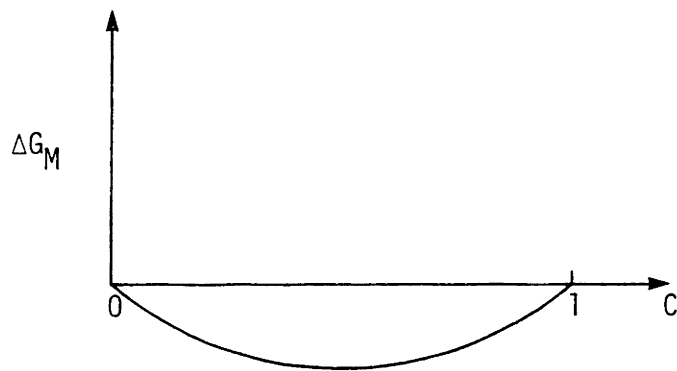


Fig. 4.1b Total miscibility.

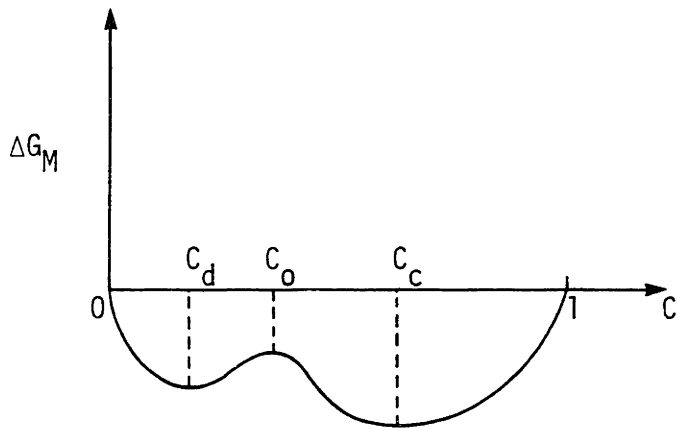


Fig. 4.1c Partial miscibility.

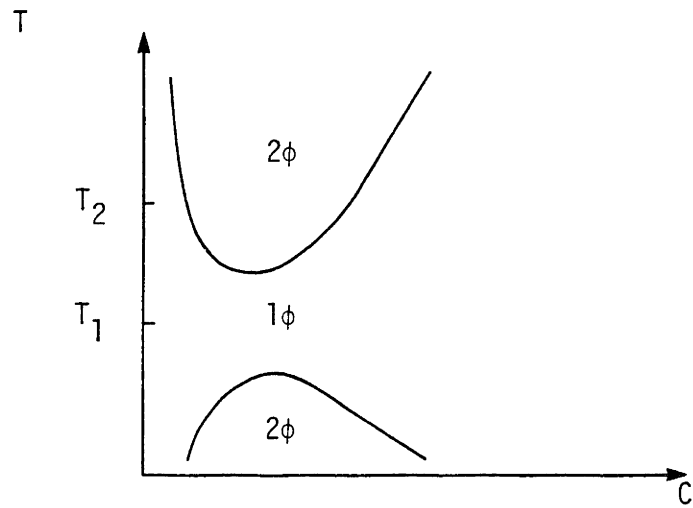


Fig. 4.2a Phase diagram for polymer-solvent system.

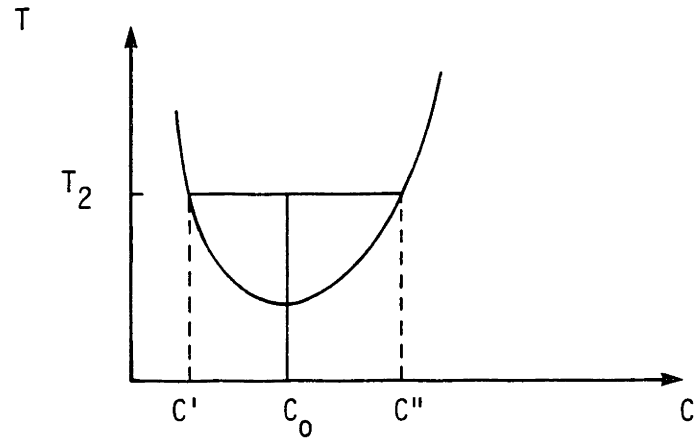


Fig. 4.2b Details of liquid-liquid phase separation at T_2 .

$$\frac{W'}{W''} = \frac{C'' - C_0}{C_0 - C'}$$

where W' = the mass of the dilute phase, W'' is the concentrated phase and $W_0 = W' + W''$, is the mass of the original solution.

Separations in this region are called liquid-liquid phase separations. If we tried to obtain total immiscibility by varying temperature alone we would degrade the polymer at the high temperatures, or crystallize the solution at the low temperatures. The pressures in Figs. 4.2a and b are the appropriate vapor pressures; increasing the pressure would only improve solubility.

It should be pointed out that phase separations at high temperatures are in general, rare phenomena for molecules of similar sizes. In many cases $\Delta S_M = \Delta S_{\text{comb}} > 0$, so as temperature is increased ΔH_M becomes insignificant and

$$\Delta G_M \cong -T\Delta S_{\text{comb}} < 0$$

So mixing usually improves at high temperatures. The unique situation for polymer-solvent systems is due to the large free volume difference between the two species. Upon mixing, the volume contraction greatly restricts the available vibrational motions of the solvent molecules. This results in an ordering effect which is accounted for in the noncombinatorial entropy term. At sufficiently high temperatures, this effect becomes overwhelming and separation occurs. The mixing of polymers and solvents at high temperatures then, with some

exaggeration, is like the condensation of a gas (solvent) into a dense medium (polymer) [4-5].

The liquid-liquid phase separations at low temperatures shown in Fig. 4.2a, are controlled largely by enthalpic differences. At sufficiently low temperatures the reduced entropic term is not adequate to overcome the endothermic heat of mixing.

Phase diagrams, similar to Fig. 4.2a have been found in biological systems and gels, as well as for polymer-solvent systems. For example, John Clark and George Benedek determined the phase diagram for cell cytoplasm from the calf lens [4-6]. In this case, the phase transition is associated with the reversible opacification known as cold cataract. In a recent paper by Tanaka, he has shown a similar phase transition in gels [4-7]. Here the volume change at separation is related to the collapse of the vitreous gel which causes eye retinal detachment.

4.2 The Thermodynamics of Separation

Since ΔG_M is written by definition between pure and mixed components, $\Delta G_M < 0$ does not guarantee that two components will be miscible in all proportions. An example of a partially miscible system that satisfies the mixing criterion is shown in Fig. 4.1c. In this case, while a solution of concentration C_0 will have a lower free energy than the individual unmixed components, a rearrangement of C_0 into C_d and C_c would have a still lower free energy. This can be shown by writing the change in Gibbs free energy locally as

$$\Delta G_{\text{LOCAL}} = G(C_o) - G(C_d) - G(C_c). \quad (4.9)$$

If $\Delta G_{\text{LOCAL}} > 0$, then separation is implied. Implicit in equation (4.9), due to the extensive nature of G , is a mass balance between the component solutions. If this is written explicitly, in terms of the Gibbs free energy of mixing per unit mass of solution, then

$$\Delta g_{\text{LOCAL}} = \Delta g_M(C_o) - \frac{C_c - C_o}{C_c - C_d} \Delta g_M(C_d) - \frac{C_o - C_d}{C_c - C_d} \Delta g_M(C_c). \quad (4.10)$$

An expansion of the right hand mixing terms according to equation (4.2) will verify the mass balance coefficients, and ultimately yield equation (4.9). Here we have used the following notation.

$$\Delta G_M = \bar{W} \Delta g_M,$$

$$\bar{W} = W/\rho_1, \quad W = \rho_1 n_1 + \rho_2 n_2, \quad \bar{W} = n_1 + \bar{\rho} n_2, \quad \bar{\rho} = \rho_1/\rho_2 \quad (4.11)$$

$$C = \frac{\bar{\rho} n_2}{\bar{W}}, \quad (1-C) = \frac{n_1}{\bar{W}},$$

W is weight, or mass, ρ is the molecular density.

Now it should be apparent from Fig. 4.1c that the separation criterion may be satisfied by a number of new solution pairs (C_d, C_c) , where $C_d < C_o$, is more dilute than the original solution, and $C_c > C_o$, is more concentrated. We are interested in the particular

values $C_d = C'$ and $C_c = C''$, that represent the lowest free energy states into which the original solution C_o can physically rearrange itself. We therefore want to maximize Δg_{LOCAL} . To do this it is helpful to recognize that for a given C_o , Δg_{LOCAL} may be thought of as a function of two independent concentration variables C_c and C_d .

$$\Delta g_{\text{LOCAL}} = \Delta g_{\text{LOCAL}}(C_c, C_d)$$

The C_c and C_d dependencies appear explicitly in the coefficients, and in the Gibbs free energy of mixing terms as follows;

$$\begin{aligned} \Delta g_M(C_o) &\text{ is independent of } C_c \text{ and } C_d, \\ \Delta g_M(C_d) &\text{ depends only on } C_d, \text{ and} \\ \Delta g_M(C_c) &\text{ depends only on } C_c. \end{aligned}$$

The concentrations C' and C'' can be obtained by applying the conditions

$$\left. \frac{\partial \Delta g_{\text{LOCAL}}}{\partial C_d} \right|_{C_d = C'} = 0, \text{ and } \left. \frac{\partial \Delta g_{\text{LOCAL}}}{\partial C_c} \right|_{C_c = C''} = 0$$

at constant pressure and temperature.

These yield,

$$\left. \frac{\partial \Delta g_M}{\partial C} \right|_{C=C'} = \left. \frac{\partial \Delta g_M}{\partial C} \right|_{C=C''} = m \quad (4.12)$$

and

$$m = \frac{\Delta g_M(C'') - \Delta g_M(C')}{C'' - C'} \quad (4.13)$$

That is, tangents at the points $(\Delta g_M(C'), C')$ and $(\Delta g_M(C''), C'')$ have the same slope as a straight line drawn through these points. This is shown in Fig. 4.3

Result (4.12) is equivalent to the well known condition that the chemical potentials of the coexisting phases must be equal [4-1]. Result (4.13) uniquely defines the coexisting phases. Since $\Delta g_M(C_0)$ was given as independent of C_d and C_c , any C_0 which satisfies $\Delta g_{LOCAL} > 0$ and does not violate conservation of mass will separate into C' and C'' . For the conditions shown in Fig. 4.3, this is true for any C_0 such that $C' < C_0 < C''$.

The chemical potential is very useful in describing this phase separation behavior because it has the following simple properties: in an equilibrium situation the chemical potential of a particular species will be equal in all phases, and in a nonequilibrium situation, a particular species will tend to migrate from a region of high chemical potential to low chemical potential [4-1]. By definition

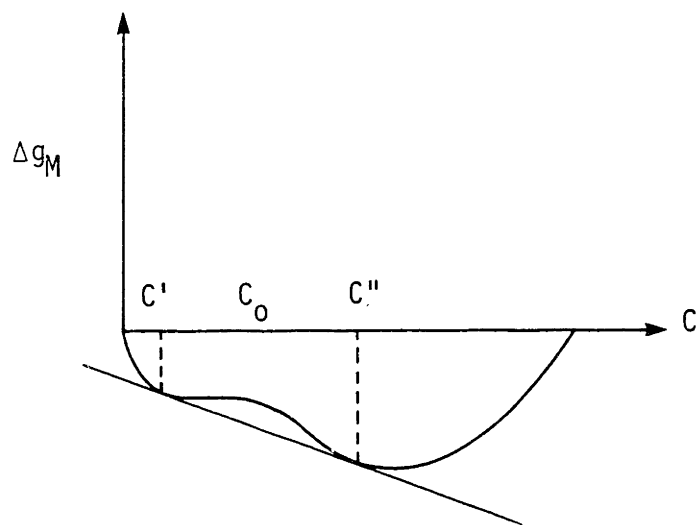


Fig. 4.3 Partially miscible system, C_0 will separate into C' and C'' .

$$\Delta\mu_1 = \left(\frac{\partial \Delta G_M}{\partial n_1} \right)_{T,P,n_2} \quad (4.14)$$

This is the difference in the chemical potential of the solvent in solution less the chemical potential of the pure solvent, $\Delta\mu_1 = \mu_1 - \mu_1^\circ$. Using the notation of equations (4.11) one can write

$$\Delta\mu_1 = \frac{\partial \Delta G_M}{\partial n_1} = \Delta g_M - C \frac{\partial \Delta g_M}{\partial C} \quad (4.15)$$

Taking the difference between the dilute and concentrated phases yields

$$\Delta\mu_1' - \Delta\mu_1'' = \Delta g_M(C') - \Delta g_M(C'') + C'' \left. \frac{\partial \Delta g_M}{\partial C} \right|_{C=C''} - C' \left. \frac{\partial \Delta g_M}{\partial C} \right|_{C=C'}$$

Substitution of equations (4.12) and (4.13) into the above expression then gives

$$\Delta\mu_1' = \Delta\mu_1'' \quad (4.16a)$$

or
$$\mu_1' = \mu_1'' \quad (4.16b)$$

In a similar manner, the chemical potential of the polymer is given by

$$\Delta\mu_2 = \left(\frac{\partial \Delta G_M}{\partial n_2} \right)_{T,P,n_1} \quad (4.17)$$

and between coexisting phases it is true that

$$\Delta\mu_2' = \Delta\mu_2'' \quad (4.18)$$

A typical phase diagram, along with a plot of Δg_M and $\Delta\mu_1$ is shown in Fig. 4.4. Note that for concentrations between the coexisting phases C' and C'' , the chemical potential goes through a minimum, an inflection point and a maximum. These points are of considerable interest because they help determine the manner in which the phase separation will occur.

4.3 Mechanisms of Liquid-Liquid Phase Separation

Gibbs, in his classic treatment of heterogeneous equilibrium derived a necessary condition for the stability or metastability of a fluid phase, namely, that the chemical potential of a component must increase with increasing concentration of that component. For a two-component system, this may be written as [4-2, 9, 10]

$$\frac{\partial^2 \Delta g_M}{\partial C^2} > 0 \quad . \quad (4.19)$$

Since C is the concentration of component 2, we may write the conditions for stability using the chemical potentials as follows,

$$\frac{\partial \Delta\mu_1}{\partial(T-C)} = - \frac{\partial \Delta\mu_1}{\partial C} = C \frac{\partial^2 \Delta g_M}{\partial C^2} > 0 \quad (4.20)$$

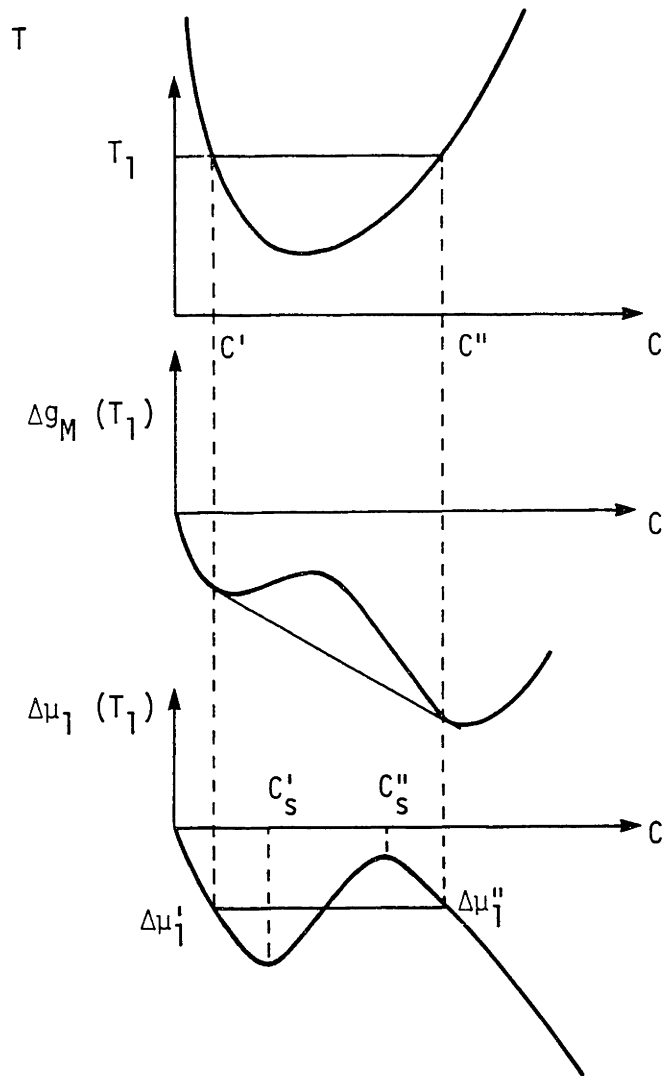


Fig. 4.4 The phase diagram, Gibbs free energy, and chemical potential for a partially miscible system.

and

$$\frac{\partial \Delta \mu_2}{\partial C} = \bar{p}(1-C) \frac{\partial^2 \Delta g_M}{\partial C^2} > 0 \quad (4.21)$$

These conditions describe the familiar situation in which a chemical species will tend to migrate from a region of high concentration to low. Fig. 4.5 shows a stable solution in equilibrium divided by an imaginary line. In real solutions the components are in a constant state of thermal motion and the concentration in any particular sub-region will tend to fluctuate about some mean value \bar{C} . If at some time a certain species 1 migrates from one region of the solution to another, as shown by A in Fig. 4.5 there will be a change in chemical potential. Since this solution is stable, it will tend to equilibrate by the migration of a molecule of this same species 1 from high concentration to low, as shown by B in Fig. 4.5. By this means, a stable solution will always maintain some mean concentration \bar{C} , with small fluctuation about that mean.

In an unstable solution where $\frac{\partial^2 \Delta g_M}{\partial C^2} < 0$ something very different happens. This is shown in Fig. 4.6. Now if a molecule of species 1 migrates from right to left as shown by A, it will lower, not raise, the chemical potential of the left side. Since chemical species always go from regions of high chemical potential to low, there is a tendency for another species 1 to migrate from right to left. This is shown as B. But this only results in lowering the chemical potential on the left hand side even more, and so more and

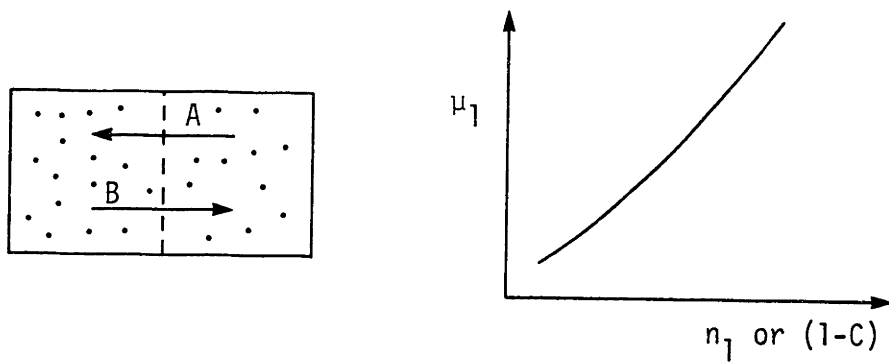


Fig. 4.5 A stable solution.

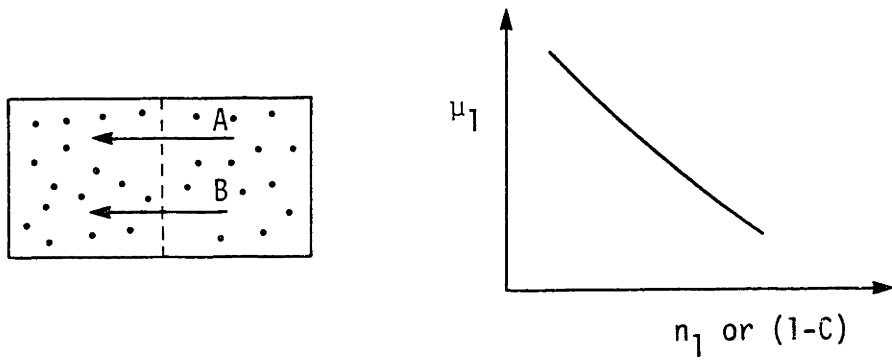


Fig. 4.6 An unstable solution.

more species 1 will migrate from right to left. Now since this is a closed system, the migration of species 1 will also affect the chemical potential of the other species 2 (not explicitly shown in Fig. 4.6). This interrelationship is shown by equations (4.20) and (4.21) i.e.

$$\frac{\partial \mu_1}{\partial n_1} < 0 \quad \text{implies} \quad \frac{\partial \mu_2}{\partial n_2} < 0 \quad .$$

So while component 1 is moving from right to left, component 2 is moving from left to right. This is the essence of unstable phase separation. Notice that the unstable region in Fig. 4.4 is in-between the minimum and maximum of $\Delta\mu_1$, marked C'_S and C''_S . Remember that $(1-C)$ is the concentration variable for species 1, so

$$\frac{\partial \mu_1}{\partial (1-C)} = - \frac{\partial \mu_1}{\partial C} ,$$

and so the slope is negative in this region. The boundary for stable liquid-liquid phase separation is then given by $\frac{\partial \mu_1}{\partial n_1} = \frac{\partial \mu_2}{\partial n_2} = 0$, or more simply,

$$\frac{\partial^2 \Delta g_M}{\partial C^2} = 0 \quad (4.22)$$

This is called the spinodal. Phase separations in the region

$$\frac{\partial^2 \Delta g_M}{\partial C^2} < 0$$

are said to take place by spinodal decomposition. For Fig. 4.4 this is the same unstable region $C_S' < C < C_S''$. In this region phase separation is by spontaneous decomposition of the original phase into two new phases. In the early stages of this mechanism, the entire composition range between the extreme compositions exists. In later stages, only the end states C' and C'' will exist. Cahn [4-10] showed that compositional fluctuations of one particular size tend to grow much faster than any other. So growth is not in extent, but in amplitude. The resulting two-phase structure can best be described by a picture. Fig. 4.7 shows computed sections through a 50:50 two phase structure [4-10]. The spacing between sections is about $1/5$ of a characteristic wavelength λ , starting at the top left, then right, and finishing at the bottom right. Notice that all of the particles are interconnected. It is obvious then, that the situation presented in Fig. 4.6 actually applies to a sub-region of characteristic dimension λ . In general then, spinodal decomposition can result in an interpenetrating network of two phased regions. Since there is no energy barrier, this process can proceed quite rapidly. This is very different from what is obtained in the other phase separation regions.

In the concentration range $C' < C < C_S'$ and $C_S'' < C < C''$, the solution is stable, but not in its lowest energy state, consequently it is called metastable. Phase separation in these regions is by nucleation and growth. By this mechanism, a new phase starts from small regions held together by surface tension, which grow in

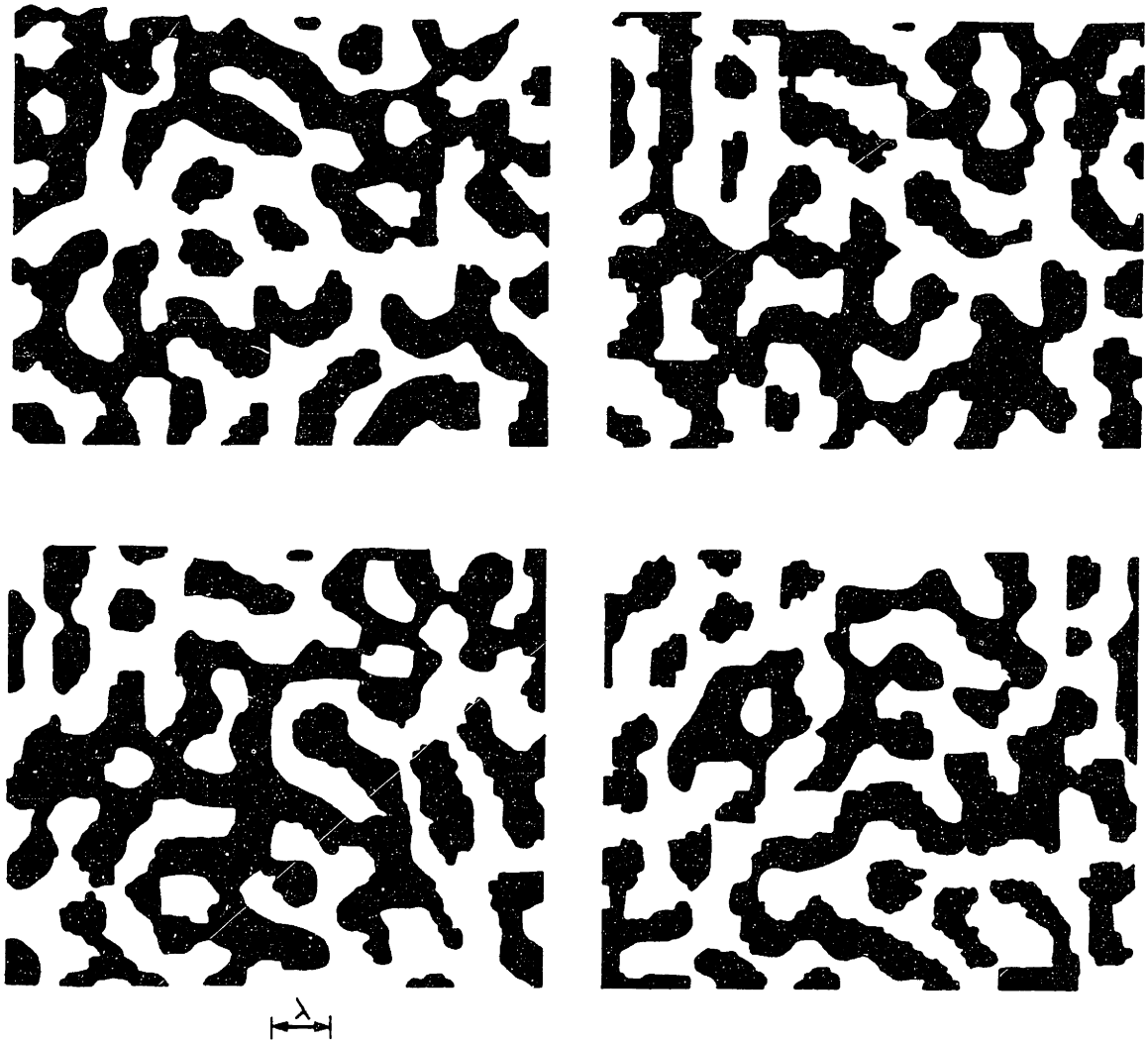


Fig. 4.7 Two phase structure (50:50) resulting from spinodal decomposition, from Cahn [4-10].

extent. At any time the structure consists of two phases, with the mother phase supplying material to the nucleated phase. Hence the mother phase changes in composition from the original solution C_0 to some end state, while the nucleated phase is at all times at the other end state. The final two phase structure would then consist of pockets, or bubbles of the nucleated phase, C' or C'' , surrounded by the other phase C'' or C' . Of considerable interest here, is the question, "Which phase nucleates?" This situation is shown in Fig. 4.8a,b and c. There are only two possibilities, 1) a polymer molecule migrates from C_0 to form C'' , or 2) a solvent molecule migrates from C_0 to form C' , any other situation would violate the conservation of mass. Now referring to Fig. 4.4 again, we can see that in the region $C_S'' < C < C''$

$$\Delta\mu_1(C) > \Delta\mu_1(C') = \Delta\mu_1(C'')$$

Hence, a solvent molecule can lower its chemical potential by migrating to form either the dilute phase C' or the concentrated phase C'' . Since only one of these is permitted, the dilute phase must be formed, as shown in Fig. 4.8c. As solvent is depleted from C_0 , the mother phase, it gradually changes to C'' . The resulting two phase structure in this case, would then be solvent rich pockets surrounded by the viscous concentrated phase (C'/C'').

In a similar manner, it can be shown that in the region $C' < C < C_S'$,

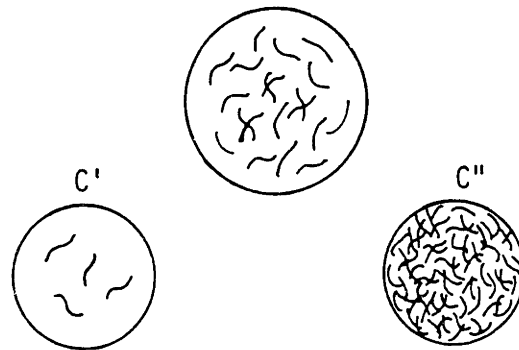


Fig. 4.8a How do the new solutions C' and C'' form from C_0 ?

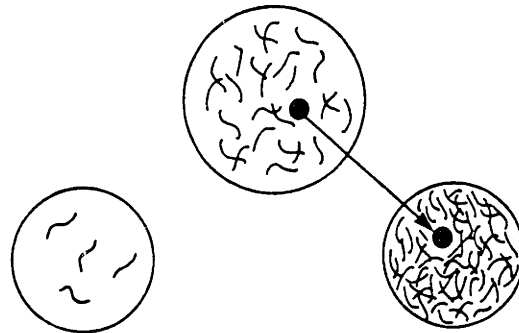


Fig. 4.8b Migration of a polymer molecule to form C'' .

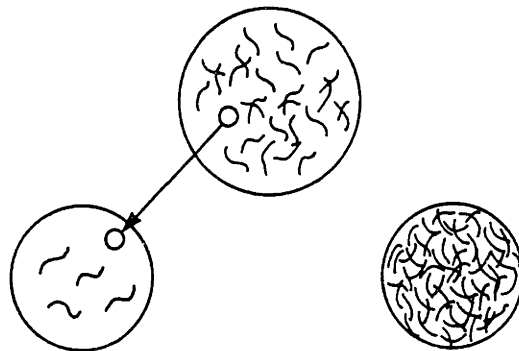


Fig. 4.8c Migration of a solvent molecule to form C' .

$$\Delta\mu_2(C) > \Delta\mu_2(C') = \Delta\mu_2(C''),$$

and the concentrated phase is nucleated by the migration of the polymer species, as shown in Fig. 4.8b. In this case, the mother phase gradually changes from C_0 to C' , and in the end we would expect polymer rich pockets surrounded by the dilute phase (C''/C').

The resulting two phase structures are then very different depending upon the particular region of the phase diagram a solution may find itself. This is particularly important, if one is concerned with the physical separation of these phases. While all of these structures; C'/C'' , C''/C' , and the spinodal structure, are unstable with respect to gravity and surface tension, the rate and form in which they rearrange themselves is vastly different. For example, one would not expect pockets of the denser concentrated phase surrounded by the dilute phase C''/C' to persist in that form for very long. In a very short time, the concentrated phase will settle due to gravity. For the reverse situation however, (C'/C'') gravity settlement (which is manifest by the dilute bubbles rising) is very slow and surface tension causes the dilute phase to coalesce. In a similar manner, the two phase structure shown for spinodal decomposition in Fig. 4.7 will also change with time and under some conditions can be made to gravity separate quite rapidly. So the phase separation mechanism has very important implications on the physical separation of the phases. This problem is discussed in detail in Chapters 6 and 7.

The locations of the different phase separation mechanisms

as well as the chemical potential of the solvent at temperature T_1 are shown in Fig. 4.9. Note that as the temperature is varied from T_1 the form of the chemical potential plot will vary. As T is decreased, for example, below T_1 the points C_S' and C_S'' will come closer together. Finally, at the point where the spinodal and binodal touch, $C_S' = C_S''$. At temperatures just below this point the solution will not separate, the chemical potential would be a smooth monotonically decreasing curve, and the Gibbs free energy of mixing would look like Fig. 4.1b. The point where the spinodal, and the binodal touch is an important point because this is the point where, going up in temperature, one would first observe phase separation. This point is called the consolute, or critical point, or the point of incipient phase separation. It occurs when the minimum, inflection point, and maximum in the chemical potential all merge into one point. Hence the conditions for incipient phase separation are

$$\left(\frac{\partial \mu_1}{\partial C}\right)_{T,P} = 0 \quad (4.23)$$

$$\left(\frac{\partial^2 \mu_1}{\partial C^2}\right)_{T,P} = 0$$

This point is of particular interest in experimental polymer solution thermodynamics and will be used in the next section of this chapter.

4.4 Flory-Huggins Theory

It is convenient to conceptualize the mixing of polymers and

metastable region (nucleation and growth of the concentrated phase)

unstable region (spinodal decomposition)

stability boundary (spinodal)

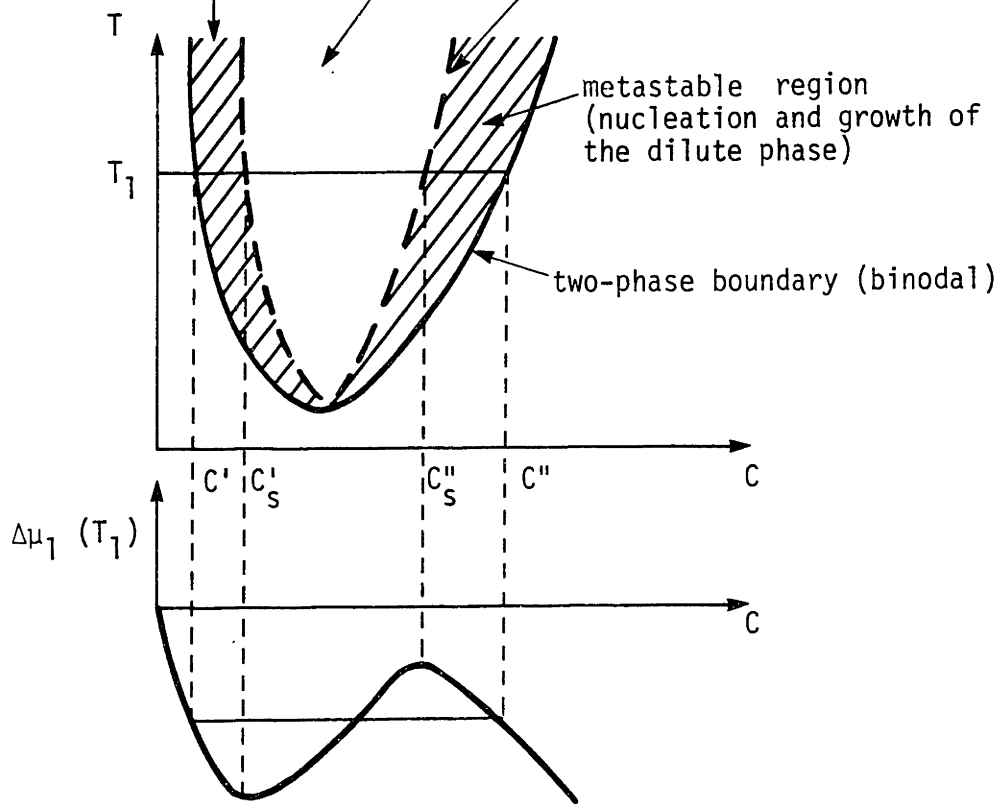


Fig. 4.9 Phase diagram for binary system, showing separation mechanisms and their relationship to the chemical potential.

solvents as taking place in a lattice of solvent sized units. Polymers are represented on this lattice as connected segments, each segment equal in size to a solvent molecule. Fig. 4.10 shows the segments of a chain polymer molecule located in a liquid lattice. Inherent to this model is the assumption that the polymer is flexible enough to conform to this lattice arrangement, also, since the lattice units are of the same size before and after mixing, there is no change in volume upon mixing, $\Delta V_M = 0$.

The mixing of polymers and solvents, then consists of arranging the polymers on the liquid lattice. By keeping track of the different possible arrangements, and using Boltzmann's equation and Stirling's approximation, Paul J. Flory [4-11], and at about the same time, Maurice L. Huggins, [4-12, 13, 14] were able to calculate the combinatorial entropy of mixing for polymer-solvent systems. For a single polymer (monodisperse molecular weight) and solvent the resulting expression is

$$\Delta S_{\text{comb}} = -k [n_1 \ln \phi_1 + n_2 \ln \phi_2] \quad (4.24)$$

where n_1 and n_2 are the numbers of solvent and polymer molecules, \ln is the natural logarithm and ϕ_1 and ϕ_2 are the volume fractions. That is

$$\begin{aligned} \phi_1 &= \frac{n_1}{n_1 + xn_2} \\ \phi_2 &= \frac{xn_2}{n_1 + xn_2} \end{aligned} \quad (4.25)$$

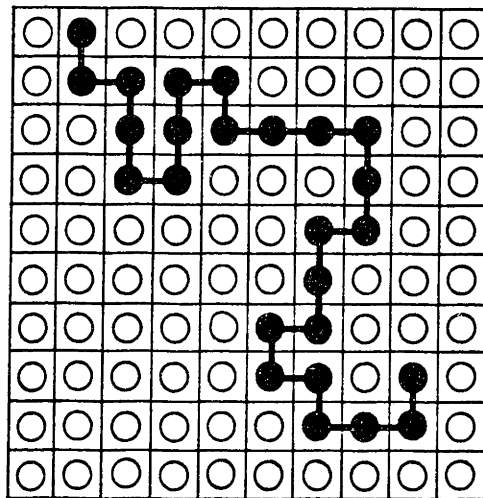


Fig. 4.10 Polymer molecule represented as connected solvent-sized segments on a liquid lattice.

and x is the number of solvent sized polymer segments, i.e. the ratio of molar volumes,

$$x = \frac{M_2/\rho_2}{M_1/\rho_1} \quad (4.26)$$

M = molecular wt., ρ = molecular density.

Equation (4.24) can be extended to the case of a broad molecular weight polymer by adding new contributions for each species or molecular weight. For convenience most of the arguments presented here will be for the monodisperse case. The more general case will be dealt with later in Chapter 5. The enthalpy and the noncombinatorial entropy terms can be handled in a similar manner once it is recognized that they both depend on interactions with nearest neighbors. ΔH_M can be written as [4-8]

$$\Delta H_M = \Delta w_{12} p_{12} \quad (4.27)$$

where w = bond energy between nearest neighbors, p_{12} = the number of unlike pairs, and

$$\Delta w_{12} = w_{12} - \frac{1}{2} (w_{11} + w_{22}). \quad (4.28)$$

This is the energy to break pairs of polymer-polymer bonds and solvent-solvent bonds subtracted from the energy to form polymer-solvent bonds, put into stoichiometric form.

In a similar fashion the noncombinational entropy depends on its specific interaction with its neighbors and can be written as [4-8]

$$\Delta S_{nc} = \Delta s_{12} p_{12} \quad (4.29)$$

where Δs_{12} can be expressed in a form similar to equation (4.28). To determine p_{12} , let z be the number of first neighbors; z is called the lattice coordination number. For a cubic lattice as shown in Fig. 4.10, $z = 6$, however other lattices are possible and in general it is expected that $6 \leq z \leq 12$ [4-8, p. 499]. If x is the number of solvent sized segments in a polymer, then the number of contacts per polymer molecule can be approximated as zx , where

$$zx \cong (z-2)x + 2 \quad .$$

Since there are n_2 polymer molecules, then there is a total of $zx n_2$ first neighbors with the polymer. Some of these will be solvent molecules, and some will be polymer segments. For reasonably concentrated solutions, and in the absence of strong preferential attractions the probability that any particular site is a solvent molecule can be estimated by ϕ_1 , the volume fraction of solvent. Then

$$p_{12} = zx n_2 \phi_1 = z \phi_2 n_1 \quad (4.30)$$

Equations (4.27), (4.29) and (4.30) can now be combined into a single contribution to the Gibbs free energy of mixing. This is conventionally written as

$$\Delta H_M - T\Delta S_{nc} = kTgn_1\phi_2 \quad (4.31)$$

where

$$g = z\Delta g_{12}/kT \quad (4.32)$$

and $\Delta g_{12} = \Delta w_{12} - T\Delta s_{12}$. g is called the interaction parameter (written as χ_1 by Flory) and it represents the interaction free energy per solvent molecule divided by kT . The final expression of the Flory-Huggins theory, for the Gibbs free energy of mixing can be obtained by combining equations (4.24) and (4.31). This gives

$$\Delta G_M = kT[n_1 \ln\phi_1 + n_2 \ln\phi_2 + gn_1\phi_2] \quad (4.33)$$

Alternatively, this can be written as the Gibbs free energy per mole of lattice sites $\Delta \bar{G}_M$, where there are $N = n_1 + xn_2$ lattice sites, and N/N_{AVO} moles, (N_{AVO} = Avogadro's number) then

$$\Delta \bar{G}_M = RT[\phi_1 \ln\phi_1 + \phi_2 x^{-1} \ln\phi_2 + g\phi_1\phi_2] \quad (4.34)$$

These expressions are of considerable use because they show the

concentration dependence explicitly. This allows us then to derive a number of important relationships including the chemical potential, the osmotic and vapor pressures, the conditions for incipient phase separations, and the spinodal. Consequently, the unknown g can be determined in a number of ways.

Equation (4.34) is particularly insightful for evaluating the effect of polymer chain length on the entropy of mixing. For mixtures of similar sized small molecules $x = 1$, however for long chain molecules x can be large, perhaps 10^3 . In effect then, the connectivity of the polymer molecule greatly reduces the number of possible mixed states, as compared to small molecules, and consequently greatly reduces the entropy of mixing. Since dissolution of polymers is usually an entropy driven process, this explains why it characteristically takes so long

Differentiation of (4.33) with respect to n_1 , and multiplication by Avogadro's number N_{AVO} yields the chemical potential per mole of the solvent,

$$\mu_1 - \mu_1^\circ = RT[\ln(1-\phi_2) + (1-\frac{1}{x})\phi_2 + g\phi_2^2] \quad (4.35)$$

where μ_1° = the chemical potential of the pure solvent. This same relationship can be derived from equation (4.34) by using

$$\mu_1 - \mu_1^\circ = \Delta\bar{G}_M + \phi_2 \frac{\partial \Delta\bar{G}_M}{\partial \phi_1} \quad (4.36)$$

In a similar manner the chemical potential of the polymer may be obtained from (4.33) or (4.34) as

$$\mu_2 - \mu_2^\circ = RT[\ln\phi_2 - (x-1)(1-\phi_2) + g_x(1-\phi_2)^2] \quad (4.37)$$

Equation (4.36) can be used to derive the vapor pressure of the solvent, and the osmotic pressure. To the extent that the vapor may be regarded as an ideal gas, the vapor pressure of the solvent p_1 , compared to its pure state p_1° , is given by [4-8],

$$\ln \frac{p_1}{p_1^\circ} = \frac{\mu_1 - \mu_1^\circ}{RT} = \ln(1-\phi_2) + \left(1 - \frac{1}{x}\right)\phi_2 + g\phi_2^2 \quad (4.38)$$

and similarly, in as much as the solvent is incompressible, the osmotic pressure π is

$$\pi = - \frac{(\mu_1 - \mu_1^\circ)}{V_1} = - \frac{RT}{V_1} [\ln(1-\phi_2) + \left(1 - \frac{1}{x}\right)\phi_2 + g\phi_2^2] \quad (4.39)$$

where V_1 is the molar volume of the solvent.

Using the osmotic pressure measurement mentioned in Chapter 3, $\pi = .07$ atm at $T = 20^\circ\text{C}$, for a 12.3% wt. solution of PBD in hexane, we can now determine the interaction parameter g , and $\Delta\bar{G}_M$ which would be the minimum thermodynamic energy necessary for separation. The various constants are, $\rho_1 = .66$ and $\rho_2 = .92$, so $\phi_1 = .909$ and $\phi_2 = .091$, $V_1 = 86/.66 = 130.3$ and $x = \frac{10^5/.92}{86/.66} = 834$. Now employing equation (4.39) yields $g = .502$. Substitution into

equation (4.34) gives $\Delta\bar{G}_M = -113 \text{ J/mole}$, or

$$\Delta\bar{G}_M(20^\circ\text{C}) = -4.3 \text{ BTU/lb-rubber}$$

At the reactor temperature of 120°C , g will be estimated in Chapter 7 to be .525, this yields

$$\Delta\bar{G}_M(120^\circ\text{C}) = -5.5 \text{ BTU/lb-rubber}$$

So the minimum energy necessary to separate hexane and polybutadiene is about 5 BTU/lb-rubber. This is three orders of magnitude less than present commercial separation processes.

The real purpose of deriving the Flory-Huggins expression for the Gibbs free energy of mixing is to gain insight into the phase separation process. To do this we will apply the conditions for incipient phase separation, equations (4.23), to equation (4.35), these yield the critical volume fraction ϕ_{2c} , and the critical value of the interaction parameter g_c .

$$\phi_{2c} = \frac{1}{1 + x^{1/2}} \quad (4.40)$$

$$g_c \cong \frac{1}{2} + \frac{1}{x^{1/2}} \quad (4.41)$$

Equation (4.40) tells us that the critical composition will occur at a very low volume fraction, for $x = 834$, $\phi_{2c} = .03$. Furthermore, we can now see that the asymmetric nature of polymer solvent phase diagrams is directly related to the dissimilarity in molecular sizes. For mixtures of similar sized small molecules $x = 1$ and $\phi_{2c} = \frac{1}{2}$ and we might expect a symmetrical phase diagram.

Equation (4.41) tells us that there is a critical value of the interaction parameter g that will cause phase separation. Smaller values of g , $g < g_c$, represent weaker interactions which can be overcome by the combinatorial entropy term, so separation does not occur. Only when $g \geq g_c$ will separation occur. To explain phase separation behavior then, it becomes very important to determine the temperature dependence of g . Recall that

$$g = \frac{z}{kT} [\Delta w_{12} - T\Delta s_{12}] \quad . \quad (4.42)$$

As a first approximation Flory assumed that Δw_{12} and Δs_{12} were roughly independent of temperature, and so g could be approximated by [4-8]

$$g = \frac{A}{T} + B \quad . \quad (4.43)$$

where A , and B were molecular constants independent of temperature and concentration, and $A > 0$ for dispersion forces. This simple function has gained fairly wide acceptance because it agrees well with the solubility parameter approach which gives [4-15]

$$g = \frac{V_1}{RT}(\delta_1 - \delta_2)^2 + \beta \quad (4.44)$$

(see equation 4.5, V_1 is the molar volume of the solvent).

The success of this approach is that it correctly predicts the low temperature phase separation phenomenon. That is, as the temperature is lowered, g becomes increasingly large until at some critical temperature T_c

$$\frac{A}{T_c} + B = g_c \quad (4.45)$$

the critical interaction parameter is obtained, and incipient phase separation occurs. Furthermore, since g_c is a function of molecular weight (equation 4.41), the Flory-Huggins Theory correctly predicts that high molecular wt. species, which have a lower critical value g_c , will come out of solution before lower molecular wt. polymers. This is shown in Fig. 4.11. These curves are labeled as the cloud point curves, because upon phase separation the solution becomes cloudy. For simple binary solutions of a polymer of one molecular weight in a solvent, the cloud point curve and the binodal are the same, and in effect are synonymous with the phase diagram. For broad molecular wt. polymers the situation is not so simple. This case is discussed in Chapter 5. Note also in Fig. 4.11 that the critical concentration shifts away from the T axis with decreasing molecular wt. as predicted by equation (4.40).

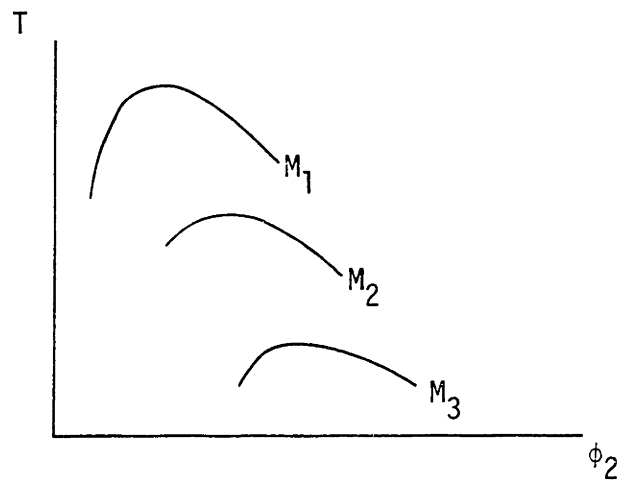


Fig. 4.11 Cloud point curves for solutions of the same polymer, but different molecular weights $M_1 > M_2 > M_3$.

The great drawback of the approximation (4.43) is that it fails to predict the high temperature phase transitions. To do this, the more recent free volume theories are needed [4-3, 5, 15]. Before getting into these rather complicated theories, however, a fairly simple approach can be used to make a slightly more sophisticated approximation of the temperature dependence of g [4-16].

The temperature dependencies of enthalpy and entropy of mixing can be related to the heat capacity ΔC_p by

$$\frac{\partial \Delta H}{\partial T} = \Delta C_p \quad (4.46)$$

and

$$\frac{\partial \Delta S}{\partial T} = \frac{\Delta C_p}{T} \quad (4.47)$$

Since for many liquids the temperature function of C_p is approximately linear, it is reasonable to assume that

$$\Delta C_p = (C_{p,0} + C_{p,1} T) \quad (4.48)$$

Since the combinatorial entropy is not strictly a temperature function, and assuming a concentration dependence for ΔC_p similar to ΔH_M and ΔS_{nc} (equation 4.34) we can integrate equations (4.46), (4.47) with (4.48) and substitute into (4.42). This yields the following approximation [4-16]

$$g = g_1 + \frac{g_2}{T} + g_3 T + g_4 \ln T \quad (4.49)$$

The fourth term in equation (4.49) is not very sensitive to variations in T and for this discussion can be ignored. This yields a temperature dependence more in keeping with physical observations of polymer solutions and one which conforms, within certain approximations, to the results of the free volume theories [4-17, 18]

$$g = g_1 + \frac{g_2}{T} + g_3 T \quad (4.50)$$

Now for $g_3 > 0$ it is apparent that at sufficiently high temperatures g will increase monotonically and it will be possible to exceed g_c and cause phase separation.

In general g behaves as the curve shown in Fig. 4.12 [4-3]. It is therefore possible to exceed g_c on heating or cooling. In both cases higher molecular weight polymers will have lower critical interaction parameters. In the limit for infinite molecular wt. $g_c = \frac{1}{2}$.

Additional topics which can be developed from the Flory-Huggins Theory will be discussed in other chapters. The effect of a broad molecular wt. distribution, and the determination of the spinodal will be discussed in Chapter 5 and Chapter 7 respectively.

4.5 Limitations of the Flory-Huggins Theory

The Flory-Huggins theory represents a significant improvement over previous mixing theories for polymer-solvent solutions. In

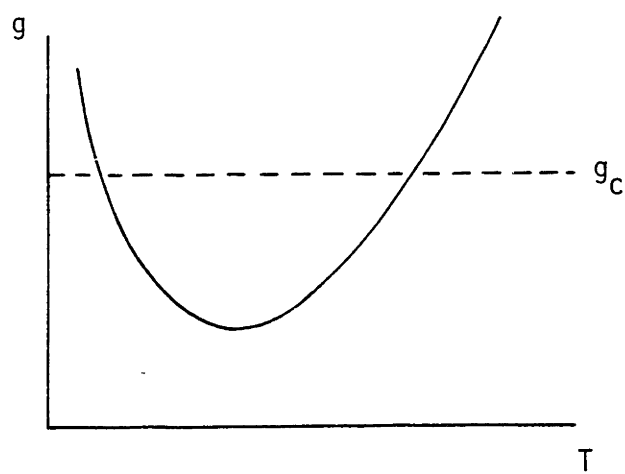


Fig. 4.12 Variation of the interaction parameter g as a function of temperature T .

particular, the combinatorial entropy term has had good success in explaining qualitative results, as well as providing insight into the polymer dissolution process [4-19, 20]. The interaction parameter however, has been less successful. Flory himself [4-8] showed that in some cases g will depend on concentration. This, of course, is contrary to its development. Further studies verified Flory's original suspicion, that the concentration dependence is most noticeable for polar systems [4-20, 21]. These same studies go on to say, and fortunately for us, that for nonpolar systems, g is virtually independent of concentration. In as much as hexane and polybutadiene are markedly nonpolar it is quite justifiable then for us to assume that the interaction parameter for our system is concentration independent.

The greatest weakness of the Flory-Huggins theory however, has been its inability to predict the high temperature phase transition. This is the problem we have already addressed by patching up the temperature dependence of the interaction term. The problem, however, runs deeper than this because the origin of the high temperature phase separation can be directly related to the free volume difference between the polymer and the solvent and the subsequent change in volume upon mixing. That is $\Delta V_M \neq 0$. This directly violates one of Flory's original implicit assumptions. Fortunately though, the volume change is sufficiently small so as not to significantly change the combinatorial entropy term as developed by Flory and Huggins. Consequently, while the development

is formidable, the end results of the newer free volume theories are similar to our previous equation for the temperature dependence of g , i.e. equation (4.50). And in essence, we may apply the results of the Flory-Huggins theory to our system with little apology. We must, however, keep in mind that the nature of the interaction term is decidedly complex, and contains many subtleties not expressed in equation (4.5). See Appendix B for a brief discussion of the free volume theories.

References, Chapter 4

- 4-1 F. Daniels and R.A. Alberty, Physical Chemistry, John Wiley and Sons, Inc. 4th ed. (1975).
- 4-2 I. Prigogine, with A. Bellemans and V. Mathot, The Molecular Theory of Solutions, North-Holland Pub. Co., Amsterdam (1957).
- 4-3 F.W. Billmeyer, Jr., Textbook of Polymer Science, Wiley-Interscience 2nd ed. (1971).
- 4-4 F. Rodriguez, Principles of Polymer Systems, McGraw-Hill (1970).
- 4-5 D. Patterson, "Review: Free Volume and Polymer Solubility, A qualitative View", Macromolecules 2, 6, p. 672 (1969).
- 4-6 J.I. Clark and G.B. Benedek, "Phase Diagram for Cell Cytoplasm from the Calf Lens," Biochemical and Biophysical Research Communications, 95, 1, p. 482 (1980).
- 4-7 T. Tanaka, "Gells", Scientific American (Jan, 1981).
- 4-8 P.J. Flory, Principles of Polymer Chemistry, Cornell U. Press (1953).
- 4-9 J.W. Gibbs, Collected Works 1, p. 105 Yale University Press (1948).
- 4-10 J.W. Cahn, "Phase Separation by Spinodal Decomposition in Isotropic Systems," J. of Chemical Physics 42, 1, p. 93 (1965).
- 4-11 P.J. Flory "Thermodynamics of High Polymer Solutions," J. of Chemical Physics 10, p. 51 (1942).
- 4-12 M.L. Huggins, "Thermodynamic Properties of Solutions of Long-Chain Compounds," Annals, New York Academy of Science 43, p. 1 (1942).
- 4-13 M.L. Huggins, "Some Properties of Solutions of Long-Chain Compounds," J. of Physical Chemistry 46, p. 151 (1942).
- 4-14 M.L. Huggins, "Theory of Solutions of High Polymers," J. American Chemical Society 64, p. 1712 (1942).
- 4-15 D. Patterson, "Role of Free Volume Changes in Polymer Solution Thermodynamics," p. 449 International Symposium on Macromolecular Chemistry, Prague, 1965.
- 4-16 R. Koningsveld, "Partial Miscibility of Multicomponent Polymer Solutions," Advances in Colloid and Interface Science 2, p. 151 (1968).

- 4-17 G. Delmas, D. Patterson, and T. Somcynsky, "Thermodynamics of Polyisobutylene-n-Alkane Systems," J. of Polymer Science 57, p. 79 (1962).
- 4-18 D. Patterson, G. Delmas, and T. Somcynsky, " A Comparison of Lower Critical Solution Temperatures of Some Polymer Solutions," Polymer 8, p. 503 (1967).
- 4-19 H. Morawetz, Macromolecules in Solution, Wiley-Interscience 2nd ed. (1975).
- 4-20 A. Tager, Physical Chemistry of Polymers, Mir Publishers, Moscow 2nd ed. (1978)
- 4-21 P.T. van Emmerik and C.A. Smolders, "Phase Separation of Polymer Solutions," European Polymer Journal, 9 p. 157 (1973).

CHAPTER 5

EQUILIBRIUM THERMODYNAMIC DATA FOR HEXANE AND POLYBUTADIENE

The feasibility of the proposed Low Energy Separation Scenario depends upon the details of the phase diagram for the hexane and polybutadiene solution we are considering. Of considerable interest is the question, to what extent can the solution be concentrated when heated above the high temperature phase transition. Furthermore it is important to point out how material variations might affect the phase diagram, so that proper monitoring and control procedures can be employed. These problems will be addressed in this chapter. Also considered here is the effect of pressure on the phase diagram. Varying pressure provides a convenient and rapid way to enter certain regions of the phase diagram. This idea will be exploited later in our discussion of spinodal decomposition and gravity settlement given in Chapters 6 and 7.

5.1 Quasi-binary Solutions

All previous discussions of the phase diagram for polymer-solvent solutions have been for strictly binary systems. Solutions that contain mixed solvents or broad molecular weight polymers are not strictly binary. Our system of hexane and polybutadiene contains both a mixed solvent, and a broad molecular weight polymer. The solvent is actually a mixture of isomers of hexane (predominantly n-hexane), and the polymer spans at least two orders of magnitude in molecular weight (from 10^4 to 10^6) with a number average value of

about 10^5 . The actual solvent mix, and the various molecular weight parameters were given in Chapter 2.

Theoretically, the solvent mix can be handled in a fairly straightforward way. Provided the solvents are similar in size and structure, as they are for our case, they can be considered as a single solvent possessing certain average characteristics. This is because their contribution to the Gibbs free energy of mixing enters primarily through the interaction parameter g . Consequently as we shall see, the details of the solvent mix can raise or lower the phase diagram, but for small variations in composition they will not significantly change the shape or nature of the diagram.

The situation for a broad molecular weight polymer is quite different from that of a mixed solvent. This is because each molecular weight constitutes a new polymer species. Because these species are all similar chemically, it is not expected that the interaction parameter will change significantly, but their differences in chain length will make new contributions to the combinatorial entropy of mixing term. To introduce this concept, it is convenient to use a slightly different notation from that given in Chapter 4. Let ϕ_0 be the volume fraction of solvent, and ϕ_i will be the volume fraction of polymer species i . The total volume fraction of polymer is then $\phi = \sum \phi_i$, summed over all polymer species. Also x_i now replaces x as the number of solvent sized polymer segments in species i . With this notation, a more general expression for the Gibbs free energy of mixing can be written for, what

Koningsveld calls a quasi-binary mixture of a solvent, and a polydisperse homopolymer [5-1,2]. This is

$$\Delta\bar{G}_M = RT[\phi_0 \ln\phi_0 + \sum \phi_i x_i^{-1} \ln\phi_i + g\phi_0\phi]. \quad (5.1)$$

The polydispersity enters in the second term, as a series of new entropy contributions. If g is strictly independent of concentration and molecular weight it will not be changed. This new contribution will change the location (somewhat) and, more importantly, the nature and shape of the phase diagram as we shall see.

5.2 Cloud Point Curves

Polymer-solvent solutions become cloudy upon phase separation due to light scattering from the interfaces of the two phases. This phenomenon is so marked that it can be easily observed with the unaided eye. When these "cloud points" are obtained for various concentrations and plotted versus temperature, the result is called a cloud point curve (c.p.c.)*

*It is not a straight forward procedure to relate the Gibbs free energy of mixing to the cloud point curves [5-1]. In general, the molecular weight distribution must be known in detail, and of course, the temperature and concentration dependences of the interaction parameter g must be known. With these dependencies measured, an iterative procedure can then be used to establish the cloud point curve. This has been done by others with mixed success [5-2,3]. A more practical approach here is to rely on measured data. The results in this chapter then, are based primarily on experimental data supplemented by occasional heuristic arguments. In later chapters, it will be useful to work backwards, and use certain data in this chapter to determine the parameters in the Gibbs free energy of mixing term.

Cloud point curves for two different monodisperse samples of polybutadiene are shown in Fig. 5.1. These were obtained by heating a solution in an apparatus as shown in Fig. 5.2 in a silicone oil bath and slowly raising the temperature (less than 1°C/min). The temperature was determined by a thermocouple in the solution to an accuracy of $\pm 1^\circ\text{C}$. These solutions were made up of a medium cis polybutadiene (45% cis, 55% trans.) in high performance liquid chromatography (HPLC) grade n-hexane (96.2% n-hexane). The polybutadiene samples were obtained from Goodyear, and the molecular weights given in the figure are their advertised values. These curves give the typical shapes, and molecular weight dependencies as discussed in Chapter 4.

Similar cloud point curves for a wide variety of polymers and solvents can be found in the literature. Two papers in particular give c.p.c.'s for monodisperse samples of polybutadiene in hexane [5-3,4]. These can not be compared directly with the data shown in Fig. 5.1 because they are for different molecular weights, and for different conformations (100% cis).

In general then, most investigators deal only with narrow molecular weight samples. If these solutions are heated above the cloud point and separated, the resulting coexisting phases will also fall on the cloud point curve. This was shown in Fig. 3.8 of Chapter 3 and in Fig. 4.2b of Chapter 4. In these cases the cloud point curve, and the coexistence curve are the same. As it turns out, this behavior is markedly different for broad molecular weight polymers.

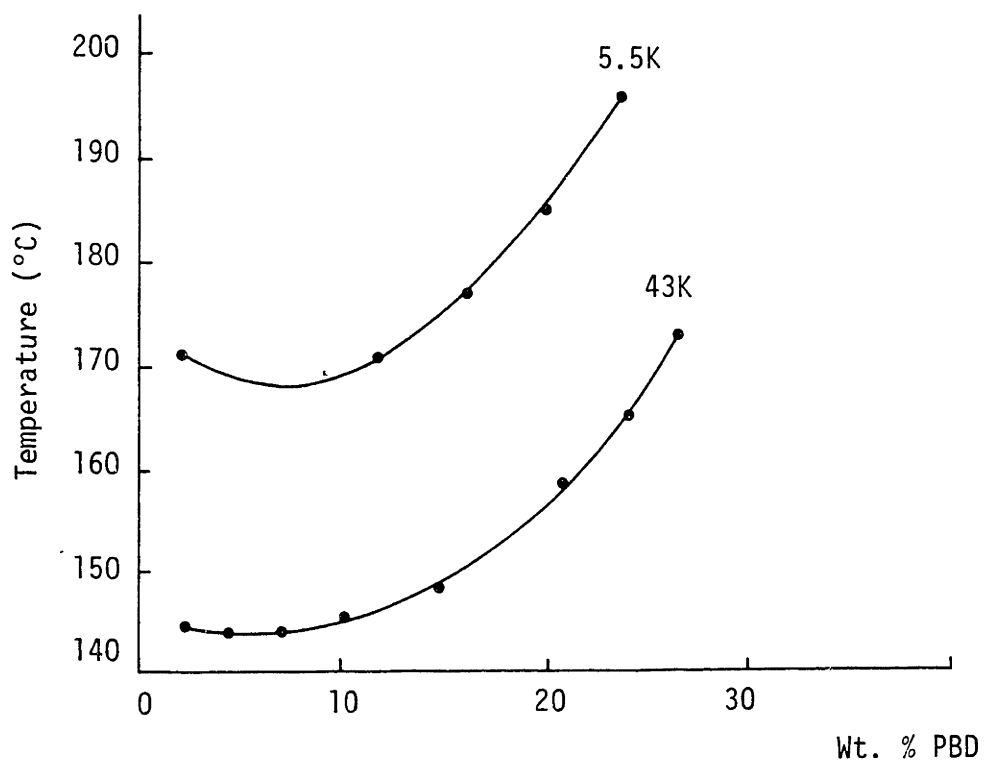


Fig. 5.1 Cloud point curves for monodisperse samples of polybutadiene in n-hexane. Molecular weights are 5,500 and 43,000.

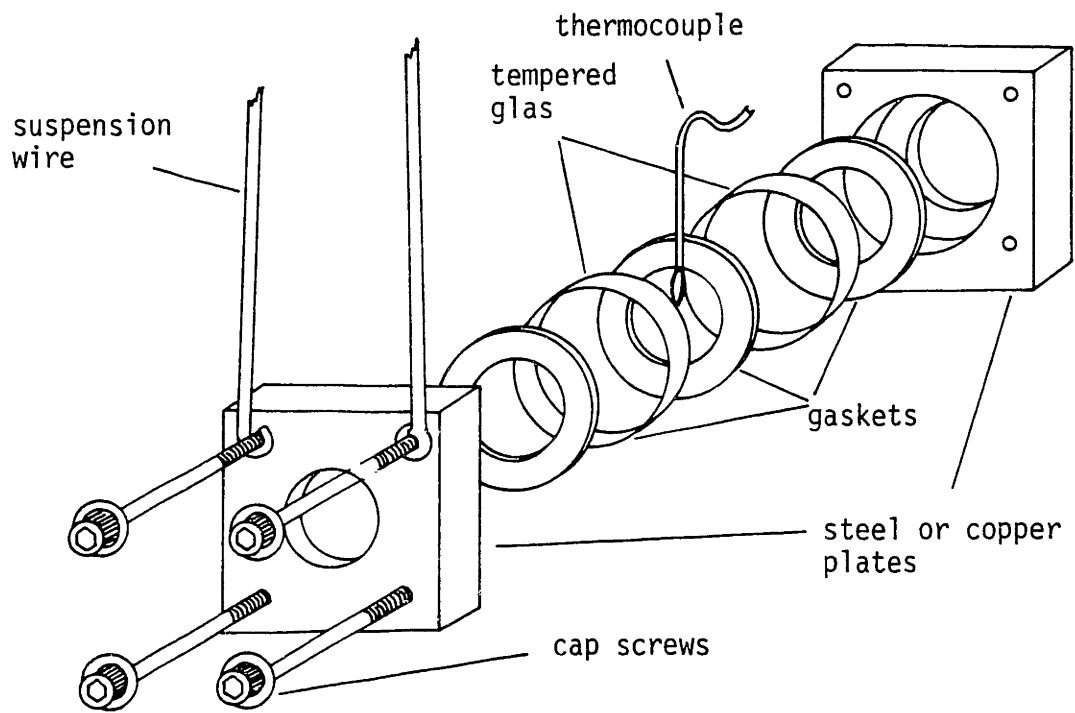


Fig. 5.2 Exploded view of apparatus used for cloud point determination.

5.3 Polymers with Broad Molecular Weight Distributions

Broad molecular weight polymers have different cloud point curves than narrow molecular weight polymers. The cloud point curve for our high cis broad molecular weight polybutadiene sample in the mixed hexane solvent is shown in Fig. 5.3 [5-5]. This curve was also obtained by heating the sample in the special glass and steel bomb shown in Fig. 5.2. The immediately obvious difference between the curves in Figs. 5.1 and 5.3 is their shape. In general, broad molecular weight polymers give straight line cloud point curves.

Perhaps the simplest way to show this effect, is to simulate a broad molecular weight sample by mixing 50:50 weight proportions of the two polymers shown in Fig. 5.1, and determining the resulting cloud point curve.* The resulting mixed polymer has a number average molecular weight of 9.7×10^3 , and its c.p.c. is shown in Fig. 5.4, along with the two pure components. Remarkably, while the new c.p.c. is in the approximate location one might expect based on the number average molecular weight, its shape is very different from the other two curves. In general, this straight line behavior is exactly what one gets for a broad molecular weight sample.

This result can be explained as follows. The curves in Fig. 5.4 are actually sections through a three-dimensional phase diagram

*This procedure was suggested and carried out by Charles Cangialose, whose inquisitiveness added tremendously to this project.

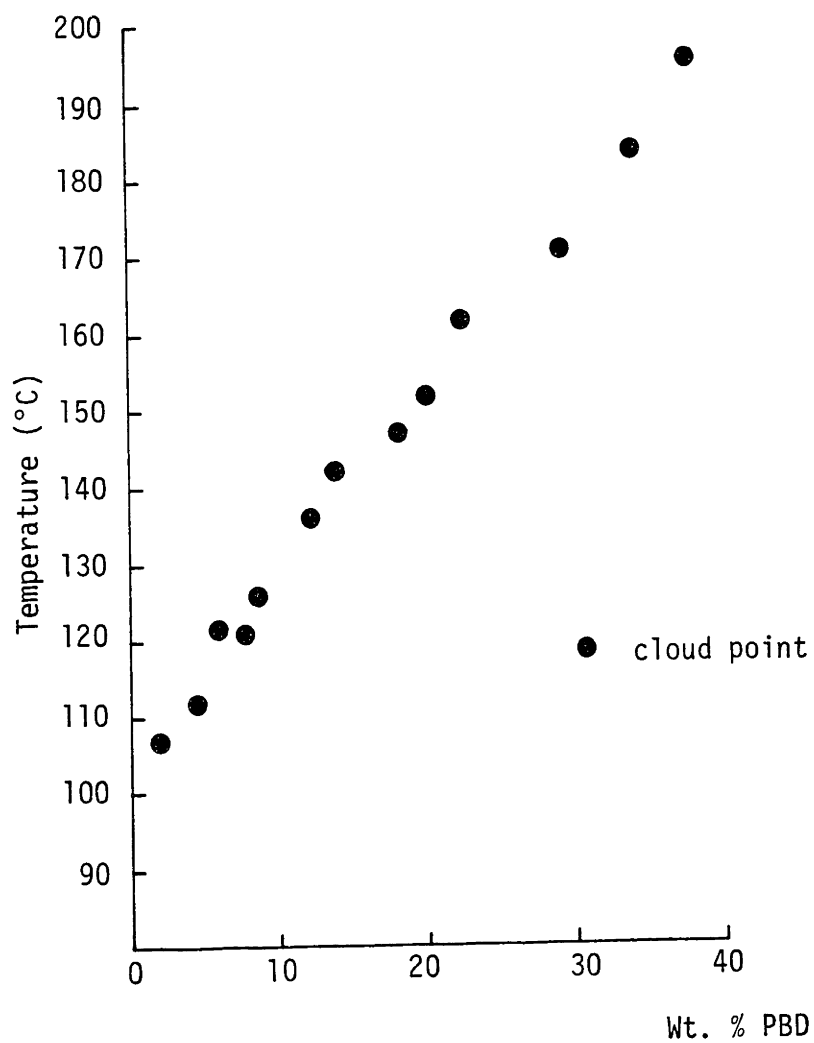


Fig. 5.3 Cloud points for broad molecular weight cis PBD in commercial grade hexane.

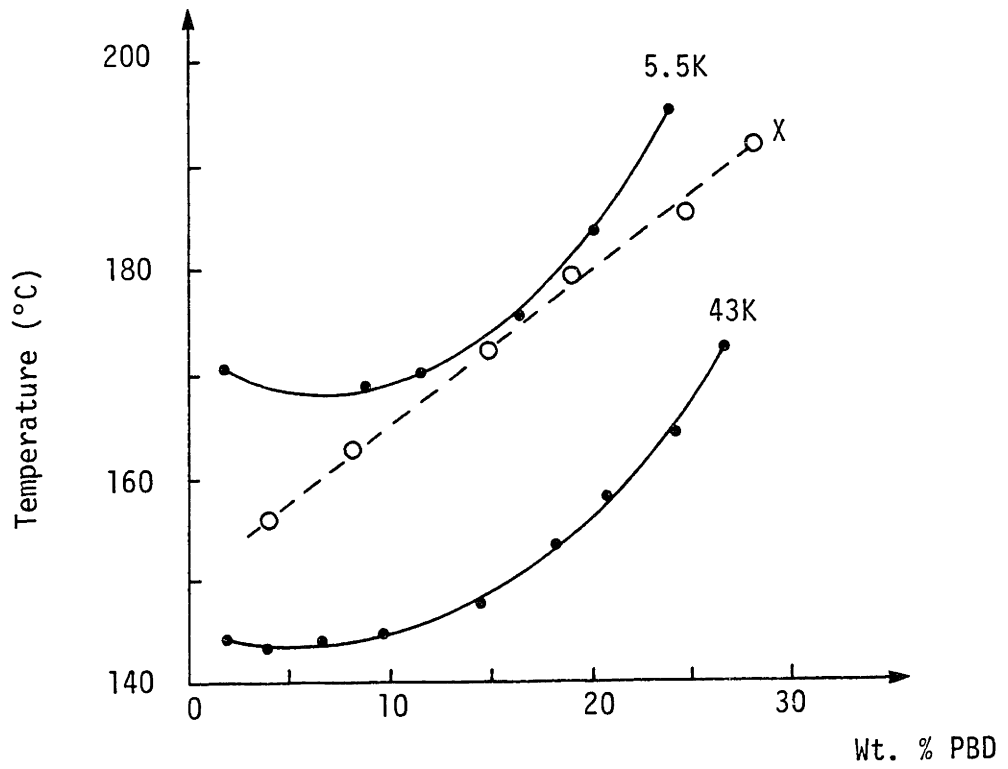


Fig. 5.4 Comparison of cloud point curves, X is 50:50 mixture of 5.5K and 43K.

made up of polymers P_1 and P_2 , and solvent 0. A constant temperature section through this diagram would be plotted on a chart as shown in Fig. 5.5. X is the mixture of P_1 and P_2 . When these charts are assembled, the resulting 3-d phase diagram would look as shown in Fig. 5.6. Here X has been displaced slightly towards P_1 for convenience of representation. The curves in Fig. 5.4 then, correspond to the sections $T-0-P_1$, $T-0-X$, and $T-0-P_2$. Conceptually then, one can see how straight line curves such as those shown in Figs. 5.3 and 5.4 can be obtained for mixed polymers. In fact, many of the essential features of the broad molecular weight diagrams can be explained using a simple two polymer system.

If we represent our broad molecular weight sample by a system of polymers P_1 and P_2 , where P_1 is of greater molecular weight, then the T_1 constant temperature plane-through Fig. 5.6 would be as shown in Fig. 5.7. The two-phase region is on the left because polymer P_1 will tend to come out of solution first, and T_1 is below the incipient phase separation temperature for P_2 . If we consider a mixture of P_1 and P_2 , X , at initial concentration X_2 it will phase separate at $T = T_1$ into two solutions, one dilute C_2' and one concentrated C_2'' . The lines joining these points are the familiar tie lines. Their specific arrangement in Fig. 5.7 can be justified using certain known results from fractionation studies [5-1]. The dilute phase, above X_2 , is known to have a higher portion of low molecular weight polymer than the original solution therefore it should be on the P_2 side of X . Conversely, C_2'' will have a higher

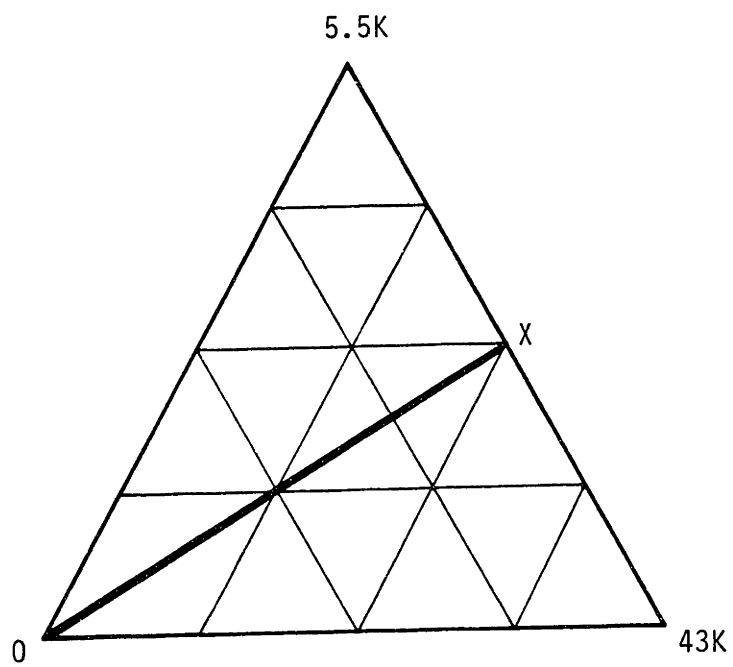


Fig. 5.5 Constant temperature plane for three dimensional phase diagram. 0 = solvent.

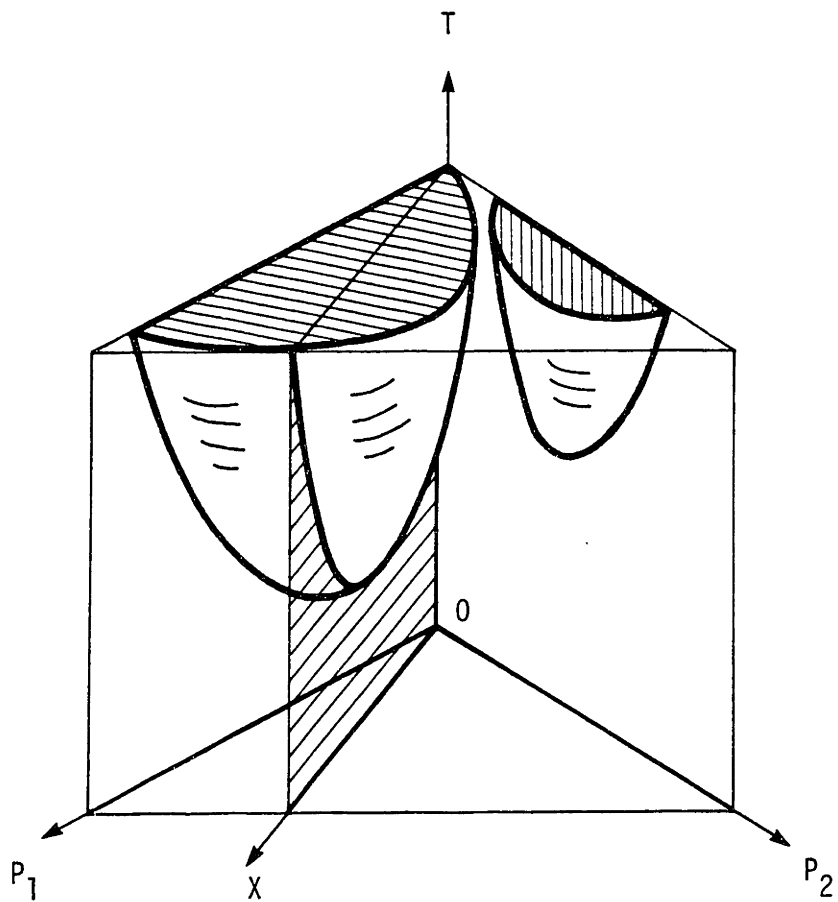


Fig. 5.6 Three dimensional phase diagram for two polymer-solvent system. $M_{P_1} > M_{P_2}$, X is some combination of P_1 and P_2 .

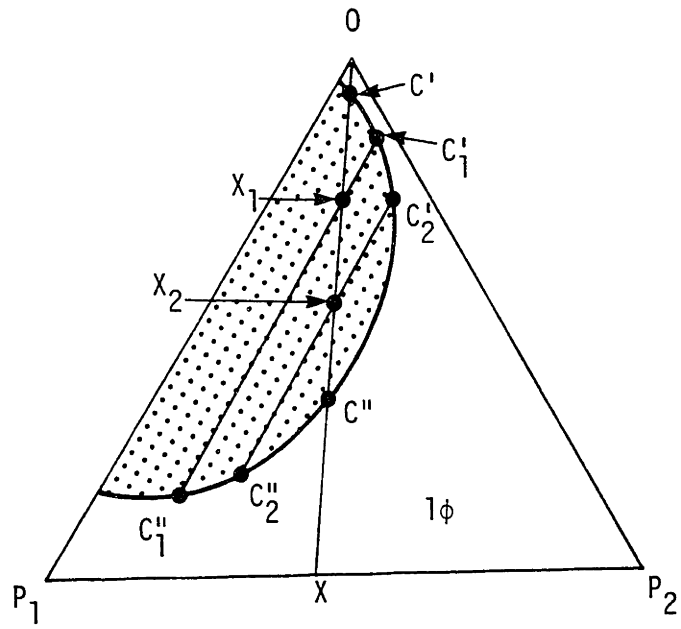


Fig. 5.7 Constant temperature plane ($T = T_1$) through three dimensional phase diagram.

portion of high molecular weight polymer P_1 , therefore it should lie below and to the right of X_2 . Now, if a different solution of the same polymer X , at concentration X_1 is heated to T_1 it will form C'_1 and C''_1 . The arrangement of these points can also be justified based on the results of fractionation studies. If solutions of X at concentrations C' or C'' were heated to T_1 , they would just become cloudy. That is, T_1 is their cloud point temperature.

Now, all of these results can be projected on the T - O - X plane as shown in Fig. 5.8. This shows that the coexistence curves do not correspond to the cloud point curve, and that the location of the coexistence curve depends upon concentration. This is a well known result that has been discussed by Koningsveld in detail [5-1]. For our broad molecular weight system, the coexistence curves of 7.9% wt. and 12.3% wt. PBD in mixed hexane are shown in Fig. 5.9. These were obtained by heating and centrifuging. The details of this process are given in Appendix C.

For the purposes of determining the feasibility of our proposed low energy separation scenario the coexistence curves are essential. These curves now tell us what extent of concentrating we can expect for a given temperature and original concentration. Also of interest, is the amount of dilute and concentrated phases the separation yields. The weight ratios can be obtained directly from tie lines in Fig. 5.9. The volume ratios can be obtained by adjusting the weight ratios as follows,

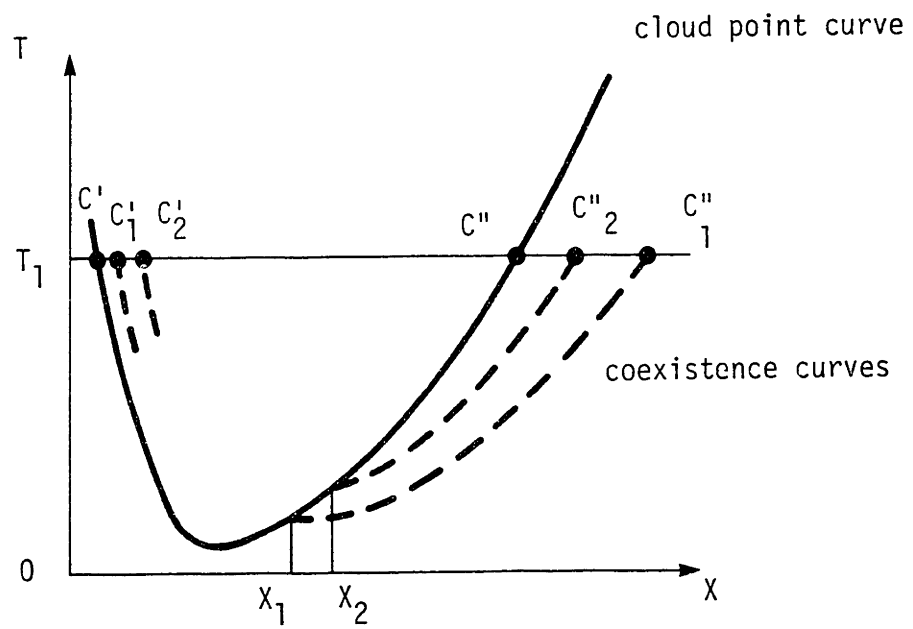


Fig. 5.8 Projections of cloud point curve and coexistence curves on T - 0 - X plane.

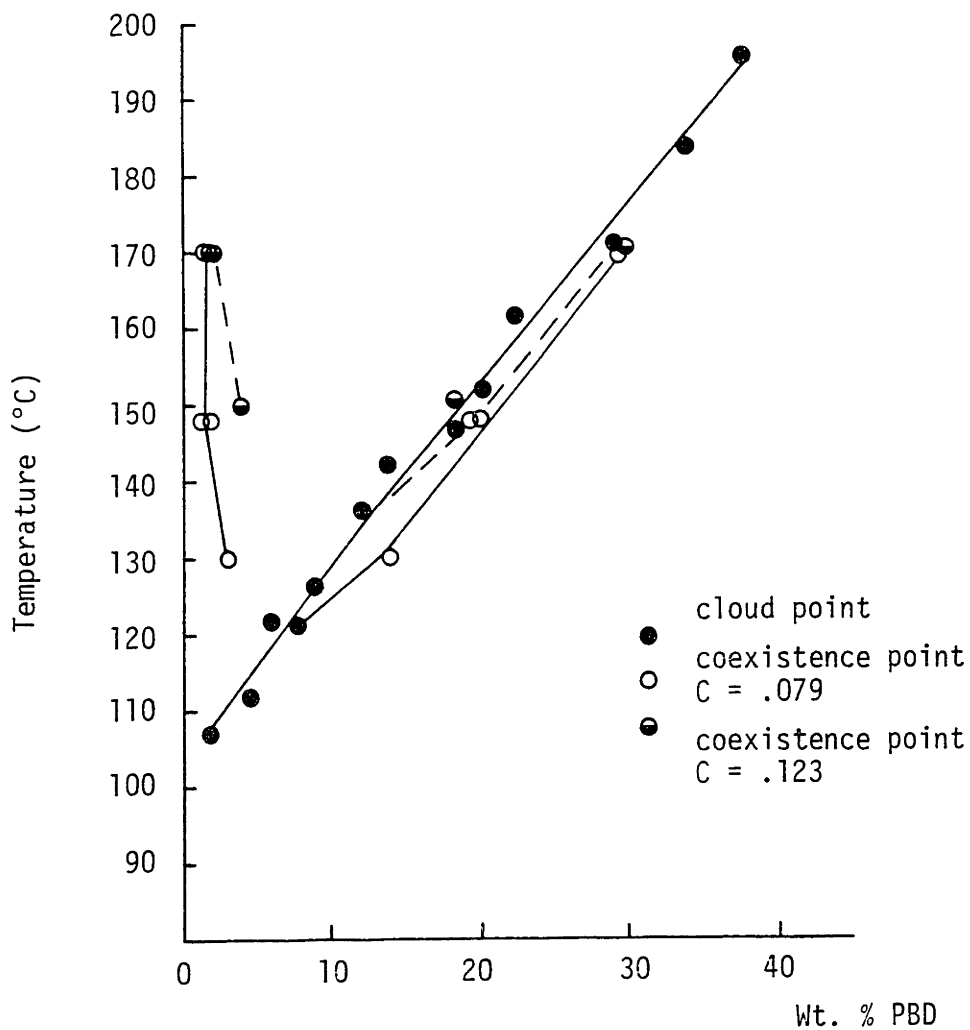


Fig. 5.9 Cloud point curves, and coexistence curves for broad molecular weight PBD in commercial grade hexane.

$$\beta_V = \frac{V'}{V''} = \frac{v'}{v''} \frac{W'}{W''} \quad (5.2)$$

where V' and V'' are the volumes of the dilute and concentrated phases respectively, the W is for weight, and the v is for specific volume. The specific volumes used were approximated as

$$v = v_R(C) + v_S(1-C) \quad (5.3)$$

where v_R is the specific volume of the rubber (about $1.087 \frac{\text{cm}^3}{\text{g}}$) v_S is the specific volume of the solvent (which depends strongly on temperature), and C is the weight fraction of polymer. Several curves are given for Equation 5.3 along with some measured data in Fig. 5.10. These curves ignore the temperature dependence of v_R , which is unimportant for low values of C . They also ignore the volume change upon mixing, which for our present purposes, is also a small effect [5-6].

Alternatively, β_V can be determined directly, by heating, centrifuging and reheating in a special glass walled test tube. This procedure is also discussed in Appendix C. Data using both methods are shown in Fig. 5.11. It is obvious that a fairly large amount of dilute phase can be generated by heating above the cloud point curve.

Before leaving the topic of the effect of the polymer on the phase diagram, it should be mentioned that the polymer

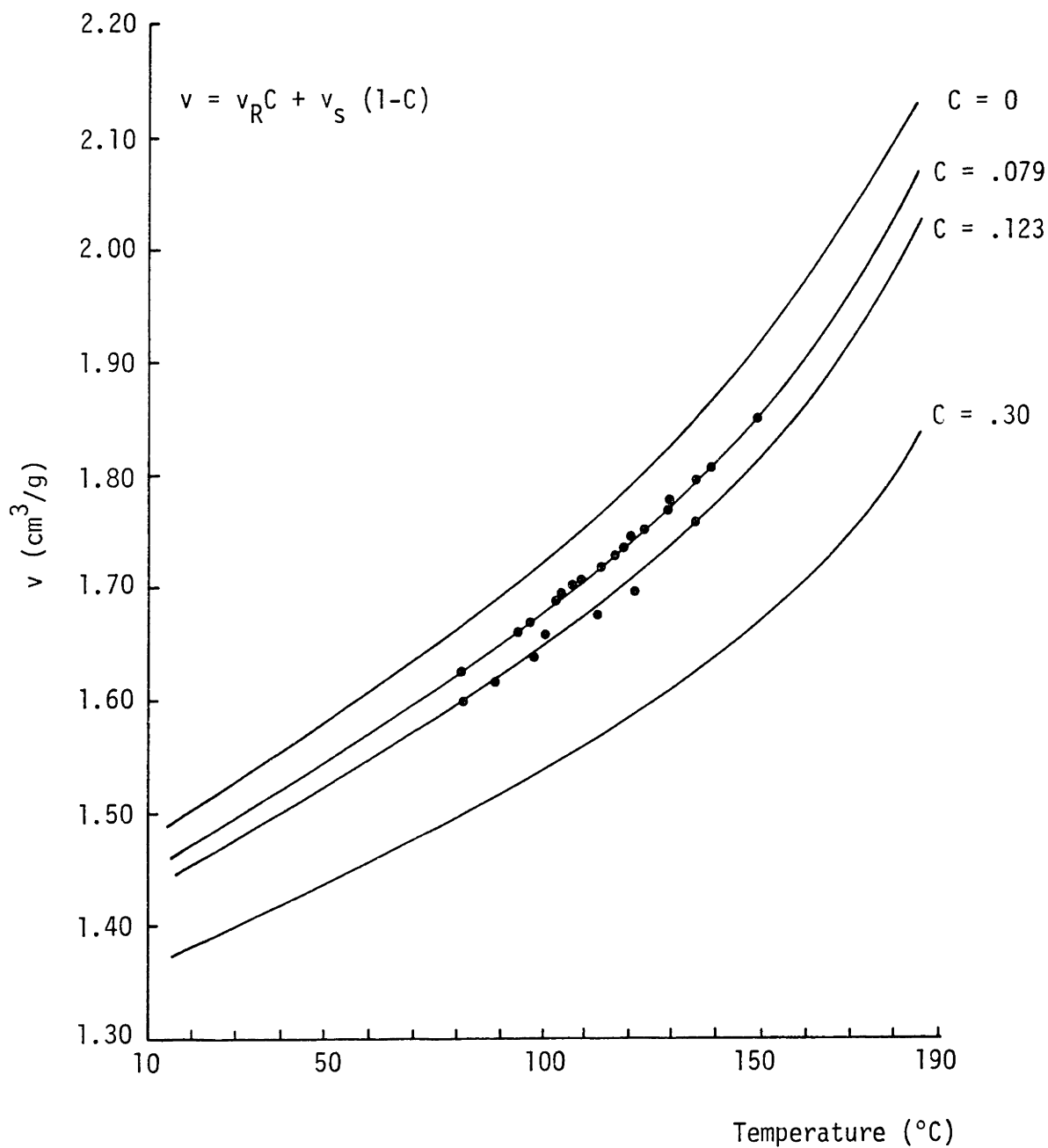


Fig. 5.10 Specific volume curves for hexane-PBD solutions.

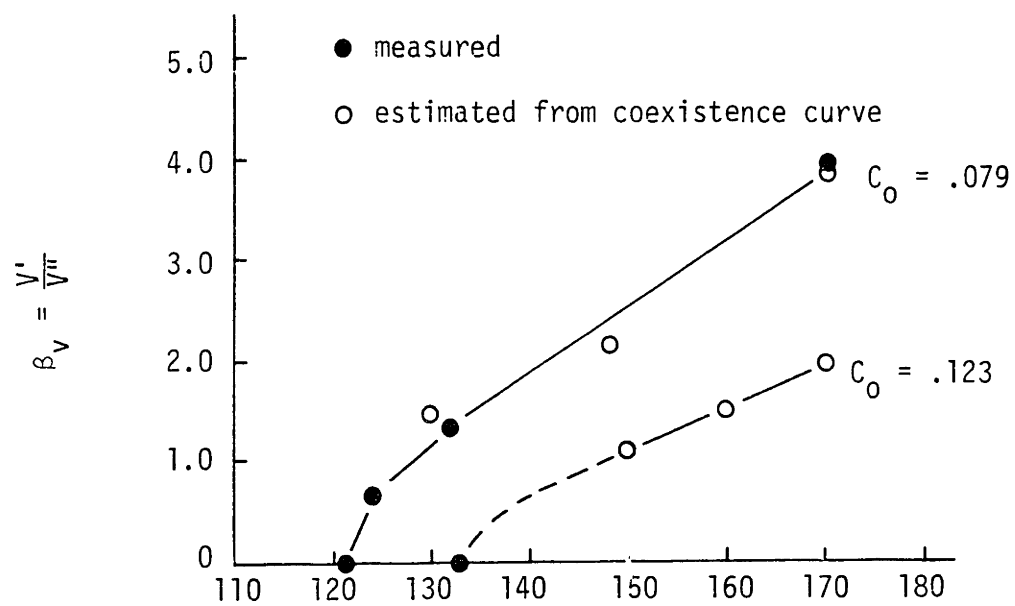


Fig. 5.11 Volume ratio vs. temperature for $C_0 = .079$ and $C_0 = .123$

conformation will change the location of the cloud point curve. This is shown in Fig. 5.12. These are the cloud point curves for two monodisperse samples of very similar molecular weights but differing in stereochemistry. The 200,000 M sample is about 55% trans and 45% cis, while the 191,000 M sample is all cis [5-3]. The difference between the two cloud point curves, about 5°C, and their order (cis comes out of solution before trans) agree with the results of Cowie and McEwen [5-7]. In effect, this phenomenon should not be a problem, however, because the stereochemistry of solution polymerized polybutadiene is closely controlled.

5.4 Mixed Solvents

Mixed solvents are used in many industrial applications because they require less refining than would be required to obtain the pure components. As a consequence they are cheaper and more readily available than the pure components. At the same time however, they will vary in the exact details of their composition from batch to batch. For example, one supplier specifies its commercial grade hexane only within the following limits:

TABLE 5.1

Suppliers Specifications for Commercial Grade Hexane

<u>Component</u>	<u>Per Cent</u>
n-hexane	66 \pm 4
methyl cyclopentane (MCP)	18 \pm 6
3. methylpentane (3MP)	9 \pm 2
2. methylpentane (2MP) and, 2,3 dimethylbutane (2,3DMB)	7 \pm 3

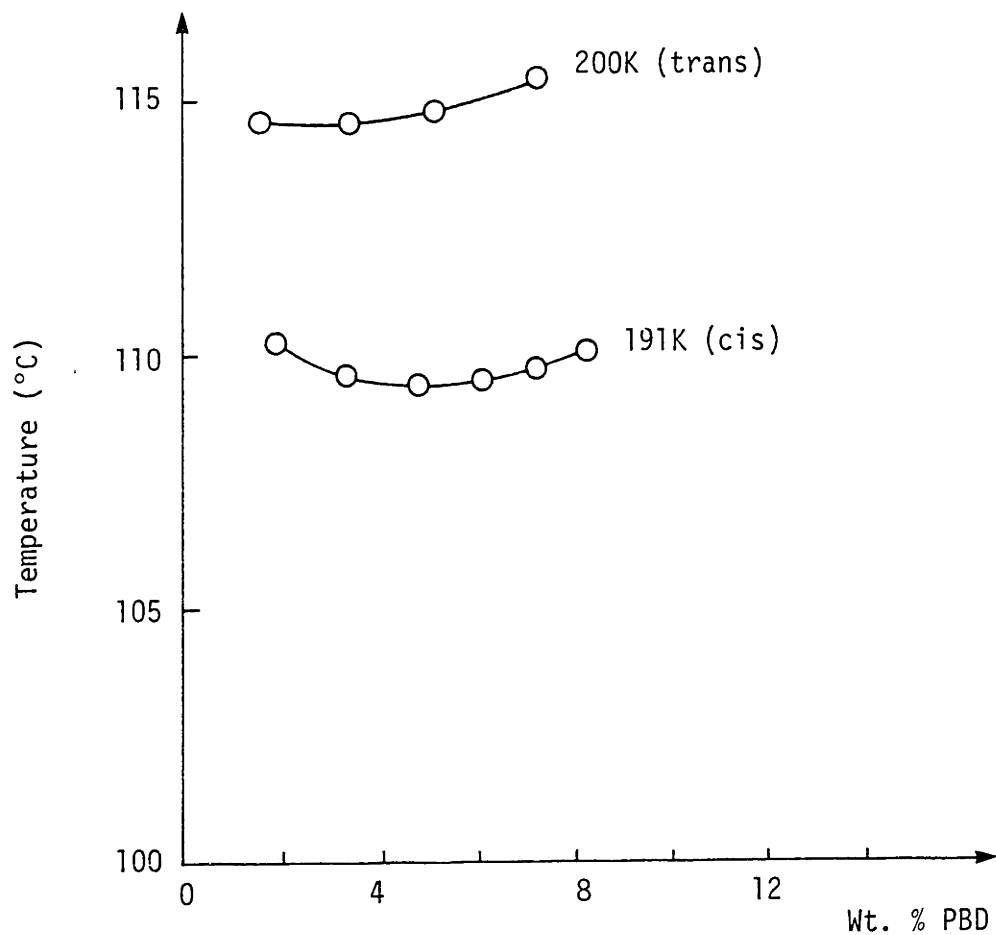


Fig. 5.12 Comparison of cis and trans conformations on cloud point curves for PBD in n-hexane.

Because of these possible variations, it is worthwhile then to investigate the nature of these solvents with respect to polybutadiene.

The standard mixed solvent we are dealing with, falls within the limits given in Table 5.1. The actual mix, as well as certain important physical properties for the individual solvents are given in Table 5.2.

These solvents can be roughly rank ordered by comparing their solubility parameters, and their boiling points. At low temperatures this difference between the solubility parameter of the solvent and the solubility parameter of polybutadiene ($\delta_2=8.6$) [5-9] will indicate the relative sizes of the enthalpy of mixing contributions and consequently the solubility. Here smaller differences indicate better solvents. At high temperatures we can look at the boiling temperature because it correlates with the solvent critical temperature. Since the high temperature phase transition will always occur before the solvent's critical temperature (see Appendix B) higher boiling points (for our case), indicate better solvents. It turns out that these two schemes give approximately the same ranking, the only difference is between 2MP and 2,3DMB which is small and unimportant for our purpose. The rank ordering, giving best solvents first, is shown in Table 5.3.

As shown, 2 MP and 2,3 DMB are quite poor solvents for PBD. In fact, at room temperature, they will not dissolve the polymer. The other three solvents are relatively good however, and MCP is

TABLE 5.2

Solvent Properties				Solubility Parameters	
<u>Solvent</u>	<u>Wt%</u>	<u>Molecular Wt.</u>	<u>Boiling Point (°C)</u>	<u>δ.(calc)</u>	<u>δ.(lit.)</u>
n-hexane	64.4	86.178	68.8°	7.21	7.24[5-8]
MCP	20.1	84.162	71.9°	7.89	
3 MP	7.6	86.178	63.3°	7.18	
3 MP & 2,3 DMB	4.9	86.178	60.3°	6.99	
		86.178	58.1°	7.01	

TABLE 5.3

Rank Ordering of the Solvents in Commercial Grade Hexane

<u>Solvent</u>	<u>$\delta_1 - \delta_2$</u>	<u>Comment</u>
MCP	.71	good solvent
n-hexane	1.39	fair solvent
3 MP	1.42	fair solvent
2 MP	1.62	poor solvent
2,3 DMB	1.59	poor solvent

quite good. These results are confirmed by high temperature cloud point curves for MCP, n-hexane, and commercial grade hexane, shown in Fig. 5.13. By comparing the cloud point curves for commercial grade hexane, and n-hexane it is apparent that, the addition of other C_6 isomers to n-hexane significantly improves the solvent quality of the resulting mixture. Since most of the additional components are only as good or worse than n-hexane, the improved solvent quality must be due to the addition of MCP. This is confirmed by the very high cloud points for methyl cyclopentane. Obviously then, this is one component that should be closely monitored between batches of solvent to ensure similar cloud point behavior.

5.5 Pressure Effects

All of our discussions concerning the details of the phase diagram for polymer solvent systems to this point, have been for the solution at its equilibrium vapor pressure. Lower equilibrium pressures can not be maintained, of course, without altering the original concentration of the solution. Higher equilibrium pressures can be maintained, and in general will increase the solubility of the two components. That is, pressures in excess of the vapor pressure will tend to translate the cloud point curve associated with the high temperature phase transition to higher and higher temperatures. The effect of pressure on the lower temperature phase transition is not so straight forward, and in magnitude is less dramatic than the effect on the high temperature region [5-10].

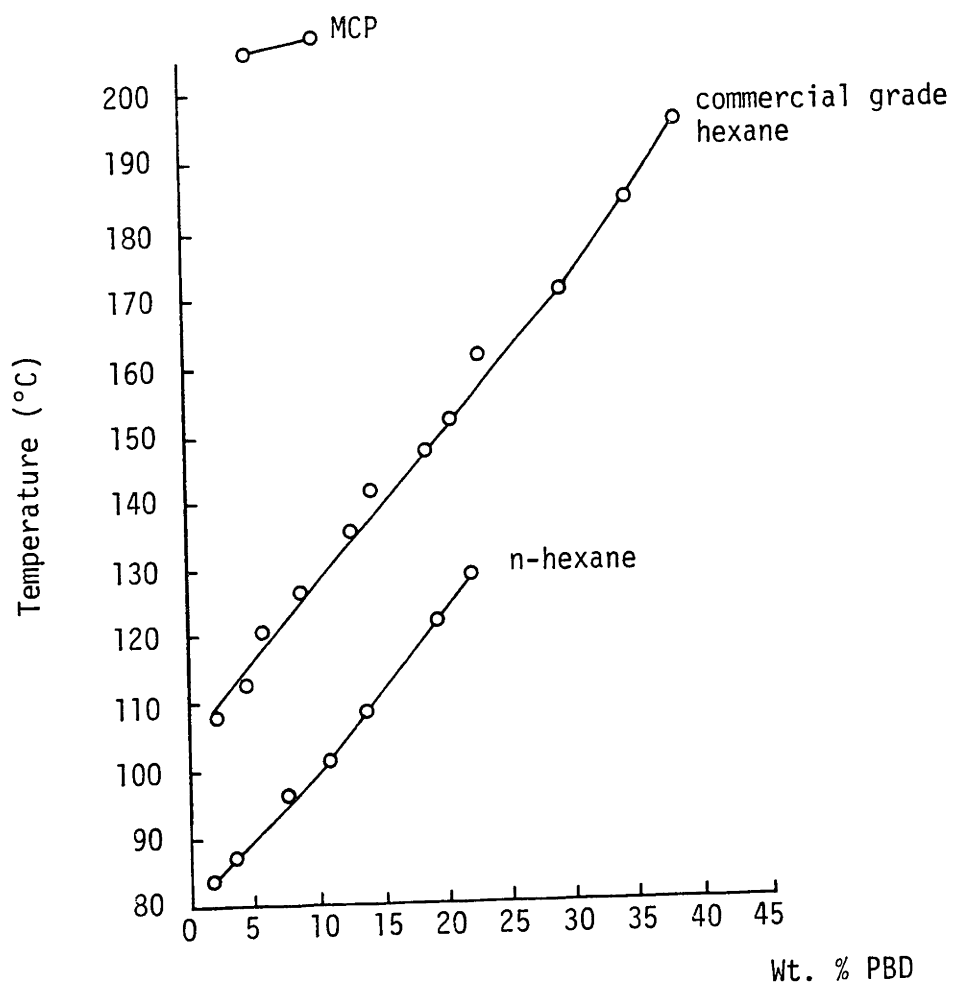


Fig. 5.13 Cloud point curves for PBD in different solvents.

urthermore, since we are only interested here in the high temperature region of the phase diagram, we will confine our comments to this region.

At high temperatures, polymer solvent systems will phase separate because of the large difference in free volumes between the two components. This difference appears as a negative noncombinatorial entropy effect which eventually overrides the combinatorial entropy and causes phase separation. Applying pressure compresses the solvent more than the polymer and reduces the free volume difference, and hence, in effect raises the phase transition temperature. This effect has been measured for many different systems with remarkably similar results. In general the phase diagram is pushed upward about $\frac{1}{2}^{\circ}\text{C}$ for every atmosphere of pressure applied above the vapor pressure. Table 5.4 gives some results for various polymer-solvent systems. The temperature-pressure increment reported here is for the incipient phase separation point, which is also (unfortunately) called the lower critical solution temperature (LCST). This designation, which is popular in the literature, is used because the point lies at the bottom of a two phase region. Contrary to intuition then, the LCST lies above the upper critical solution temperature (UCST) which is associated with the lower temperature phase transition.

The effect of pressure on the cloud point curves for a polystyrene-diethyl ether system [5-10] is also shown in Fig. 5.14. The fact that pressure can be used to raise or lower the phase

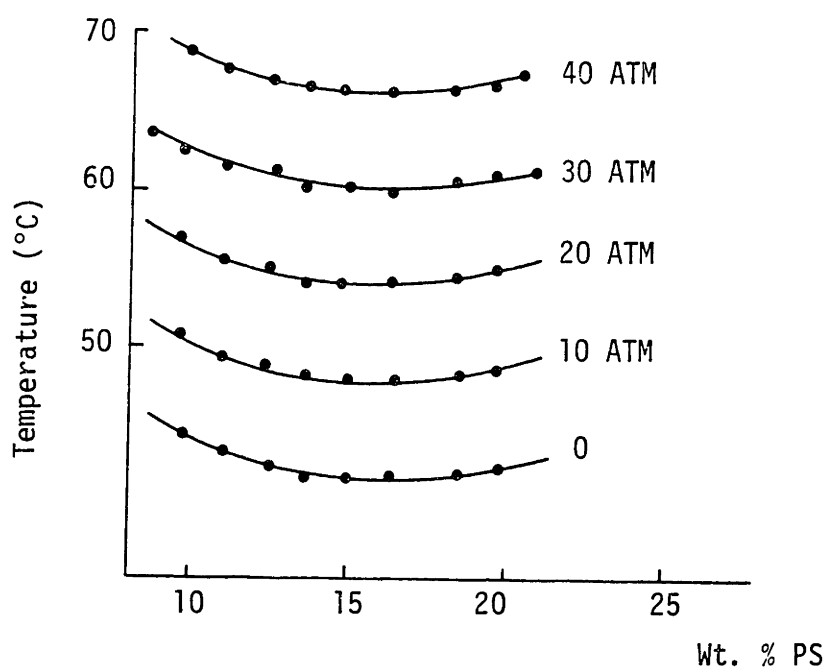


Fig. 5.14 Effect of pressure on cloud point curves for polystyrene-diethyl ether [5-10].

TABLE 5.4

The Effect of Pressure on the LCST

<u>System</u>	<u>M_w</u>	<u>(dT/dP)_{LCST}</u>	<u>Reference</u>
Polyisobutylene (PIB) - Butane	1.7x10 ⁶	.37 °C/atm	[5-11]
PIB - Pentane	1.7x10 ⁶	.45 °C/atm	[5-11]
PIB - Hexane	1.7x10 ⁶	.61 PC/atm	[5-11]
Polystyrene (PS) - Methylacetate	10 ⁵	.45 °C/atm	[5-12]
PS - Methylacetate	1.8x10 ⁶	.48 °C/atm	[5-12]
PS - diethyl ether	2 x 10 ⁴	.62 °C/atm	[5-10]
Polyethylene - pentane	---	.59 °C/atm	[5-10]

diagram will be used to advantage in Chapter 7 on spinodal decomposition.

References, Chapter 5

- 5-1 R. Koningsveld, "Partial Miscibility of Multicomponent Polymer Solutions." *Advances in Colloid and Interface Science*, 2 p. 151 (1968).
- 5-2 P.J. Flory, "Principles of Polymer Chemistry." Cornell University Press, (1953).
- 5-3 G. Delmas and P. de Saint-Romain, "Upper and Lower Critical Solution Temperatures in Polybutadiene-Alkane Systems." *European Polymer Journal*, 10 p. 1133 (1974).
- 5-4 E. Vanzo, "Lower Critical Solution Temperatures of Polybutadiene Solutions." *Rubber Chemistry and Technology*, 41, p. 1285 (1968).
- 5-5 C. Cangialose, "The High Temperature Phase Separation Behavior of Hexane-Polybutadiene Solutions." S.B. Thesis, Massachusetts Institute of Technology (1980).
- 5-6 B.E. Eichinger and P.J. Flory, "Thermodynamics of Polymer Solutions." *Transactions, Faraday Society* 64, p. 2035 (1968).
- 5-7 J.M.G. Cowie and I.J. McEwen, "Upper and Lower Theta Temperatures for Solutions of cis and trans-1,4-polybutadiene." *Polymer*, 16, p. 933 (1975).
- 5-8 F.W. Billmeyer, Jr., Textbook of Polymer Science, Wiley-Interscience 2nd ed. (1971).
- 5-9 F. Rodriguez, Principles of Polymer Systems, McGraw-Hill (1970).
- 5-10 S. Saeki, N. Kuwahara, and M. Kaneko, "Pressure Dependence of Upper and Lower Critical Solution Temperatures in Polystyrene Solutions." *Macromolecules* 9, 1, p. 101 (1976).
- 5-11 L. Zeman, J. Biros, G. Delmas, and D. Patterson, "Pressure Effects in Polymer Solution Phase Equilibria I." *The Journal of Physical Chemistry*, 76, 8 p. 1206 (1972).
- 5-12 L. Zeman and D. Patterson, "Pressure Effects in Polymer Solution Phase Equilibria II." *The Journal of Physical Chemistry* 76, 8 p. 1214 (1972).

CHAPTER 6

GRAVITY SETTLEMENT BEHAVIOR

One of the key problems associated with using the high temperature phase transition to remove hexane from polybutadiene is the physical separation of the phases. After phase separation, which takes place on a microscopic scale, and for original concentrations around 12% wt. PBD (required for efficient reactor usage) gravity settlement is very, very slow. In fact, even after five hours, less than 10% of the potential settlement will take place. This is too slow for any practical separation process. Accelerating this process by centrifuging is possible, but to do so on a continuous basis is made difficult by the high viscosity (10^5 to 10^6 c.p.) of the concentrated phase. Some other method is needed.

This settlement problem was also noted by Anolick and Goffinet [6-1] for the separation of ethylene-propylene rubbers. These authors noted that, low mooney viscosity rubbers will settle more cleanly. While this is true, it turns out that the gravity settlement behavior of two phased polymer-solvent solutions is more related to the phase separation mechanism, than it is to the viscosity of the polymer.

6.1 Gravity Settlement Model

In order to draw some conclusions from the gravity settlement data to be presented in this chapter, it will be extremely useful to have some simple mathematical model for gravity settlement. The

purpose of this model is to determine the relative importance of various factors that can influence settlement. For convenience, this model will be developed from the view point that the discontinuous phase is denser than the continuous phase. So small dense particles will tend to fall to the bottom. In fact, with a minor modification, this model will also be able to represent the opposite case, when the less dense discontinuous phase rises to the top.

Taken individually, the dense particles can be considered as solid particles provided their viscosity is sufficiently high to prevent internal circulation. For example, if the particle is one hundred times more viscous than the continuous medium the error in this solid particle approximation is about 1% [6-2]. For our case, the difference in viscosity between the concentrated and dilute phases is always at least a factor of 100. (This error approximation also applies if the phases are reversed. Now internal circulation is a small effect compared to the motion of the viscous continuous medium.) Furthermore, to within a factor of 2, we may assume that the settling particles are spherical in shape.

Now, for very small particles, and therefore a very low Reynolds Number (Re) we do not expect flow separation. Consequently, gravity and viscous forces are the only ones acting on the particle. Writing Newton's 2nd law, for an individual particle yields,

$$\rho V_{ol} \frac{d^2x}{dt^2} = (\rho - \rho_c) g V_{ol} - 6\pi\mu_c r \frac{dx}{dt} \quad (6.1)$$

where ρ_c and μ_c are the density and viscosity of the continuous phase, Vol. = $\frac{4}{3} \pi r^3$ is the volume of a sphere of radius r , which has density ρ , and g is gravity. At equilibrium $\frac{d^2x}{dt^2} = 0$, and $\frac{dx}{dt} = v_0$, this is the well known Stoke's law terminal settling velocity, where

$$v_0 = \frac{2}{9} \frac{g \Delta \rho r^2}{\mu_c} \quad (6.2)$$

The time constant for equation (6.1) is

$$\tau = \frac{2}{9} \frac{\rho r^2}{\mu_c} \quad (6.3)$$

This model is for individual spheres falling in large containers. It ignores the fact that conservation of mass requires, that as the dense particles fall down, the less dense continuous phase must move up. This effect remains small until the volume fraction of particles exceeds about .01. At this point the interparticle distance is on the order of three particle diameters. When the concentration of these particles of mixed sizes is such that collisions and interactions become common, it will happen that the particles will tend to settle en masse. This process is known as hindered settling. It is easy to observe experimentally because there is a sharp border between the settling particles, and the continuous phase they have left behind. Should a particle lag behind the interface for some reason, it will catch up to the rest of the particles because the hindered settling velocity is quite a bit slower than the settling velocity for an individual particle.

Consequently the phenomenon is stable.

Hindered settling, then, is not unlike flow through a porous plug. This is easy to conceptualize, if for the moment, the particles are imagined stationary with the continuous phase flowing through them. In fact, the hindered settling velocity correction factor can be derived directly from the Carmen-Kozeny equation for laminar flow of a fluid through a porous medium [6-2]. The hindered settling velocity is [6-2, 3]

$$v = v_0 \frac{(1-\alpha)^3}{10\alpha} \quad (6.4)$$

where v_0 is given by equation (6.2) and α is the volume fraction of particles in the continuous phase. The factor of 10 is an empirical constant.

Two examples of hindered settlement are shown in Fig. 6.1a, and b. These show two extreme cases. In Fig. 6.1a the particles stoically settle on the bottom of the tube without warning their upstairs neighbors about what is to come. As a consequence, the concentration of settling particles remains fixed, $\alpha = \text{constant}$, and equation (6.4) can be integrated directly to obtain a linear relationship between interface distance x and time t . In reality the act of the particles meeting the bottom of the container is likely to cause a disturbance that will be propagated back to the interface at x . This may cause concentration inhomogeneities to propagate back and forth between the two interfaces [6-4]. The most

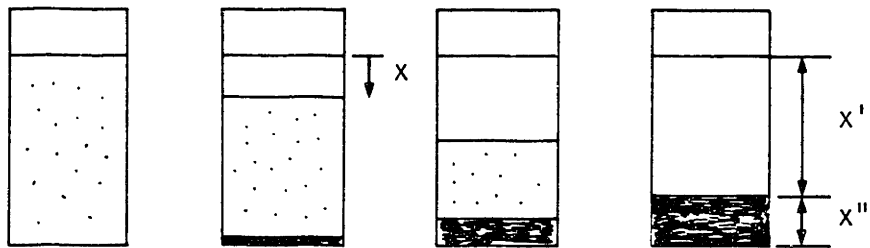


Fig. 6.1a Case I, lower bound hindered settlement.

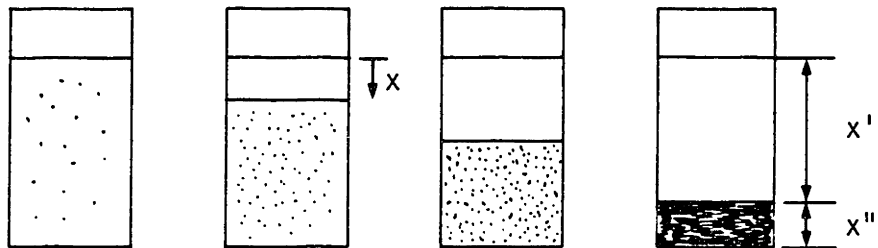


Fig. 6.1b Case II, upper bound hindered settlement.

extreme case of this phenomenon is shown in Fig. 6.1b. Here the entire disturbance is propagated back in an average form. Now the concentration of settling particles is constantly growing. This leads to much longer settlement times than for case I in Fig. 6.1a. To obtain a mathematical expression for this case requires integrating equation 6.4 with variable α . This is most conveniently done by changing variables. Let

$$\beta = \frac{x' - x}{x''} \quad (6.5)$$

where x' and x'' are shown in Fig. 6.1. β is then a nondimensional distance that starts at some value that indicates the amount of potential settlement, and ends at zero. For a constant cross sectional area container A , β also represents a volume ratio. For example, at $t = 0$, $x = 0$, and

$$\beta(t=0) = \frac{x'A}{x''A} = \frac{V'}{V''} \quad (6.6)$$

where V' is the volume of the dilute phase, and V'' is the volume of the concentrated phase, so $\beta(x=0)$ is the same as β_V defined in Chapter 5. At times greater than zero, β represents the volume ratio for the remaining two phase fluid below the x interface. For $\beta = 0$, only the dense phase lies below x . So β may be thought of as a dimensionless distance variable, or as an average concentration variable, for case II. As a consequence, α can be related to β by

noting that

$$\alpha = \frac{1}{\beta + 1} \quad (6.7)$$

Recasting equation (6.4) in terms of β , yields

$$\frac{d\beta}{dt} = \frac{-v_0}{10} \left(\frac{1+\beta}{\ell} \right)^{v_0} \frac{\beta^3}{(\beta+1)^2} \quad (6.8)$$

where $\ell = x' + x''$ gives the scale of the separation device, and $\beta_V = \beta(t=0) = \text{constant}$.

We can now integrate equation (6.8) to obtain the time history of β . For case I, shown in Fig. 6.1a, β is replaced by β_V on the right hand side of the equation, with the result,

$$t = \frac{10}{v_0} \ell \frac{(\beta_V+1)}{\beta_V^3} (\beta_V - \beta) \quad (6.9)$$

This gives the linear relationship between time t , and β . In this case β is a dimensionless distance variable, when $\beta = 0$, settlement is complete. This will occur in time t^* , where

$$t^* = \frac{10}{v_0} \ell \frac{(\beta_V+1)}{\beta_V^2} \quad (6.10)$$

For case II, integration of equation (6.8) yields

$$t = \frac{10\ell}{v_0(1+\beta_V)} \left\{ \ln \frac{\beta_V}{\beta} + 2 \left(\frac{1}{\beta} - \frac{1}{\beta_V} \right) + \frac{1}{2} \left(\frac{1}{\beta^2} - \frac{1}{\beta_V^2} \right) \right\} \quad (6.11)$$

Now, infinite time is needed for complete settlement. For many of the cases we are interested in, β_V is between 1 and 4. Fig. 6.2 compares equations 6.9, and 6.11 for $\beta_V = 2$. Real situations will lie between the bounds given by cases I and II. Measured cases for hexane and polybutadiene, look more like case II.

Equation (6.11) does predict a certain settlement time dependence on the volume ratio β_V . That is, settlement should be more rapid for large β_V . This is shown in Fig. 6.3. The cross-over phenomenon shown in the figure is an artifact of the way β is scaled.

6.2 Gravity Settlement Observations

Gravity settlement data were obtained by heating hexane and polybutadiene samples in a special stainless steel and glass test tube immersed in a silicone oil bath as shown in Fig. 6.4. Markings on the side of the tube housing allowed measurement of the settlement distance x . The temperature of the solution was measured by a thermocouple in a thin well (diameter = .166cm) at the bottom of the tube. The inside dimensions of the glass tube are; length = 7.5 cm, and diameter = .83 cm. Note that the solution in Fig. 6.4 has separated a small distance, and the vapor-dilute phase, and dilute phase-mixed phase interfaces are clearly visible.

In general, it was difficult to obtain settlement data that conformed exactly to the requirements of the simple mathematical models that were just developed. The major reason for this is related to the heating time. For rather dilute solutions ($C_0 = .079$), heating

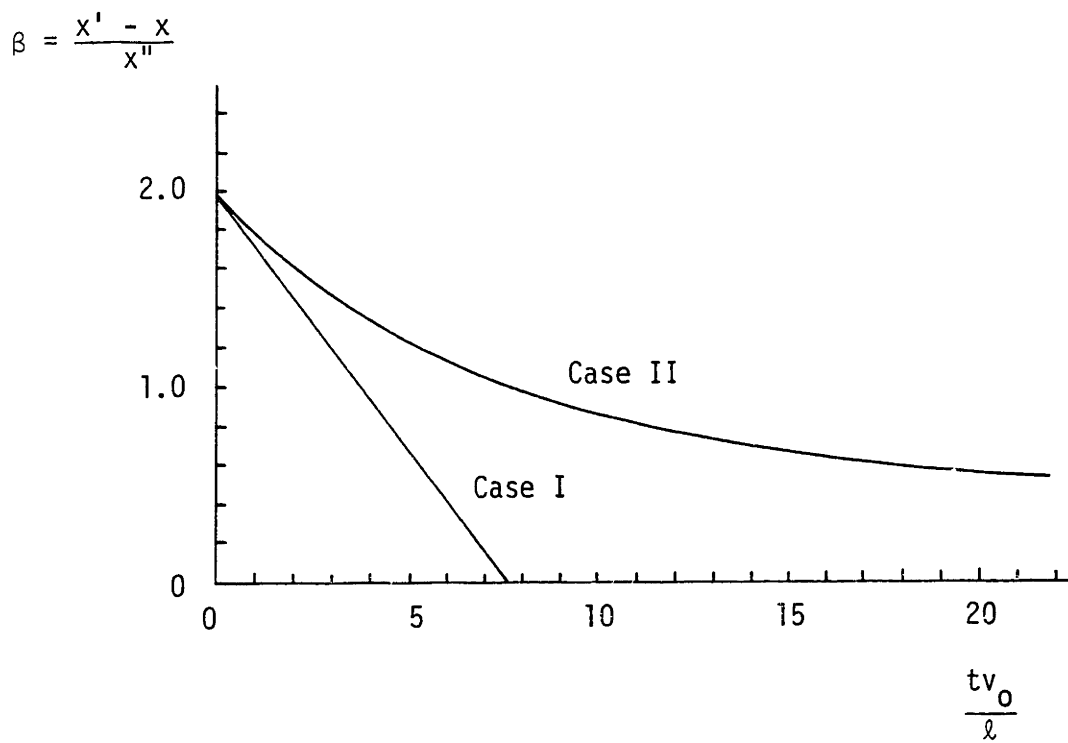


Fig. 6.2 Comparison of Case I and Case II type hindered settling.

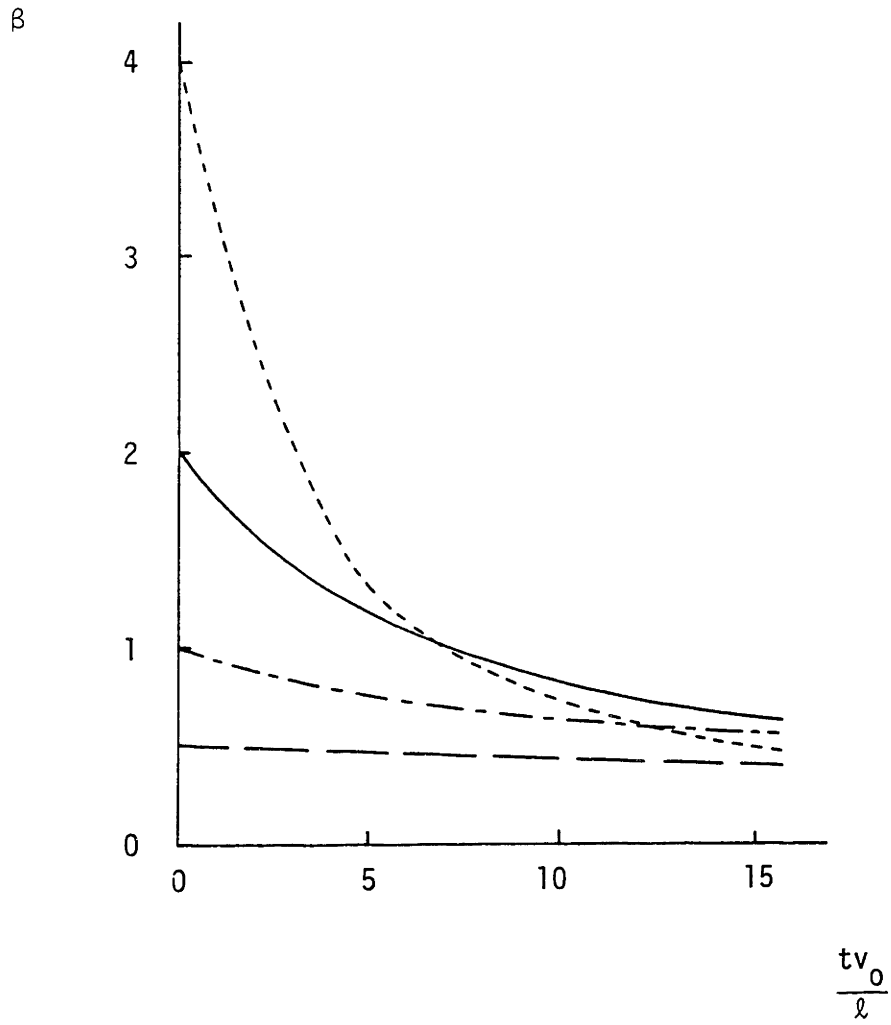


Fig. 6.3 Comparison of settling times for different initial values of β .

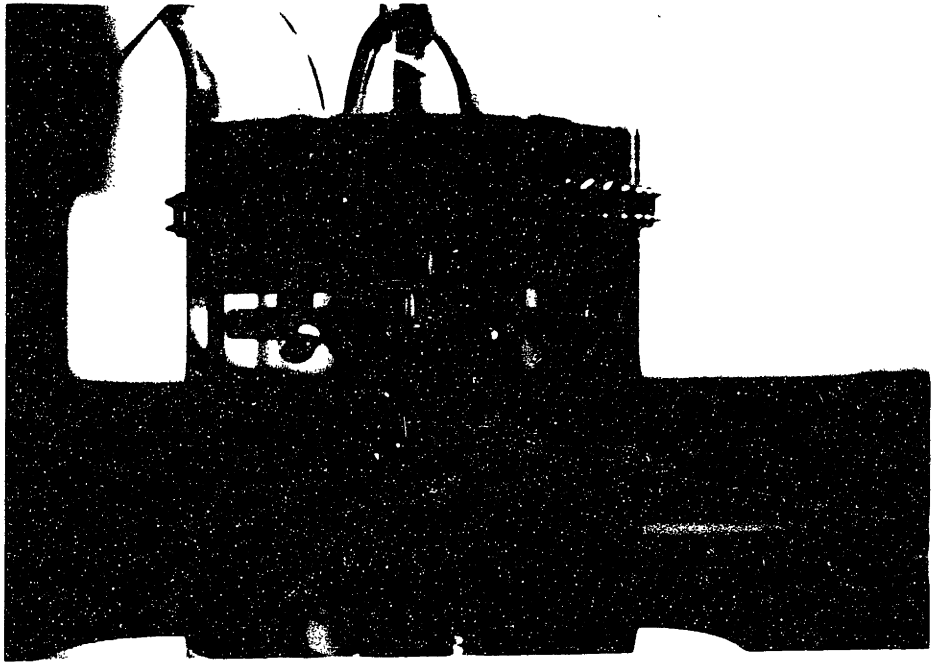
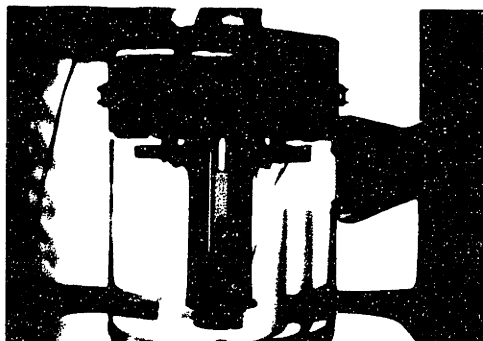
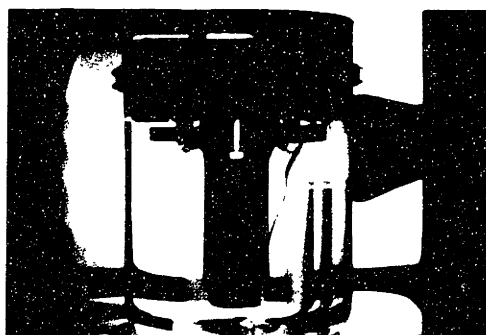


Fig. 6.4 Thick walled glass tube in stainless steel housing used for gravity settlement observations. Note partial settlement at cross bar location.

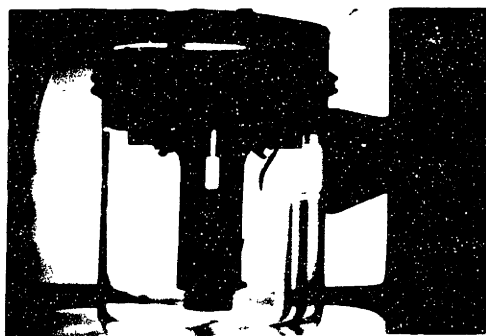
too rapidly caused thermal gradients and instabilities that lead to what looked like "turbulent" settlement. Heating too slowly however, while producing "orderly" settlement, caused some gravity settlement to occur before the desired equilibrium temperature was obtained. Examples of these two cases are shown in the series of photographs in Figs. 6.5 and 6.6. The first figure shows orderly settlement for a 7.9% wt. PBD solution heated only a small amount above the cloud point. Fig. 6.6 shows the same solution heated more rapidly, and to a higher temperature, resulting in unstable settlement. This instability problem was not encountered at higher concentrations ($C_0 = .123$), but then neither was gravity settlement. To avoid the unstable settlement case, samples were heated slowly and the temperature histories were reported with the settlement data. For our purpose, which is to make an order of magnitude estimate concerning the structure of the two phased medium, this procedure turns out to be adequate. Data for the orderly settlement of a 7.9% wt. PBD solution are shown in Fig. 6.7, along with the temperature history of the sample. The solid circle points shown in this figure are scaled using the final equilibrium values for x' and x'' . Therefore, the curve they yield indicates the motion of the interface x as a function of time. In reality, the actual values of x' and x'' varied somewhat due to the temperature variations in the early part of the experiment. The actual values of x' and x'' can be ascertained by comparing the temperature in Fig. 6.7 with the value of β_V ($\beta_V = x'/x''$ for a constant cross-sectional container) given in Fig. 5.11. After two minutes the actual β_V value is 83% of



$T = 121^{\circ}\text{C}$ (cloud point)
 $t = 0$

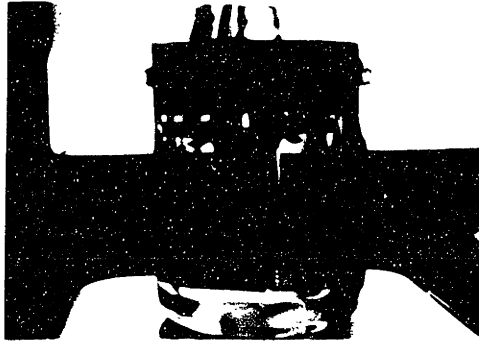


$T = 124^{\circ}\text{C}$
 $t = 10 \text{ min.}$



$T = 125^{\circ}\text{C}$
 $t = 17 \text{ min.}$

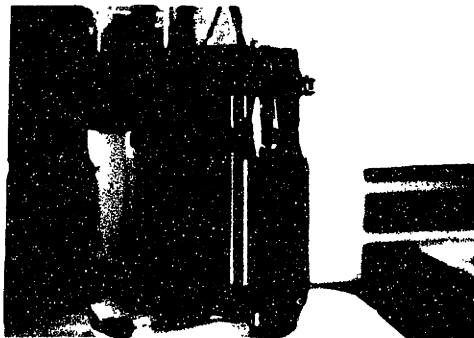
Fig. 6.5 Orderly gravity settlement of 7.9% wt. PBD solution.



$T = 142^{\circ}\text{C}$
 $t = 1 \text{ min.}$



$T = 163^{\circ}\text{C}$
 $t = 4 \text{ min.}$



$T = 165^{\circ}\text{C}$
 $t = 34 \text{ min.}$

Fig. 6.6 Unstable gravity settlement of 7.9% wt. PBD solution

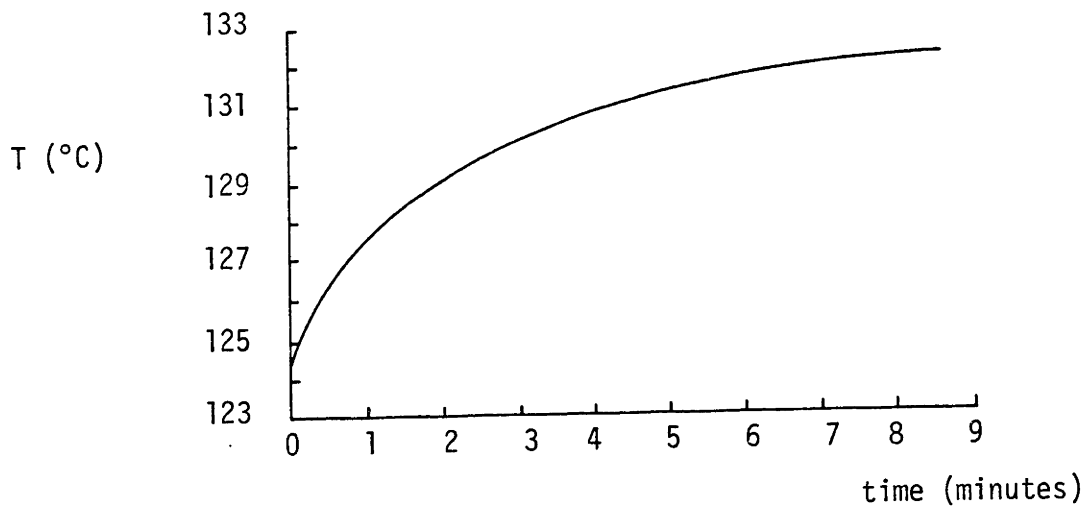
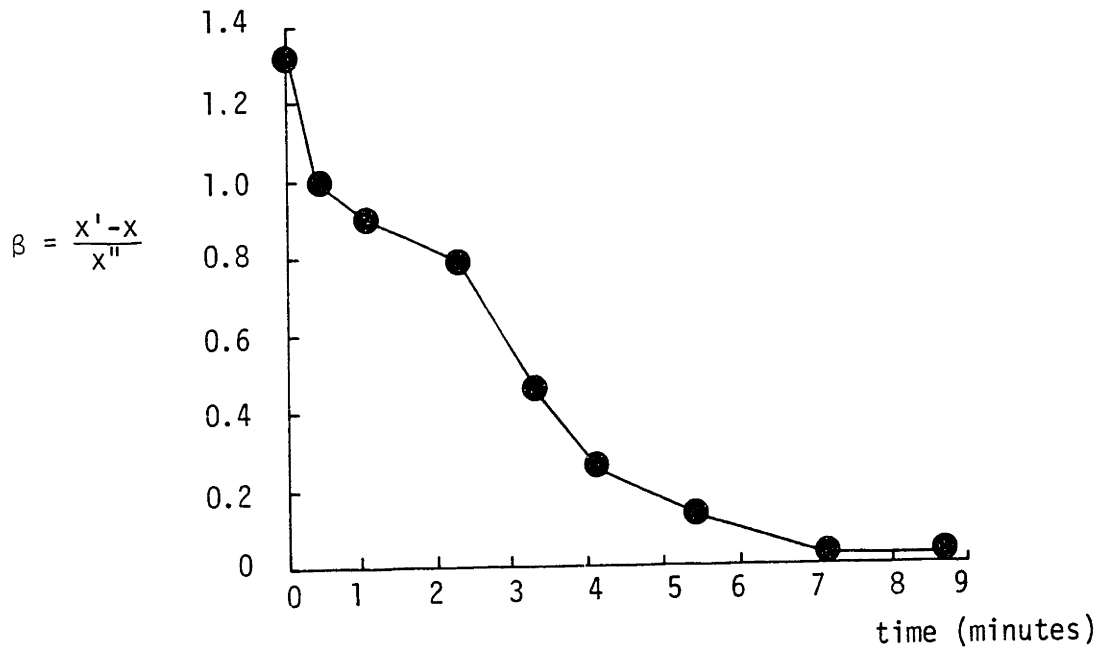


Fig. 6.7 Gravity settlement and temperature history for 7.9% Wt. PBD solution.

equilibrium value, and after four minutes the two are essentially the same.

A comparison of the upper bound model and the data in Fig. 6.7 can be done directly, once it is recognized that the "real" settlement curve, would start at $\beta = 1.32$, $t = 0$, and decay in a fashion so it could just meet, but never exceed, the solid data points. By "real" curve is meant, the curve that would be obtained if the sample could be instantaneously and uniformly heated to its equilibrium value. The lower bound to this data is much more difficult to set since it depends on an initial slope, which is completely obscured by the temperature variation. Therefore no estimate of the lower bound is made.

Two different plots of equation (6.11) are compared with the settlement data in Fig. 6.8. One is an upper bound curve ($\frac{v_0}{\ell} = 4 \text{ min}^{-1}$) and the other is a best fit through $\beta = 1.32$, $t = 0$, ($\frac{v_0}{\ell} = 8 \text{ min}^{-1}$). Using these curves, equation (6.2) now allows us to make an order of magnitude estimate of the particle size ($d=2r$). This is of interest because two possibilities exist. We could be seeing bubbles (or droplets) of the dilute phase rising to the top, denoted as C'/C'' (i.e. the dilute phase C' surrounded by the concentrated phase C''), or it may be that the concentrated phase is falling as particles to the bottom, denoted as C''/C' .^{*} In fact, it turns out that it is the latter that is taking place. The details of the calculation are

*This calculation is made because it was impossible to observe, even with a low powered microscope, the nature of the two-phased structure during gravity settlement.

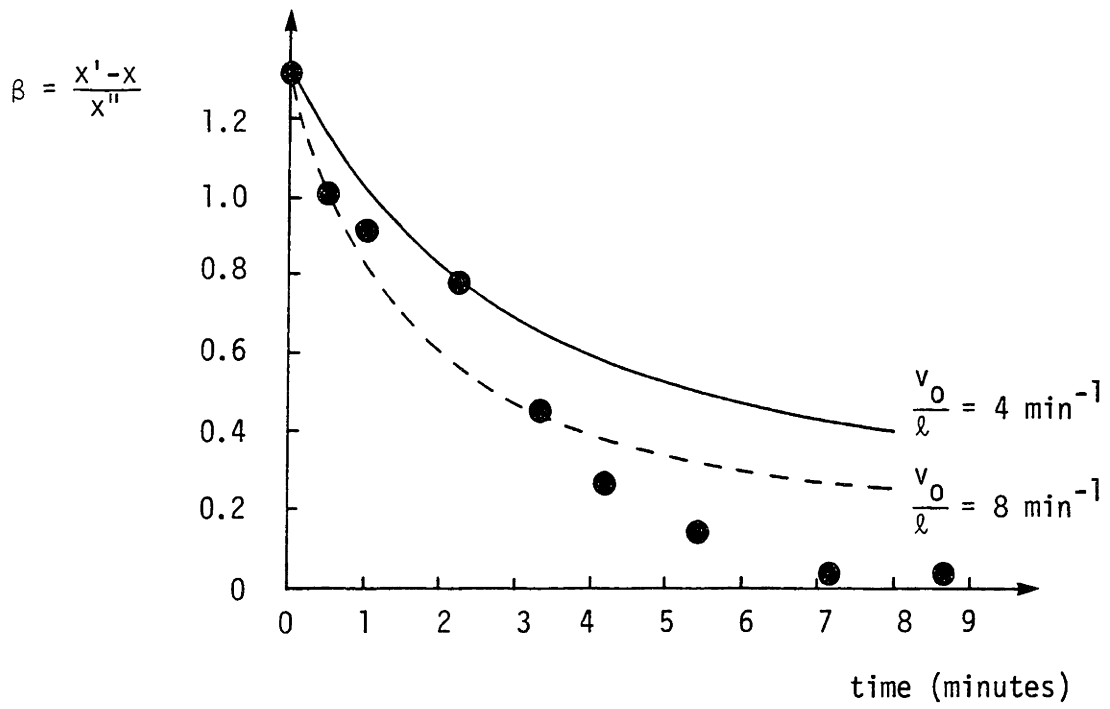


Fig. 6.8 Comparison of upper bound settlement model with data.

given in Table 6.1. Immediately, we see that the particle sizes for the C'/C" case are too large, in fact, they exceed the inside diameter of the settlement device (.83 cm). The particle sizes for the other case however, i.e. C'/C" are quite plausible.

This result is, in a way, surprising, since it was stated earlier in Chapter 4, that thermodynamics arguments say, for temperatures just above the cloud point, and for concentrations greater than the critical one, that phase separation is by nucleation and growth of the dilute phase. This can be easily confirmed at higher concentrations. For example, if a 12.3% wt. PBD solution is heated and observed under a microscope, the two phased C'/C" structure can be clearly seen. This is shown in Fig. 6.9 (the hot stage set up), Figs. 6.10, 6.11, 6.12, 6.13, 6.14, and finally in Fig. 6.15. These show the sequence of nucleation and growth, with the final bubble structure. The structure shown in Fig. 6.15 can not be C"/C' since it would rapidly settle due to gravity (i.e., in all photographs gravity acts from the top to the bottom of the page).

This is further confirmed by comparing the gravity settlement behavior of the two concentrations, shown in Fig. 6.16, (the small amount of settlement for $C_0 = .123$ is in fact what was shown in the photograph in Fig. 6.1. This small amount of settlement will essentially remain unchanged for hours.) If the two curves in Fig. 6.16 were for similar structures and roughly similar particle sizes, we would expect them to look more like the model results shown in Fig. 6.3. These two solutions then, apparently have very different two-phased structures. In one case ($C_0 = 1.23$), we clearly have C'/C". In the other case

TABLE 6.1

Calculation of Particle Sizes for
Two Different Phase Arrangements

Parameters:

$$T \cong 130^{\circ}\text{C}, C_0 = .079$$

$$C' = .03, C'' = .14 \text{ (from Fig. 5.9)}$$

$$\Delta\rho = .065 \text{ g/cm}^3$$

$$\mu(C') = .18 \text{ g/cm S}$$

$$\mu(C'') = 90 \text{ g/cm S}$$

$$l = 5 \text{ cm}$$

$$g = 980.7 \text{ cm/S}^2$$

Results:

	<u>C''/C'</u>	<u>C'/C''</u>
$\frac{v_0}{L} = 4 \text{ min}^{-1}$	$d = .08 \text{ cm}$	$d = 3.0 \text{ cm}$
$\frac{v_0}{l} = 8 \text{ min}^{-1}$	$d = .12 \text{ cm}$	$d = 4.20 \text{ cm}$
	$\tau \cong .01 \text{ sec.}$	$\tau \cong .02 \text{ sec}$
	$R_e \cong .5$	$R_e \cong .01$

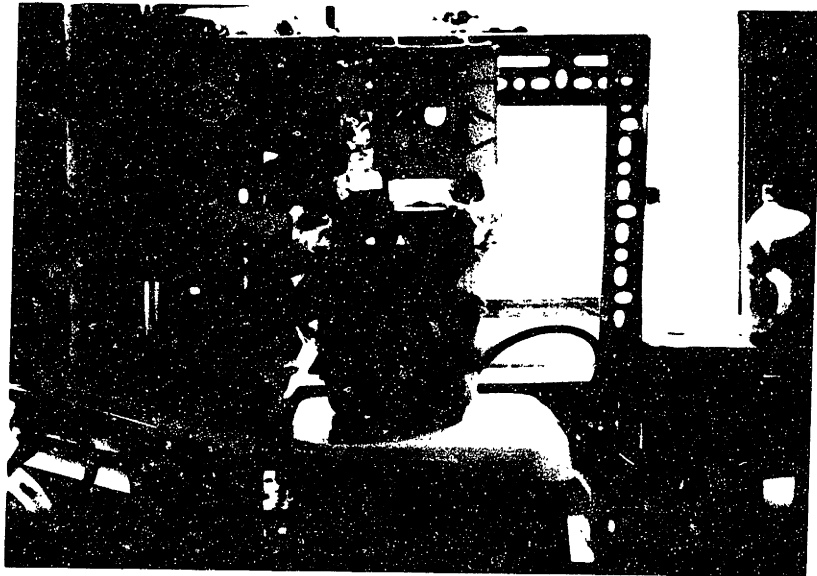
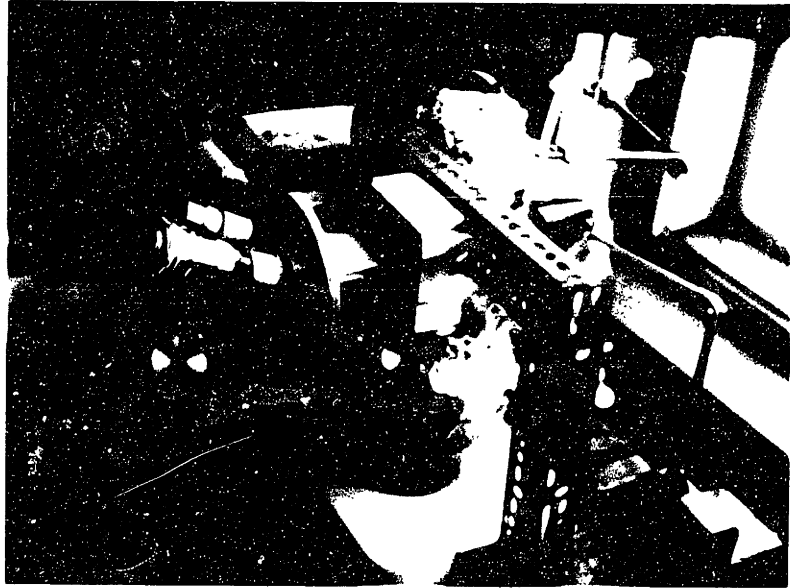


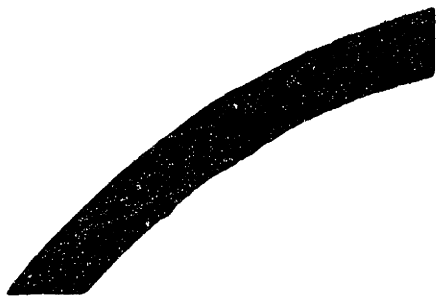
Fig. 6.9 Hot stage set-up. Microscope with camera attachment, top. Pump, heater, oil beaker and hot stage, bottom.



$T = 132^{\circ}\text{C}$ (before cloud
 $t = 0$ point)

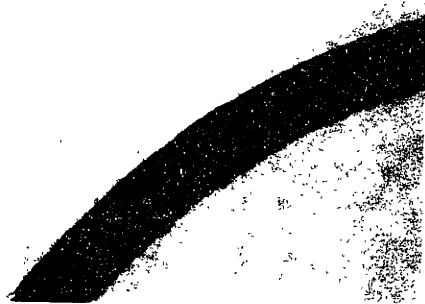


$T = 136^{\circ}\text{C}$ (after cloud
 $t = 4$ min. point)

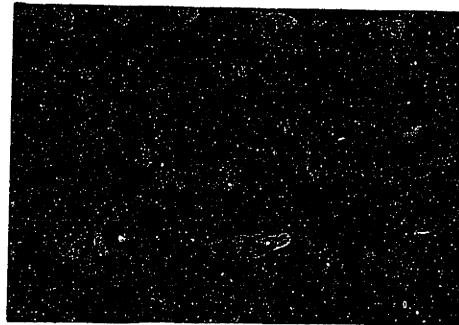


$T = 141^{\circ}\text{C}$
 $t = 11$ min.

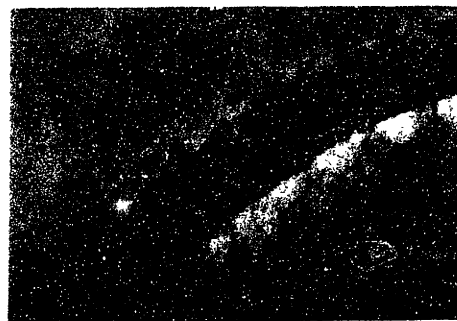
Fig. 6.10 Nucleation and growth sequence, diameter of thermocouple wire = 0.3 mm.



$T = 143^{\circ}\text{C}$
 $t = 13 \text{ min.}$



$T = 148^{\circ}\text{C}$
 $t = 23 \text{ min.}$

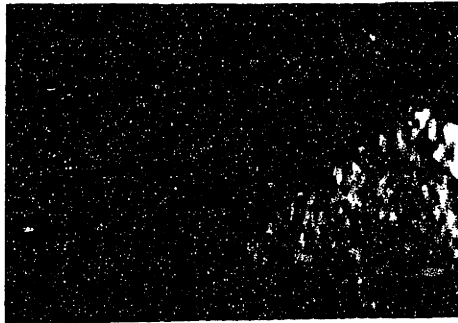


$T = 151^{\circ}\text{C}$
 $t = 28 \text{ min.}$

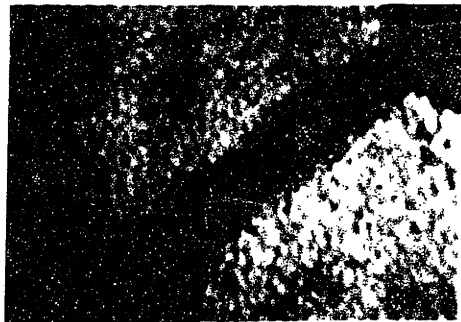
Fig. 6.11 Nucleation and growth sequence, diameter of thermocouple wire = 0.3 mm.



$T = 152^{\circ}\text{C}$
 $t = 45\frac{1}{2} \text{ min.}$



$T = 152^{\circ}\text{C}$
 $t = 46 \text{ min.}$

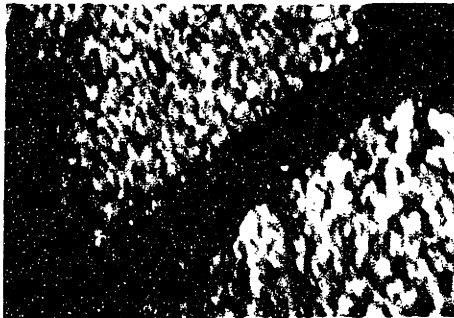


$T = 152^{\circ}\text{C}$
 $t = 46\frac{1}{2} \text{ min.}$

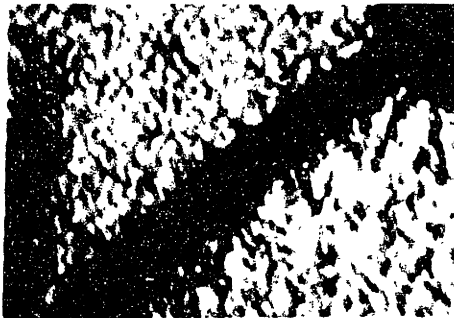
Fig. 6.12 Nucleation and growth sequence, diameter of thermocouple wire = 0.3 mm.



T = 149°C
t = 53 min.

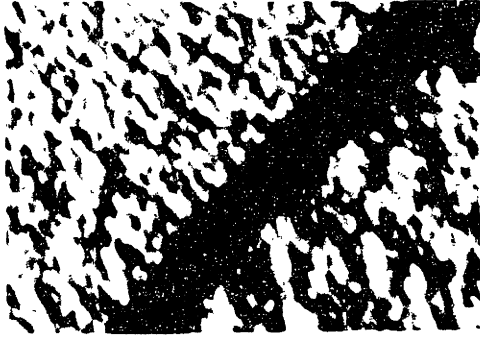


T = 150°C
t = 58 min.

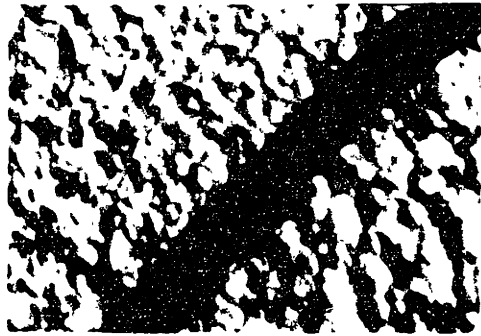


T = 151°C
t = 1 hr. 4 min.

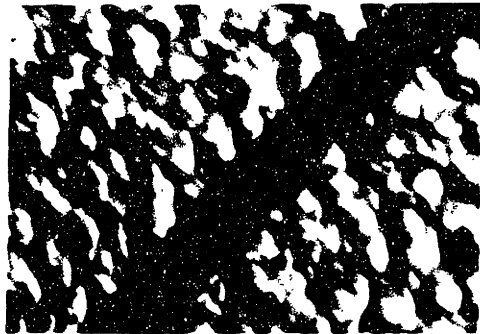
Fig. 6.13 Nucleation and growth sequence, diameter of thermocouple wire = 0.3 mm.



$T = 149^{\circ}\text{C}$
 $t = 1 \text{ hr. } 16 \text{ min.}$

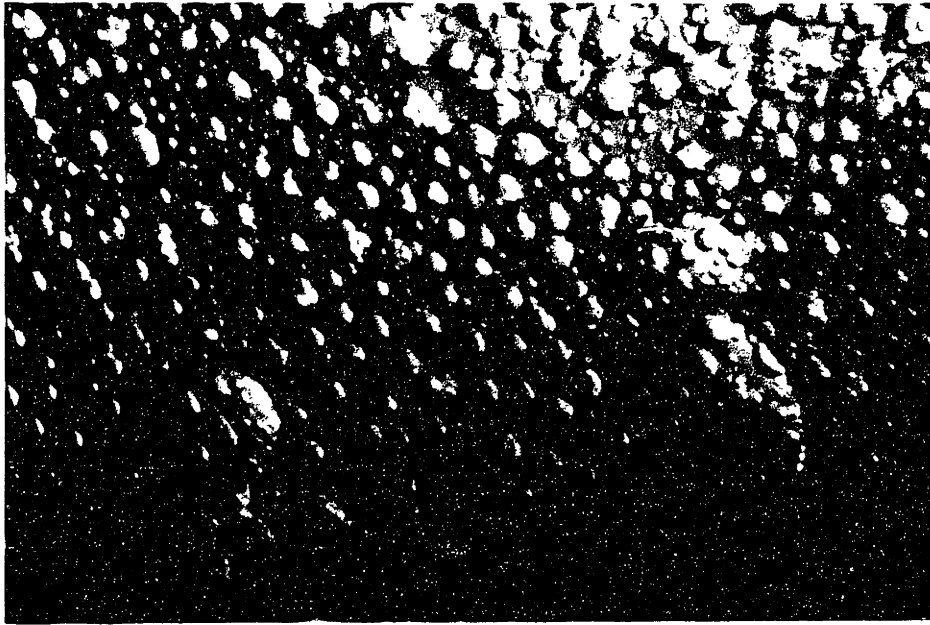


$T = 147^{\circ}\text{C}$
 $t = 1 \text{ hr. } 18 \text{ min.}$



$T = 144^{\circ}\text{C}$
 $t = 1 \text{ hr. } 20 \text{ min.}$

Fig. 6.14 Nucleation and growth sequence, diameter of thermocouple wire = 0.3 mm.



$T = 143^{\circ}\text{C}$ $t = 1 \text{ hr. } 30 \text{ min.}$

Fig. 6.15 Resulting two phase structure after nucleation and growth of the dilute phase. Typical bubble diameter 0.2 to 0.3 mm, largest bubble diameter 0.7 mm.

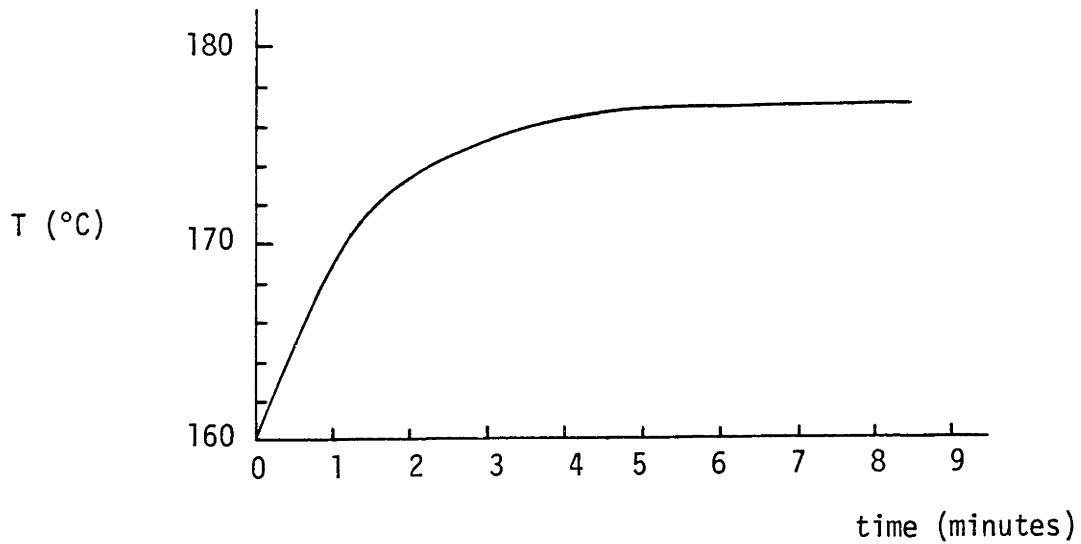
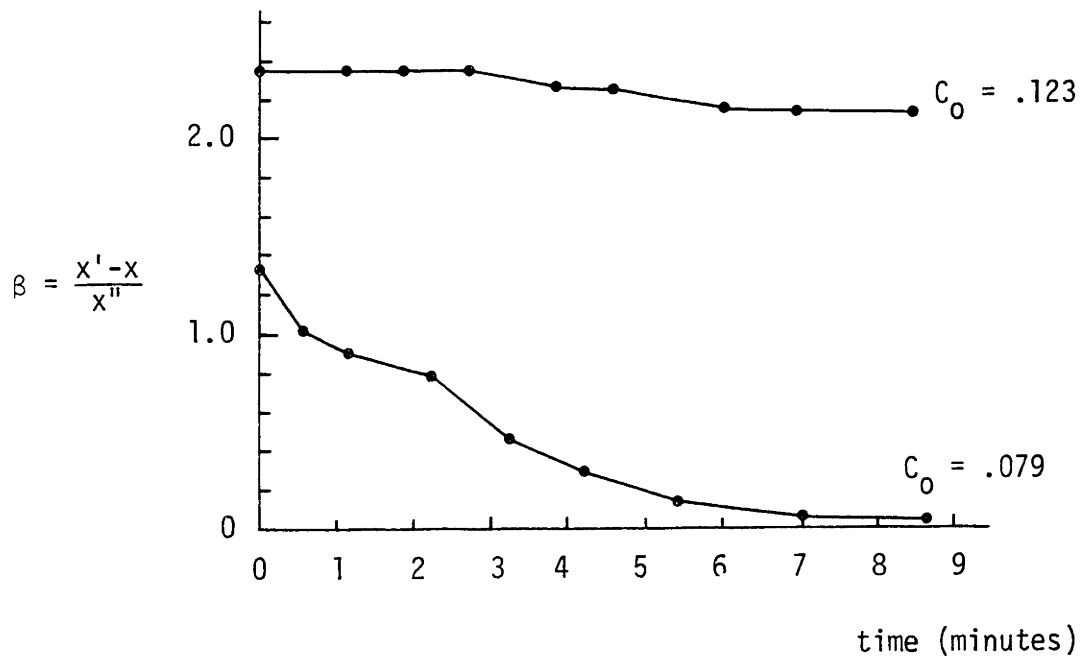


Figure 6.16 Comparison of gravity settlement for two different concentrations, and temperature history for $C_0 = .123$.

($C_0 = .079$) we have C''/C' . The dramatic difference in the settlement behavior of these two structures is due to the difference in viscosity between the dilute and concentrated phases. Viscosity data for polybutadiene in hexane are shown in Fig. 6.17. This curve can be extended down to pure hexane which has a viscosity of about 0.01 c.p. The difference in viscosity between the dilute and concentrated phases then can easily be three or four orders of magnitude. Consequently, the same order of magnitude difference can be expected for the settlement times.

The difference in structure is probably due to passing through the nucleation and growth regime and into the spinodal decomposition regime for the 7.9% wt. sample. In this case, it is likely that the spinodal lies only a few degrees above the cloud point curve. For the more concentrated solution (12.3% wt.) on the other hand, it is likely that the spinodal lies a considerable distance, perhaps 20°C, above the cloud point curve. In this case it is difficult to prevent extensive nucleation and growth of the dilute phase before entering the spinodal region. In fact, even when very thin samples (1 mm) were rapidly heated, no appreciable settlement was observed at this concentration.

Some indication that rapid heating does influence the gravity settlement behavior however, is shown in Fig. 6.18. Here thin samples of 12.3% Wt. PBD were rapidly heated in a glass and copper apparatus similar to the one used for the cloud point determination. Very rapid heating produced some noticeable separation, while for the slower heating cases, no separation was observed even

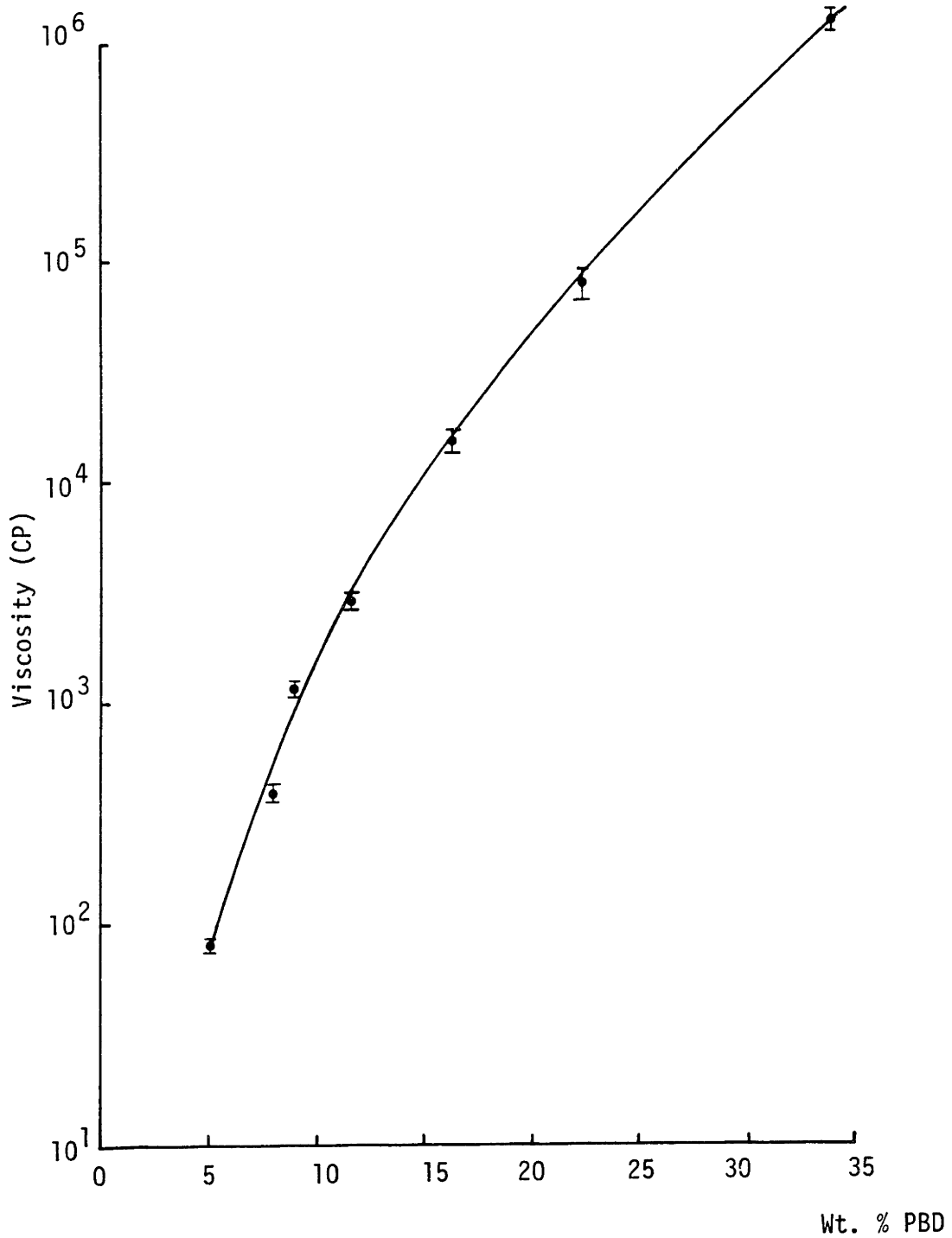


Fig. 6.17 Viscosity of polybutadiene in hexane at 24°C.

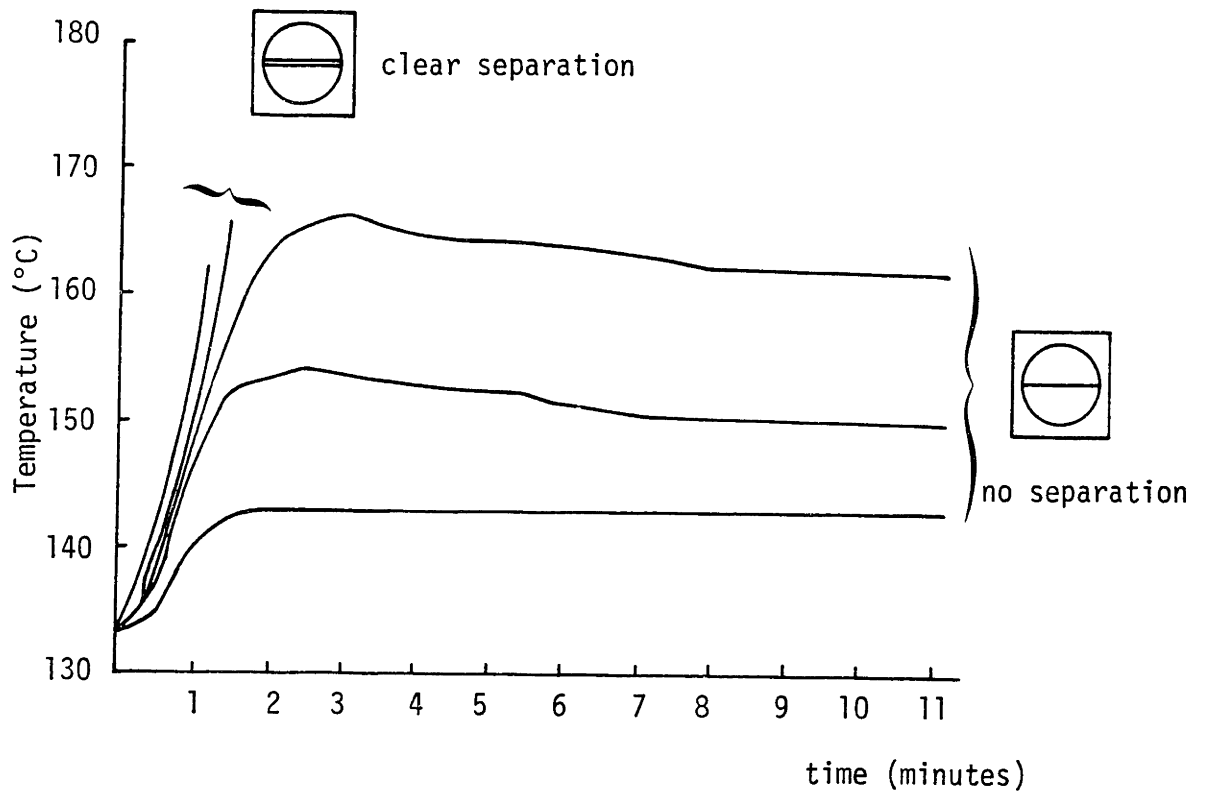


Fig. 6.18 Separation behavior of polybutadiene in hexane solution (12.3% Wt.).

after 11 minutes.

The crux of the gravity settlement issue then, is to obtain a favorable arrangement of the two phases. This is made difficult for concentrations greater than the critical one (about $C = .04$ for our case) because the dilute phase tends to nucleate. If the nucleation and growth regime can be passed through rapidly though, there is some hope that the spinodal structure will allow gravity settlement. In this case a fairly continuous path for the dilute phase can be formed, allowing it to drain while the viscous material can collapse to the bottom. Furthermore, since there is no energy barrier to spinodal decomposition as there is for nucleation and growth we may expect fairly rapid kinetics for this process.

The problem of inducing gravity settlement then, boils down to one of figuring out how to rapidly enter into the spinodal decomposition regime. This can be done by taking advantage of the pressure effect discussed in Chapter 5. The idea now is not to heat rapidly, which is hopeless anyhow, but to pressurize, heat, and then rapidly drop the pressure. This means one would essentially raise the phase diagram above a target temperature, heat to that temperature, and then rapidly drop the phase diagram so that the target temperature now lies in the spinodal decomposition regime. This idea which is shown schematically in Fig. 6.19, is presented in the next chapter, along with an estimate of the location of the spinodal.

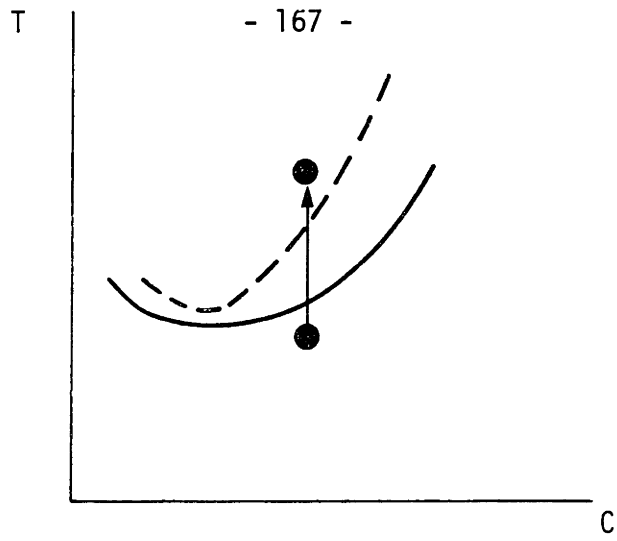


Fig. 6.19a Rapid heating into the spinodal decomposition regime.

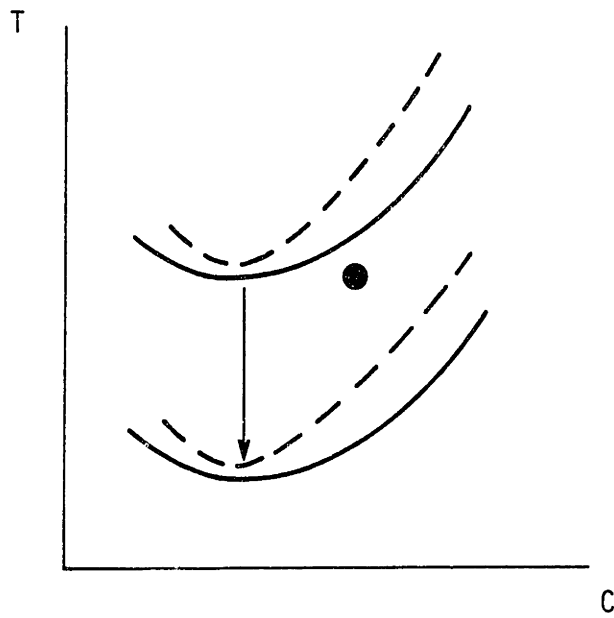


Fig. 6.19b Rapid pressure drop into the spinodal decomposition regime.

References, Chapter 6

- 6-1 C. Anolick and E.P. Goffenet, Jr., "Separation of Ethylene Copolymer Elastomers from Their Solvent Solutions," U.S. Patent No. 3,553,156 (1971).
- 6-2 G.W. Govier and K. Aziz, The Flow of Complex Mixtures in Pipes, Van Nostrand Reinhold (1972).
- 6-3 J.M. Kay and R.M. Nedderman, Fluid Mechanics and Heat Transfer, 3rd ed., Cambridge University Press (1977).
- 6-4 G.B. Wallis, One-Dimensional Two-Phase Flow, McGraw-Hill (1969).

CHAPTER 7

SPINODAL DECOMPOSITION

While spinodal decomposition is a well known phenomenon to metallurgists, it only recently has been discussed by polymer scientists [7-1,2,3,4]. The reason for this is related to the relatively high thermal conductivity of metals. This allows rapid entry into the spinodal regime, and then rapid freezing of the spinodal pattern for later observation. The characteristically low thermal conductivity of polymer-solvent solutions on the other hand, impedes easy access to the spinodal regime. Spinodal decomposition has been observed for only a very few polymer-solvent systems and then only by the rapid heating or cooling of very thin samples (0.2 mm). [7-2,3,4,]. The proposition that the spinodal regime can be entered by dropping pressure, and that this might induce rapid gravity settlement in a concentrated polymer solution is new.

In principle, spinodal decomposition may occur in any liquid-liquid phase separation. Gibbs [7-5] described the conditions for unstable phase separation, and Cahn, [7-6] and Cahn and Hilliard [7-7] described the early kinetics of spinodal decomposition, and the free energy for a nonuniform system. Van Aartsen [7-8] later applied Cahn's work to polymer solutions by using the Flory-Huggins expression for Gibbs free energy.

The essential features of spinodal decomposition were presented in section 4.3 of Chapter 4 of this thesis. Basically, it is an unstable phase separation phenomenon. It differs from nucleation and

and growth in that the energy barrier associated with the formation of a new interface no longer exists. This is because unstable phase separation is by the propagation of concentration fluctuations. In the early stages of spinodal decomposition all concentrations between the yet-to-be-formed dilute and concentrated phases exist. Therefore there is no sharp interface. In later stages, of course, the boundaries become well defined. Cahn [7-6] showed that concentration fluctuations of one particular wave number propagate more rapidly than others. This wave number defines the scale of the resulting spinodal pattern. By using the work of van Aartsen [7-8], Cahn [7-6], and Nishi, Wang and Kwei [7-2] it is possible to estimate the characteristic length scale λ_m for the spinodal pattern as

$$\lambda_m = 2\pi\ell\{3(\frac{T}{T_s} - 1)\}^{-1/2} \quad (7.1)$$

ℓ is the range of molecular interaction estimated to be of order $\langle S^2 \rangle^{1/2}$ (the root-mean-square radius of gyration of the polymer chain), T is the temperature and T_s is the spinodal temperature. Using an estimated value of 520\AA for ℓ , and 150°C for T_s (to be discussed later) yield the following results.

TABLE 7.1

Estimated Length Scale λ_m for PBD-hexane	
<u>Temperature</u>	<u>$\lambda(\mu\text{m})$</u>
151°	3.9
155°	1.7
160°	1.2
165°	1.0
170°	.9

This scale applies to the spinodal pattern shown in Fig. 4.7 of Chapter 4. These numbers are consistent with other observations and calculations [7-2,3,4,8] which give roughly the same size scale for all polymer-solvent systems that have been observed so far. Of course, the spinodal pattern is not stable to surface tension and gravity forces which will alter this pattern in the later stages of separation.

7.1 Estimate of the Spinodal

The proposed pressure drop method requires some estimate of the location of the spinodal for our polybutadiene-hexane system. This can be done by applying the spinodal condition

$$\frac{\partial^2 \Delta G_M}{\partial C^2} = 0 \quad (7.2)$$

to the Gibbs free energy of mixing expression for a broad molecular weight polymer (equation 5.1). This has been done by Koningsveld [7-9], with the remarkable result that under certain conditions the spinodal depends only on the weight average molecular weight of the polymer and not on the details of how the polymer is distributed. The conditions are that the interaction parameter g is independent of molecular weight and concentration, two conditions which we have assumed earlier for our system. Koningsveld's result is

$$\text{(spinodal)} \quad 2g = \frac{1}{\phi_0} + \frac{1}{m_w \phi_1} \quad (7.3)$$

where ϕ_0 and ϕ_1 are the solvent and polymer volume fractions respectively ($\phi_0 + \phi_1 = 1$) and m_w is similar to x defined in equation 4.26,

$$m_w = \frac{\bar{M}_w / \rho_1}{\bar{M}_0 / \rho_0} \quad (7.4)$$

but now the weight averaged molecular weight \bar{M}_w is specified. The spinodal intersects the cloud point curve at the critical point,

$$\text{(critical point)} \quad \phi_{1,c} = \frac{1}{1 + m_w / \sqrt{m_z}} \quad (7.5)$$

where g takes on its critical value

$$\text{(critical point)} \quad 2g_c = 1 + \frac{1}{m_z^{1/2}} + \frac{1}{m_w} [1 + m_z^{1/2}] \quad (7.6)$$

where

$$m_z = \frac{\bar{M}_z / \rho_1}{\bar{M}_0 / \rho_0} \quad (7.7)$$

is based on the z average molecular weight. Note that for a monodisperse sample $m_w = m_z = x$ and the original expressions derived in Chapter 4 are obtained (equations 4.40 and 4.41).

Because of the three-dimensional nature of the phase diagram for a broad molecular weight polymer, the critical point does not correspond to the lowest point on the cloud point curve [7-9].

Therefore, the spinodal-cloud point arrangement will be slightly different than previously shown (Fig. 4.9) for a strictly binary solution. The critical point, derived from equation (7.5) is at $\phi_{1,c} = .032$, this corresponds to a weight fraction of about .044.

Our problem now boils down to determining the temperature dependence of g . This has been discussed in detail in Chapter 4 and Appendix B. There are three points that are readily available for fitting these curves. One is the osmotic pressure measurement discussed in Chapters 3 and 4 and the other two are the critical points associated with the upper and lower temperature cloud points. These points are listed below.

TABLE 7.2

Data Used to Estimate Temperature Dependence of g

<u>Temperature</u>	<u>Interaction Parameter g</u>
112.5°C	.521
20°C	.502
-12°C	.521

Using this data to fit equation (4.50) yields* the following estimate for the interaction parameter

$$g = \frac{188.9}{T} - .692 + 1.875 \times 10^{-3} T \quad (7.8)$$

*Since equation (4.50) is of the form $g = \frac{A}{T} + B + CT$, the three points in Table 7.2 can be used in a straight forward way to determine the constants A, B and C.

where T is in $^{\circ}\text{K}$. Using the first two points in Table 7.2 to fit equation (B.12) yields

$$g = \frac{.171}{\theta}(1-\theta)^{1/2} + .201(1-\theta)^{-1/2} \quad (7.9)$$

where $\theta = T/T_c$, and $T_c = 508^{\circ}\text{K}$ is the vapor-liquid critical point for hexane. These two curves along with other results are shown in Fig. 7.1. Now inspection of Equation 7.3 for the spinodal will show that the higher curve in Fig. 7.1 (equation 7.9) will yield a lower spinodal in temperature-concentration space. To be conservative then, Equation 7.8 will be used as an estimate of the spinodal. This choice is partially justified by the other curve in Fig. 7.1. The data points shown in the figure were obtained from cloud point curves found in the literature for monodisperse samples of cis polybutadiene in pure n-hexane [7-10]. Matching the chemical potentials for the left and right branches of these curves yields a value for g . Now if we assume that the spinodal for the pure n-hexane curve is similar in its relationship to the cloud point curve as the spinodal for the commercial grade hexane curve, we may shift the data points shown in Fig. 7.1 by the amount shown in Fig. 5.13. Where Fig. 5.13 showed us that the cloud point curves for commercial grade hexane, and pure n-hexane are very similar in shape but shifted by 27°C . This approximation is probably not too bad since commercial grade hexane is 64% pure n-hexane so the interaction parameters are likely to be similar in nature. This shifted curve lies very close to equation (7.8).

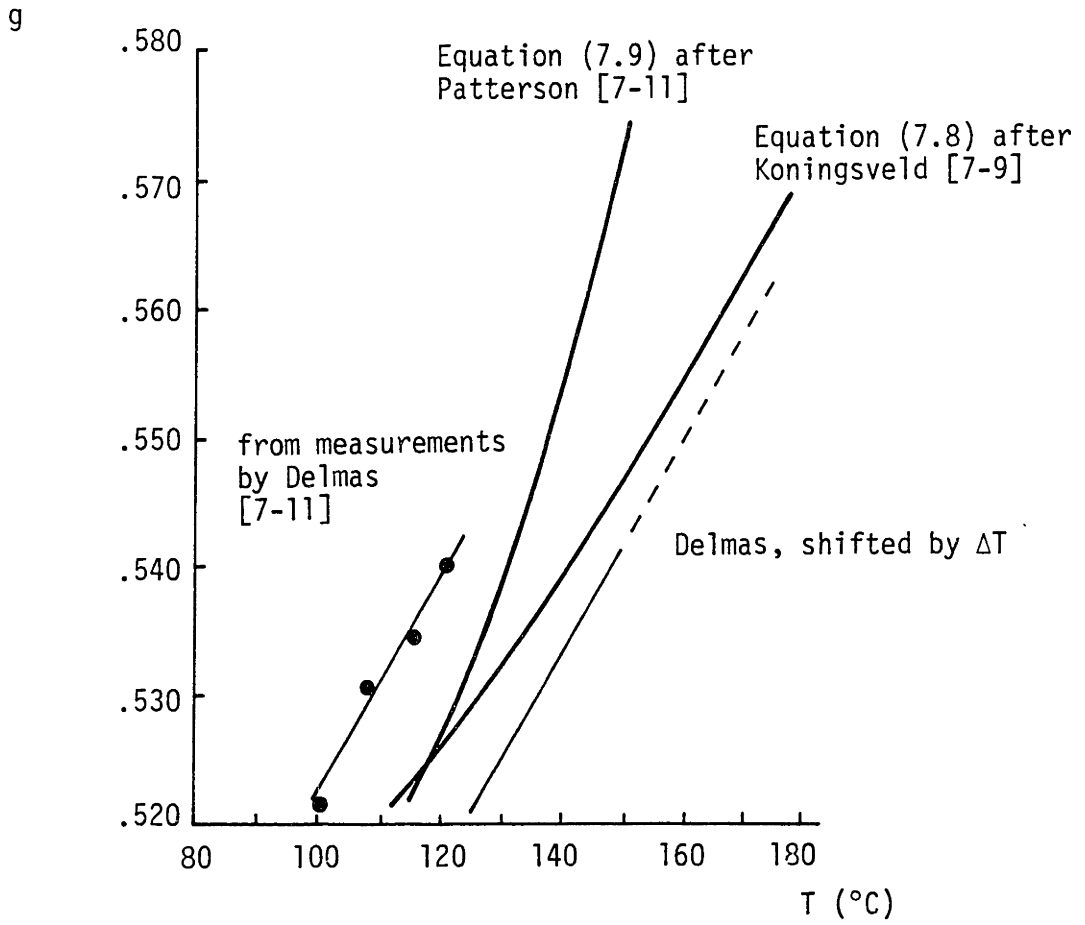


Fig. 7.1 Comparison of approximations to the interaction parameter g .

Using equations (7.8) and (7.3) and converting from volume fraction to weight fraction allows us to estimate the spinodal. This is shown in Fig. 7.2. The fact that the spinodal appears to drop below the cloud point curve for very low values of C cannot be correct. Rather the spinodal should lie close to, or slightly above the cloud point curve. This small error indicates the rough nature of this approximation. On the other hand, the curve in Fig. 7.2 possesses all of the essential features of the spinodal. It touches the cloud point curve at the critical point ($C=.044$) and then gradually, and later much more rapidly rises, above the cloud point curve for concentrations far removed from the critical one. The left hand branch of the spinodal is of no interest for our present discussion, but the right hand branch performs approximately as expected. Indeed the nucleation and growth regime grows rapidly for concentrations greater than about 8% wt. This curve can now be used for comparison with the pressure drop experiments discussed in the next section.

7.2 Pressure Drop Method

The proposed pressure drop method for entering the spinodal decomposition regime is based upon our knowledge, that the high temperature phase transition is due to the large free volume difference between a polymer and a solvent. That is, as temperature is increased the solvent becomes much more expanded than the polymer. This difference can be significantly lessened by applying pressure. As discussed in Chapter 5, the phase diagram is pushed upward

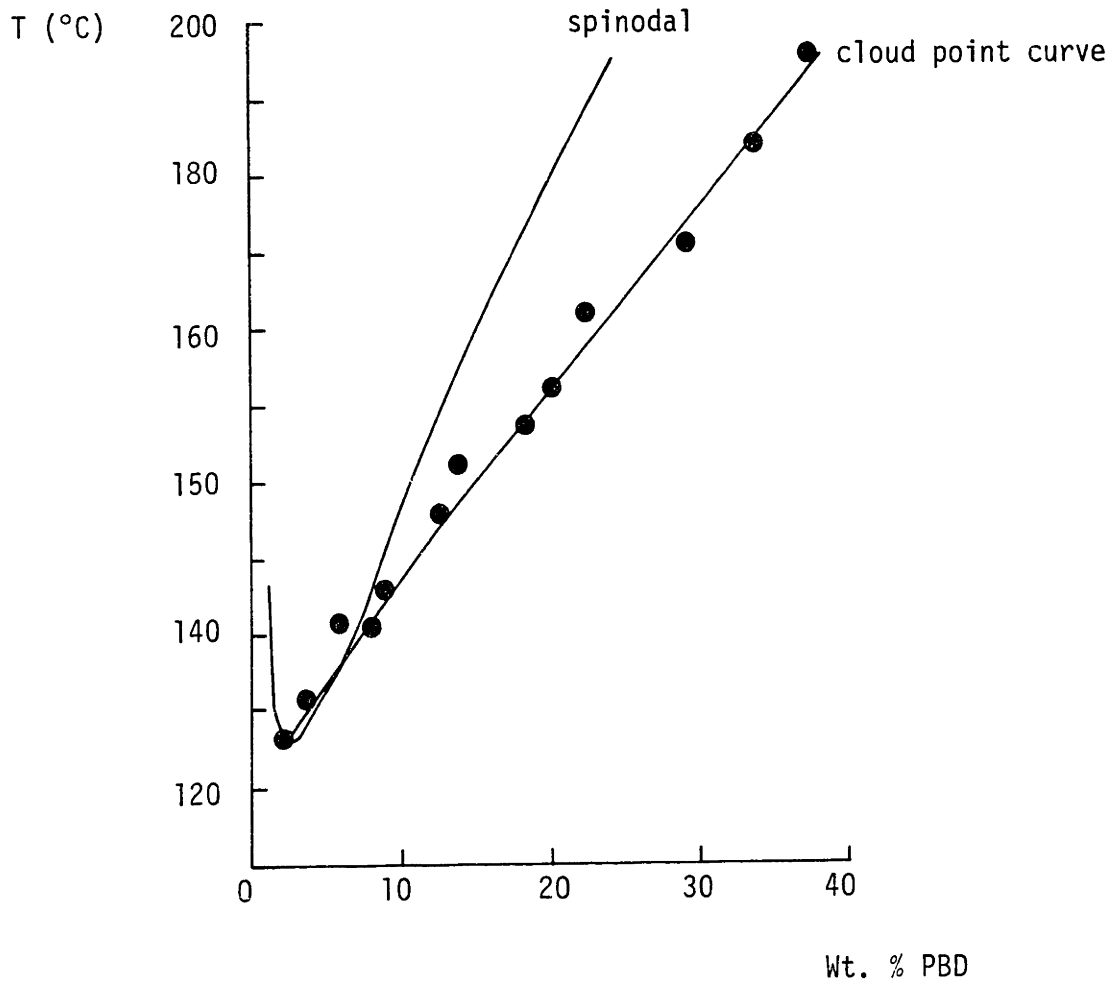


Fig. 7.2 Estimated spinodal with cloud point curve for hexane-PBD solutions.

approximately $1/2^{\circ}\text{C}$ for every atmosphere of pressure applied above the vapor pressure. This approximation is true for almost every polymer-solvent system that has been investigated to date.

Referring to Fig. 5.3, the cloud point for a 12.3% wt PBD solution is about 133°C . From Fig. 7.2 on the other hand, it appears that the spinodal for this concentration will occur at about 148°C . For safe measure however, heating was carried out to 170°C . This requires an excess pressure P_{ex} of 74 atmospheres or about 1090 psi. It was found that this pressure could be obtained at 170°C if the experimental vessel was charged to about 800 psi while at room temperature. The vessel pressure, the estimated cloud point boundary for a single concentration in temperature-pressure space, and the vapor pressure of the solution are shown schematically in Fig. 7.3. Heating samples along the vessel pressure curve then, allowed us to avoid the high temperature phase transition. Once the target temperature was reached, the pressure was dropped over some time Δt , down to the approximate vapor pressure. By this means then, the solution could be very rapidly located almost anywhere in the phase diagram. A schematic of the pressure history during the pressure drop is shown in Fig. 7.4.

These experiments were carried out in an apparatus as shown in Fig. 7.5. Because of the high pressures involved, the solution was contained in a stainless steel "bomb," so direct observations could be made only after the experiment was complete. The rather large volume of tubing allowed the hexane to evaporate and later

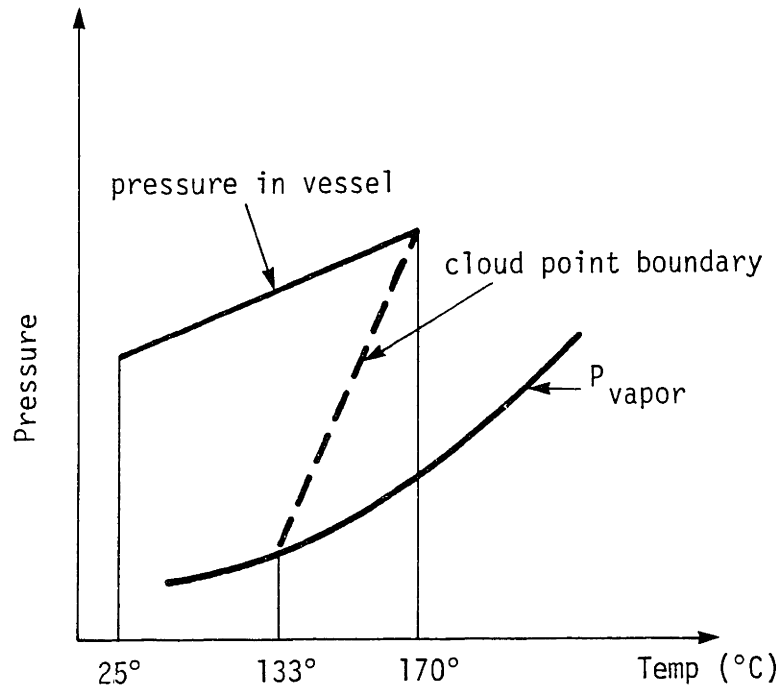


Fig. 7.3 Estimated cloud point boundary, and vessel pressure used to avoid phase transition.

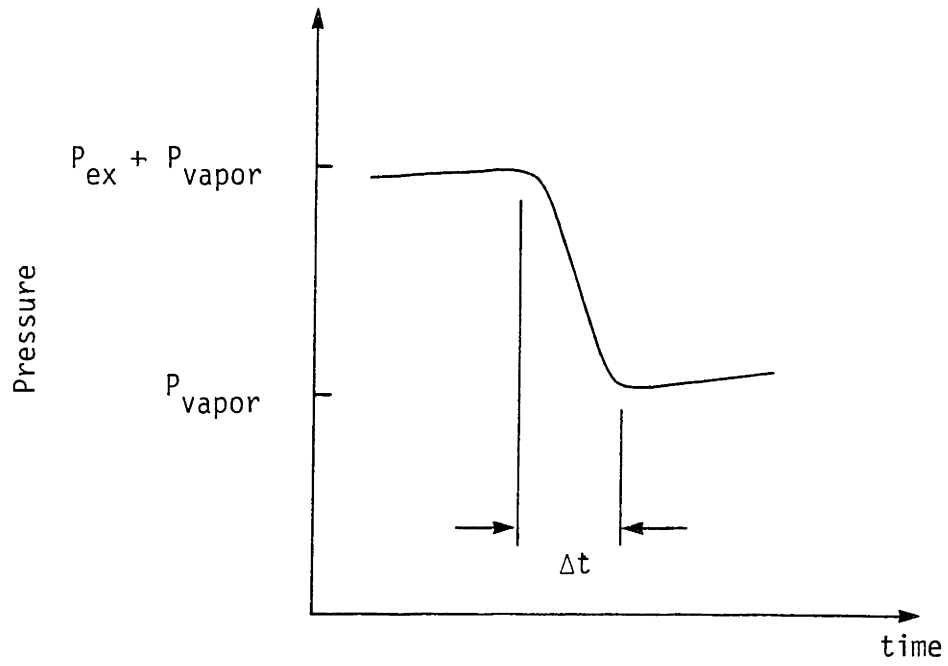


Fig. 7.4 Schematic of pressure drop over time Δt .

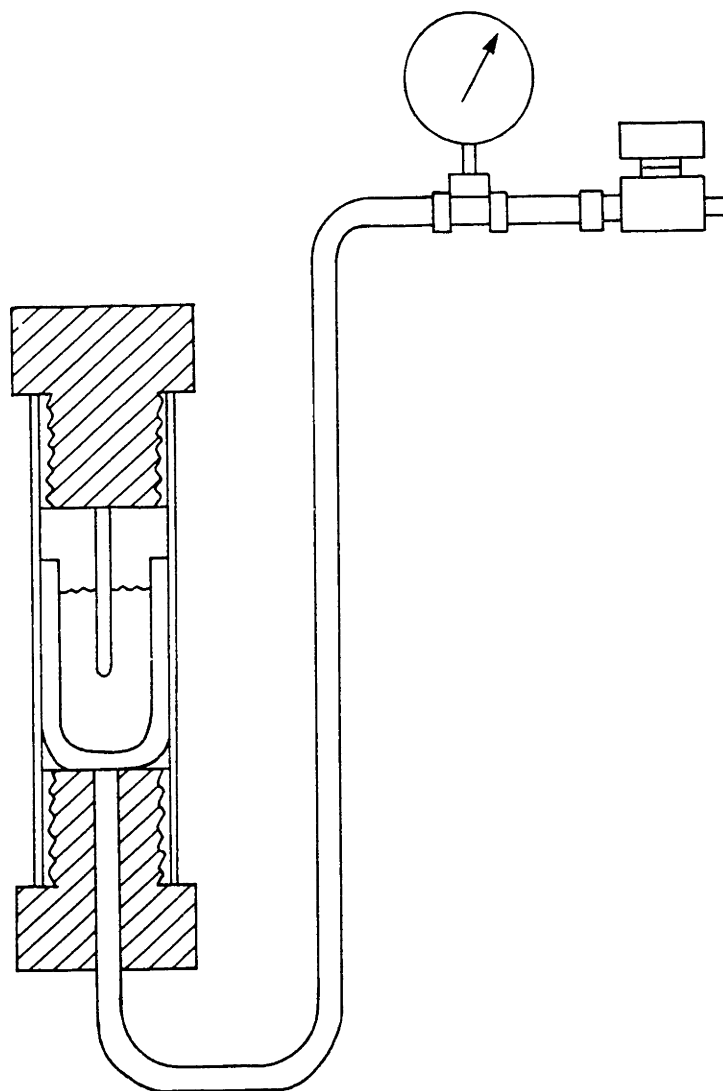


Fig. 7.5 High pressure apparatus.

condense and collect upon cooling, at the bottom of the tube. A mass balance including the collected hexane, and the hexane lost during the pressure drop allowed the calculation of the resulting concentrations.

In general it was found that very rapid pressure drops (on the order of 1 sec.) were not necessary, and in fact were undesirable because they blew rubber all over the inside of the pressure vessel. More gradual pressure drops, on the order of 12 sec. or even 35 sec. were adequate to induce substantial settlement. The gravity settlement results are shown in Fig. 7.6. On the y axis is plotted the difference between the observed concentrated phase C_{obs} , and the original concentration C_0 , divided by the difference between the equilibrium concentrated phase C'' (given in Fig. 5.9) and C_0 . So this number is zero for no separation, and one for complete separation. The fact that several points go beyond 1.0 reflect the roughness of the mass balance correction. The trend exhibited by the data however, is clear. For rapid pressure drops at temperatures above about 150°C, appreciable and in some cases complete gravity settlement can be obtained. The exact settlement times here, were not possible to observe because the sample was in a closed bomb. In all cases, however, they are less than 1/2 hr., and in reality are probably much shorter than 1/2 hr.

A second, and even more dramatic result was also obtained from these experiments, when the mass of solvent lost ΔS_ℓ , during the pressure drop was plotted for the different drop times Δt , and temperatures. These results are shown in Fig. 7.7, where S_0

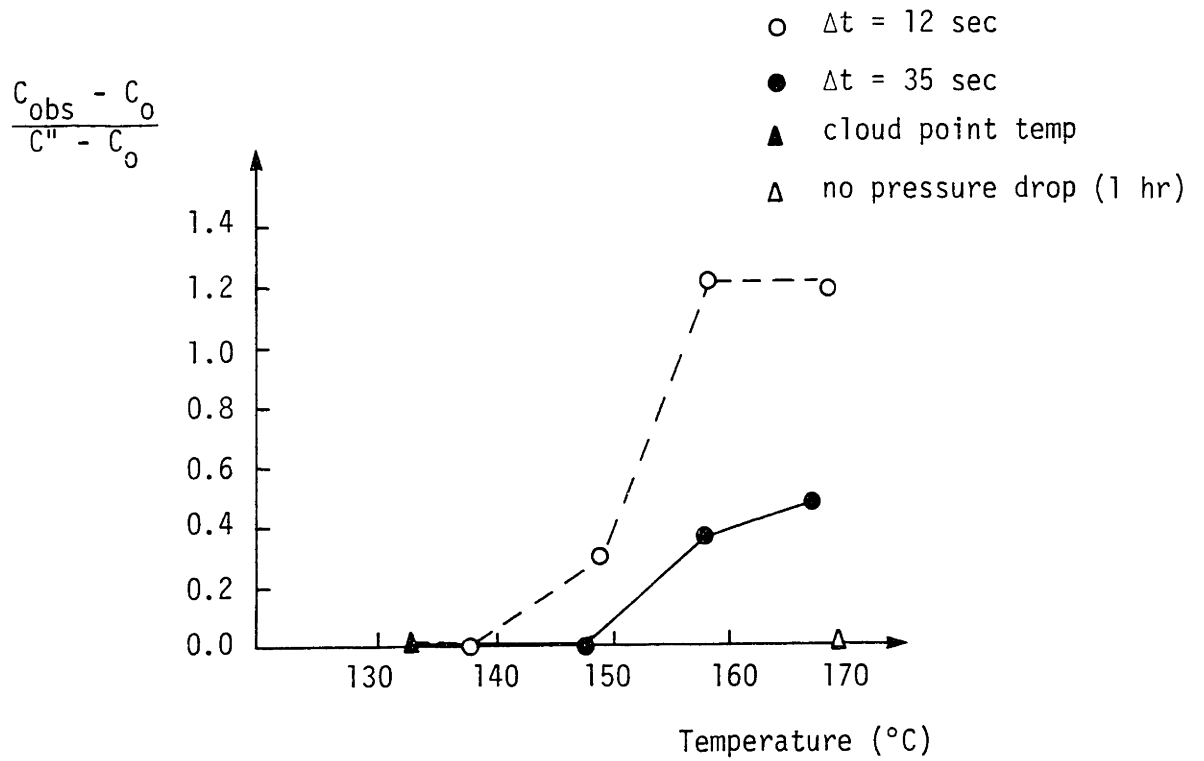


Fig. 7.6 Gravity settlement data for pressure drop experiment.

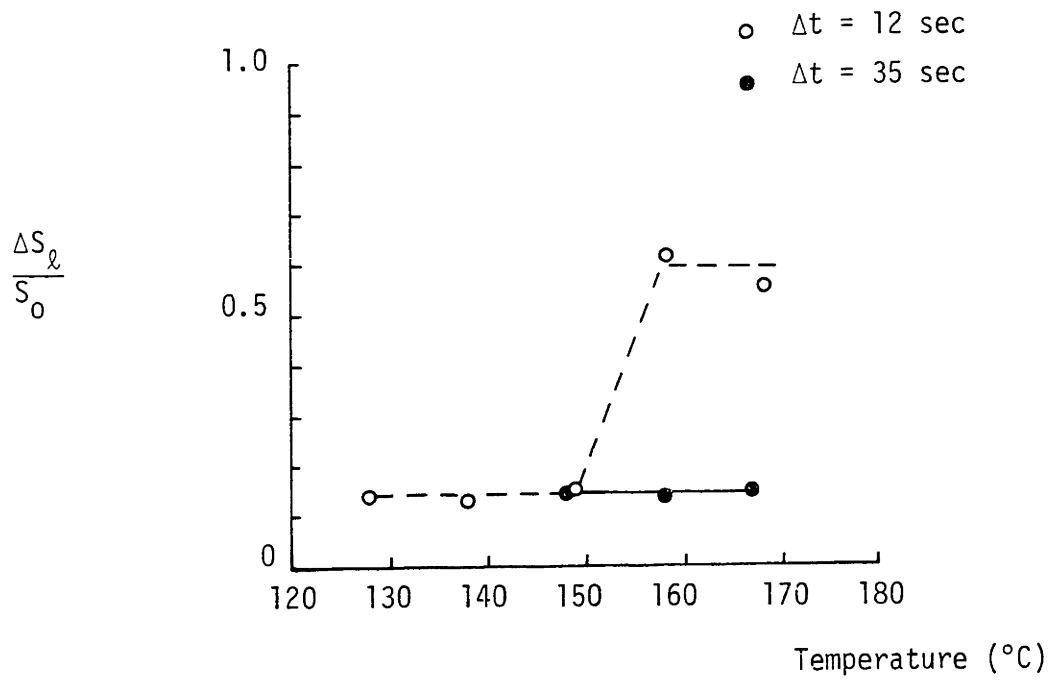


Fig. 7.7 Weight ratio of solvent lost during pressure drop.

represents the original amount of solvent. Under most circumstances, the ratio of solvent lost to the original solvent weight, stays at about 15%. When the spinodal region is entered very rapidly, however, the solvent lost ratio jumps to about 60%. This is because solvent evaporation from solutions is always diffusion limited, but when the spinodal structure is obtained, a fairly continuous pathway is created that allows solvent molecules deep below the surface almost instantaneous access to the vapor phase. Furthermore, this figure indicates that the spinodal kinetics are quite fast. For the two upper data points in Fig. 7.7 only 12 sec. were available for the solvent to escape. This indicates that the spinodal structure probably forms within times less than 12 sec.

The results of these experiments show that rapidly entering the spinodal decomposition regime dramatically changes certain transport properties associated with solutions. As we have seen, both gravity settlement, and solvent evaporation can be sped up enormously. The second observation could be used to advantage, in the spray drying of rubbers. As was mentioned earlier in Chapter 3, a heat pump cycle could be used between the evaporation and condensation of hexane to reduce the separation energy requirement. One of the problems associated with that method was the diffusion limitation on the spray drying of particles. It appears, from Fig. 7.7 that spinodal decomposition could be used to greatly accelerate the drying process. It should probably also be mentioned at this time that spray drying solutions into powdered rubber has many potential advantages for the later mixing of the rubber with other

components. Mixing is about as energy intensive as solvent separation is in the overall scheme of rubber processing. (See Appendix D).

Finally, it appears that the results in Fig. 7.6 and Fig. 7.7 indicate that the estimate of the spinodal in Fig. 7.2 for $C_0 = .123$ is approximately correct. Fig. 7.6 seems to place the spinodal somewhere between 138°C and 158°C. Fig. 7.7 would place the spinodal between 148°C and 158°C.

References, Chapter 7

- 7-1 O. Olabisi, L.M. Robeson and M.T. Shaw, Polymer-Polymer Miscibility, Academic Press (1979).
- 7-2 T. Nishi, T.T. Wang, and T.K. Kwei, "Terminally Induced Phase Separation Behavior of compatible Polymer Mixtures," Macromolecules, 8, 2, P. 227 (1975).
- 7-3 C.A. Smolders, J.J. van Aartsen, and A. Steenbergen, "Liquid-Liquid Phase Separation in Concentrated Solutions of Non-crystallizable Polymers by Spinodal Decomposition," Kolloid-Zeitschrift und Zeitschrift für Polymere, 243, p. 14 (1971).
- 7-4 P.T. van Emmerik, C.A. Smolders and W. Geymayer, "Liquid-Liquid Phase Separation in Concentrated Polymer Solutions Studied By Electron Microscopy," European Polymer Journal, 9, p. 309 (1973).
- 7-5 J.W. Gibbs, Collected Works 1, Yale University Press (1948).
- 7-6 J.W. Cahn, "Phase Separation by Spinodal Decomposition in Isotropic Systems," The Journal of Chemical Physics 42, 1, p. 93 (1965).
- 7-7 J.W. Cahn and J.E. Hilliard, "Free Energy of a Nonuniform System. I. Interfacial Free Energy," The Journal of Chemical Physics, 28, 2 p. 258 (1958).
- 7-8 J.J. van Aartsen, "Theoretical Observations on Spinodal Decomposition of Polymer Solutions," European Polymer Journal 6, p. 919 (1970).
- 7-9 R. Koningsveld, "Partial Miscibility of Multicomponent Polymer Solutions," Advances in Colloid and Interface Science, 2, p. 151 (1968).
- 7-10 G. Delmas, and P. de Saint-Romain, "Upper and Lower Critical Solution Temperatures in Polybutadiene-Alkane Systems," European Polymer Journal, 10, p. 1133 (1974).
- 7-11 D. Patterson, "Role of Free Volume Changes in Polymer Solution Thermodynamics," International Symposium on Macromolecular Chemistry, p. 449, Prague (1965).

CHAPTER 8

THE LOW ENERGY SEPARATION SCENARIO AND CONCLUSIONS

The proposed low energy separation scenario was introduced in Chapter 1, and presented in more detail in section 3.5 of Chapter 3. Chapters 4, 5, 6 and 7 then presented back up material to support and amplify the previous statements in section 3.5. In this chapter, the significance of the previous results will be summarized, with conclusions, and suggestions for future work.

8.1 The Low Energy Separation Scenario

The separation method which has been referred to in this thesis as the Low Energy Separation Scenario is a new process for separating rubbers from their solvents after solution polymerization. Based upon discussions with four major manufacturing companies who produce solution polymerized synthetic rubbers, it is the authors impression that no one is presently using this method for solvent separation^{*}. There is evidence, on the other hand, that there is significant interest among these companies to improve upon their present separation methods.

The advantage of the proposed Low Energy Separation Scenario is that it can greatly reduce the energy required for solvent separation. As energy costs rise, this issue becomes more and more important. Furthermore, the principles involved in our proposed

* Three of these companies are members of the MIT-Industry Polymer processing program which supported this research.

method are universally true and should be applicable to almost any polymer-solvent system. It is true that hexane and polybutadiene are a particularly attractive system for this method because the reactor temperature can be only a few degrees below the cloud point temperature ($\cong 13^{\circ}\text{C}$). However, other systems could be made to behave this way by altering the solvent, and/or applying pressure.

The steps involved in the Low Energy Separation Scenario can now be stated as;

- 1) bring the solution above the spinodal,
- 2) gravity separate the dilute phase from the concentrated phase,
- 3) "dry" the dilute phase
- 4) recycle the dilute phase, and
- 5) remove the remaining hexane from the concentrated phase by some evaporation technique, perhaps by using a vented barrel extruder.

These steps are slightly different from the original statement in section 3.5, because they reflect new knowledge that was gained, particularly in Chapters 6 and 7. Also note, that the steps in this process can be accomplished with existing equipment.

If the solution can be brought into the spinodal regime by simply heating (as is the case for $C_0 = .079$), the basic energy cost for this process can be expressed as

$$\bar{E} = \bar{m} C_p \Delta T + \bar{S}'' \Delta h_V \quad (8.1)$$

where \bar{E} is the energy per pound of rubber, \bar{m} is the mass of cement per pound of rubber, C_p is the heat capacity of the cement, ΔT is the temperature rise, \bar{S}'' is the mass of solvent remaining in the concentrated phase per pound of rubber, and Δh_V is the latent heat of vaporization for the solvent. Now, \bar{m} is a constant, but C_p and of course T increase with temperature, \bar{S}'' on the other hand decreases with temperature as does Δh_V^* . Consequently, the first term in equation (8.1) increases with temperature, and the second term decreases. A minimum is found at 170°C, where

$$\bar{E} = 610 \text{ BTU/lb-rubber.}$$

Variations from 170°C by $\pm 10^\circ\text{C}$ change \bar{E} by only +2%, so variations in this operating temperature do not dramatically affect the energy consumption. The viscosity of the concentrated phase at this temperature, ($C'' = .30$ for either $C_0 = .079$ or $C_0 = .123$, see Fig. 5.9) can be estimated from Fig. 6.17 to be about 5.5×10^5 c.p. This is at the lower bound for handling in a vented barrel extruder. So if a slightly higher viscosity were desired it could be obtained by increasing temperature and C'' .

* \bar{m} and \bar{S}'' can be written explicitly in terms of the known concentrations C_0 , C' and C'' as

$$\bar{m} = \frac{1}{C_0} \left[\frac{\frac{1}{C'} - \frac{1}{C''}}{\frac{1}{C'} - \frac{1}{C_0}} \right], \text{ and } \bar{S}'' = \frac{1-C''}{C''} .$$

To the approximation that the rubber in the concentrated phase is equal to the rubber in the original cement $\bar{m} = \frac{1}{C_0}$. Note that C'' increases with temperature, so \bar{S}'' decreases.

If entering the spinodal regime required the application of pressure, then a new term for compressor work would have to be added to equation (8.1). The magnitude of this term would depend upon the details as to how the pressure is applied. If the pressure is applied isothermally, then all of the compressor work W_p must be added to equation (8.1). However, if the pressure is applied primarily to the solution, and not to a large vapor space, then the pressure-volume work given below, will be small, owing to the incompressibility of the solution, i.e. $\Delta V \cong 0$.

$$W_p = P\Delta V \quad (8.2)$$

Consequently $\bar{E} = 610$ BTU/lb-rubber is a good estimate for the energy requirement for the proposed Low Energy Separation Scenario, regardless of the details as to how step one, given above, is carried out.

In fact, the pressure drop method discussed in Chapter 7 is probably not the most practical way to enter the spinodal regime. While this method will work, it will also require special equipment to handle the 1000 psi pressures. An alternative way could be employed, based upon our knowledge that a 7.9% wt. PBD solution can be heated into the spinodal regime.

This method, called the "7.9% solution," is shown in Fig. 8.1. In principle the method could work at other concentrations, but since data is available at 7.9%, it is the concentration used. Here, the reactor operates at its original high concentration (12.3%) so there is no loss in reactor efficiency. But now the reactor output

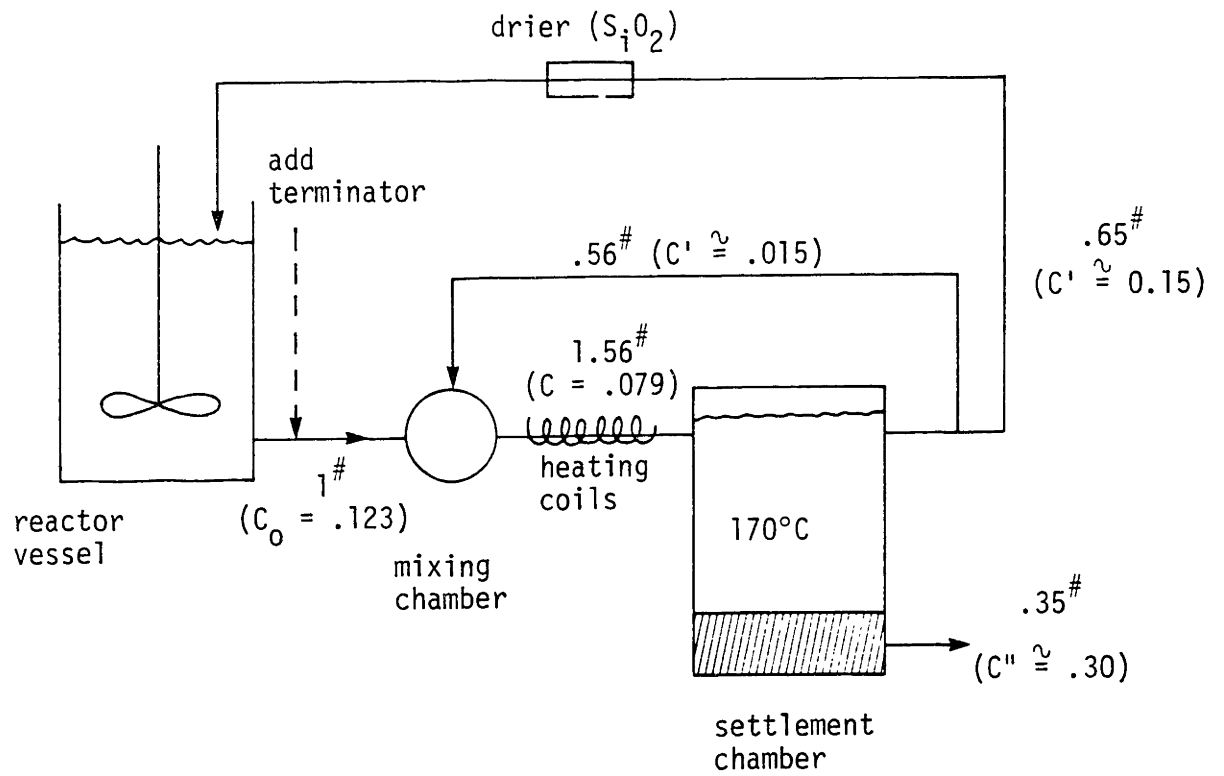


Fig. 8.1 "The 7.9% Solution"

is diluted in a mixing chamber with some of the hot dilute phase from a previous separation. Some additional heating is required, and then the diluted solution (7.9%) enters the settling tank. The concentrated phase, goes to a vented barrel extruder, and the dilute phase is split into two streams so that some goes to preheat and dilute the reactor output, and some is dried and then recycled into the reactor. In addition to speeding up gravity settlement while avoiding the pressure drop step, this method has the decided advantage of providing intimate heat transfer in the mixing chamber. This step alone makes the "7.9% solution" attractive by improving the heat transfer efficiency. For comparison, a pressure drop scenario is shown in Fig. 8.2. Note that the final outputs for the two schemes are slightly different. This is probably because, within experimental error, the coexistence curves shown in Fig. 5.9 appear to be approximately the same for $C_o = .123$ and $C_o = .079$ at 170°C , i.e. $C' = .015$ and $C'' = .30$.

The drier stage shown in both figures is included to clean up the dilute phase before recycling. This is a standard procedure for all ionic polymerizations; its intent is to eliminate all potentially troublesome polar material that may have gotten into the system. Usually this is water, but in our case, the drying material (SiO_2), may help to clean up any excess terminator. As indicated in Figs. 8.1 and 8.2, the polybutadiene reaction requires a terminator or stopper to bind with the reactive ends of the polymer chains. While this terminator is added in near stoichiometric

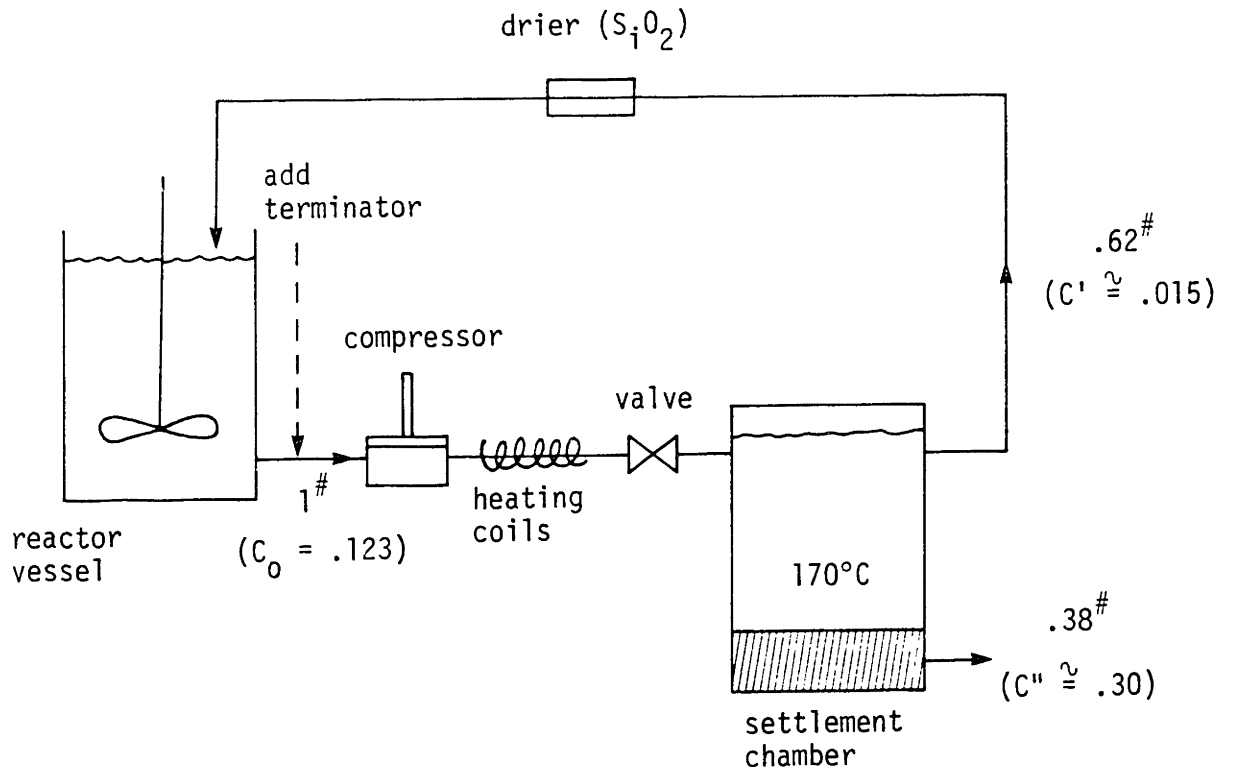


Fig. 8.2 Low energy separation scenario using pressure drop method to enter spinodal regime.

quantities, even small excesses could have an adverse affect if recycled into the reactor vessel. This result is shown in Table 8.1. These are the results of bottle polymerization trials with raw recycle (dilute phase with terminator), and dried recycle (dilute phase with terminator). The results show that raw recycle dramatically reduces the polymer conversion, whereas the dried recycle gives almost identical results to those obtained when pure hexane is used in place of the recycle.

8.2 Conclusion

The major conclusions of this thesis are listed below.

1. The proposed Low Energy Separation Scenario appears to be a feasible solvent separation method for hexane and polybutadiene systems with the potential to greatly reduce the required separation energy. Furthermore the method should be applicable to other polymer-solvent systems.
2. The dilute phase for the hexane-polybutadiene system can be recycled to the reactor vessel without affecting the polymer conversion.
3. Gravity settlement can be used as the physical separation process if the solution can be rapidly brought into the spinodal decomposition regime.
4. Rapid entry into the spinodal decomposition regime will also dramatically affect other important solution transport properties. In particular, solvent evaporation can be greatly enhanced by this method.

TABLE 8.1

Bottle Polymerization Results

<u>Sample No.</u>		<u>% Conversion</u>
1.	Control-20% butadiene in hexane	85.5%
2.	1 part hexane/9 parts 20% premix-Control	74.2%
3.	1 part dried recycle/9 parts 20% premix	74.3%
4.	1 part raw recycle/9 parts 20% premix	43.3%
5.	1 part hexane/4 parts 20% premix-Control	70.7%
6.	1 part dried recycle/4 parts 20% premix	71.4%
7.	1 part raw recycle/4 parts 20% premix	0.3%
8.	Control-20% butadiene in hexane	91.3%
9.	1 part hexane/9 parts 20% premix-Control	85.5%
10.	1 part dried recycle/9 parts 20% premix	86.4%
11.	1 part raw recycle/9 parts 20% premix	65.9%
12.	1 part hexane/4 parts 20% premix-Control	78.9%
13.	1 part dried recycle/4 parts 20% premix	76.8%
14.	1 part raw recycle/4 parts 20% premix	5.9%

A brief description of a possible separation scenario based upon rapid solvent separation is given in Appendix D.

8.3 Future Work

In spite of the optimistic conclusions just presented, considerable work is still needed before the proposed Low Energy Separation Scenario could be used as an actual industrial process. The first step would require scaling up the process and performing the required steps on a continuous basis. In the process shown in Fig. 8.1, the gravity settlement behavior is likely to be greatly affected by the temperature history and residence time in the mixing chamber and heating section. And, of course, the settlement time will be a function of the settlement chamber size. Furthermore, recycling of the dilute phase may cause a build up of low molecular weight material in the reactor. This will likely manifest itself by a shift in the molecular weight distribution for the "cement" exiting from the reactor. As a consequence, the cloud point curve will also probably shift, requiring an adjustment in operating conditions. Since some of the low molecular weight material also goes with the concentrated phase, the issue of low molecular weight build-up is not seen as a serious one, but only as a subtle one that may require some small adjustment to deal with it on a continuous basis.

Finally, if the pressure drop method is employed, many additional details concerning the pressure-temperature behavior of the solution would be desirable. The experiments in Chapter 7 were performed

using a rather conservative excess pressure. An actual investigation of the cloud point boundary in pressure-temperature space would provide useful information to determine optimum operating conditions.

In addition to the many problems to be solved in order to implement an actual industrial process based on the Low Energy Separation Scenario, some of the work in this thesis raises more open ended questions. These questions might be more of a scientific interest, but with potential practical payoffs. The whole issue of polymer solution behavior in the spinodal regime appears to be one that is rich with possibilities but until now has received very little attention. It is probable that many different transport properties of polymer-solvent solutions could be dramatically altered by use or avoidance of the spinodal decomposition regime. In addition some unique polymeric structures might be obtainable in the spinodal regime. Some examples that come to mind are paint drying, the formation of porous membranes, and the formation of interpenetrating polymer-polymer networks.

APPENDIX A

VORTEX REACTOR VESSEL

This appendix describes some of the theoretical and experimental aspects of a special reactor vessel with a cooled, rotating inner core (See Figure 3.1 in Chapter 3). The original motivation for such a vessel was to improve heat transfer from a reacting, hot, viscous liquid to the cooled walls and core. Later, when separation by the high temperature phase transition was being considered, this vessel was evaluated for heating rather than cooling. In principle, the applications are similar but not identical. The chief difference is due to the accumulation of high molecular weight, viscous material near the cooled walls.* This additional thermal resistance greatly reduces the heat transfer coefficient for cooling applications. For example, Kenics [A-1] advertises an overall heat transfer coefficient of 20-60 BTU/hr.ft².°F for heating a polymer melt in their STATIC MIXER; for cooling, they only advertise a value of 10-20 BTU/hr.ft².°F. In many cases reactor vessel walls are scraped to reduce this problem. This appendix does not directly address the polymer fouling problem, and in fact all of the data presented here are for the heating rather than the cooling application.

A.1 Fluid Mechanics

Consider the motion of a fluid confined to the annulus between two concentric cylinders. At low rotational rates ω , the flow is laminar

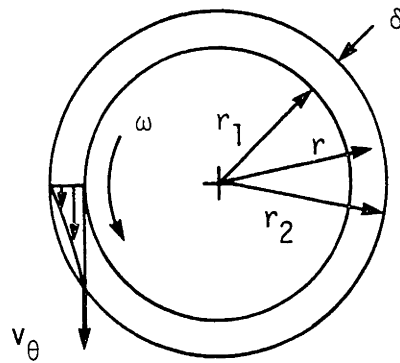
*In a reactor vessel, the no slip boundary condition at the wall gives the reacting species infinite residence time. This means high molecular weight material will accumulate here. Furthermore, for either a reacting or non-reacting system the lower temperature at the cooled wall will increase the viscosity of the system.

and the linearized Navier-Stokes equations can be solved exactly [A-2]. Here, only the v_{θ} fluid velocity component is important and it varies parabolically between the walls, see Figure A.1. As the rotational rate is increased, however, a fluid instability will occur. This instability will manifest itself as ring vortex pairs, see Figure A.2. Their significant feature is that they contribute a nonzero v_r component to the fluid motion [A-3], thereby affecting both the heat transfer and the mixing of fluids in the annulus. G. I. Taylor solved this instability problem in 1923 [A-4]. He predicted the onset of instability to occur at a precise value of a dimensionless group we now call the Taylor Number, Ta . For an infinitely narrow gap, the critical Taylor Number is:

$$Ta_c = \frac{\omega R \delta}{\nu} \sqrt{\frac{\delta}{R}} = 41.3 \quad (A.1.)$$

where the terms in equation (A.1) are defined in Figure A.1. (For finite narrow gaps Haas and Nissan [A.5] give a corrected Ta_c , which in general is slightly higher than 41.3)

For a given geometry, equation (A.1) predicts the critical rotational rate to increase linearly with viscosity. Consequently, viscous liquids, such as the one's we are concerned with, require very high rotational rates to produce this instability. Rotz and Suh [A.6] suggested grooving the inner core to lower the instability criterion. Their finite difference program and experimental results suggest that the vortices generated in the grooved core annulus are now a stable feature of the flow field. In this case the vortex size grows with increasing rotational rate. While their goal was to analyse the effect of these vortex motions on mixing, we are concerned here with the effect of these motions on heat transfer.



$$v_\theta = \frac{r_1^2 \omega}{r_2^2 - r_1^2} \left(\frac{r_2^2}{r} - r \right)$$

$$Ta = \frac{\omega \bar{R} \delta}{\nu} \sqrt{\frac{\delta}{\bar{R}}} < 41.3$$

$$\bar{R} = \frac{r_1 + r_2}{2}$$

Fig. A.1 Laminar motion of a fluid of kinematic viscosity ν in a gap between two concentric cylinders.

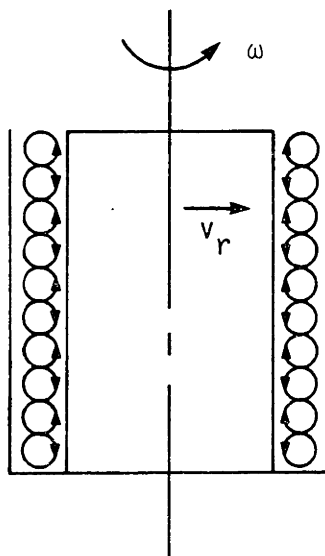


Fig. A.2 Vortex instability between concentric cylinders.

A.2 Heat Transfer

While we are interested in heat transfer from the core and walls of the vessel shown in Figure 3.1 to a fluid (or to the walls and core for the cooling case), considerable work has been already done for a slightly different case for vessels with essentially smooth walls. This is the case of heat transfer across the gap from the inner cylinder to the outer one. This existing work offers us an excellent opportunity to compare the expected heat transfer characteristics of a grooved core vessel with these known results. This comparison will be presented in this and the next sections.

Heat transfer across an air gap with Taylor vortices has been analysed in considerable detail [A-5, 7, 8, 9]. This problem is of practical importance to the functioning of electric motors. In this case the goal is to transfer heat from the inner cylinder (the motor), through the air gap and outer cylinder (motor housing), to the atmosphere. At $Ta < Ta_c$ heat transfer through the air gap is by conduction. However at $Ta > Ta_c$, $v_r \neq 0$, and we now have a fluid velocity component in the direction of the temperature gradient $\partial T/\partial r$. As a consequence, heat transfer is now by convection and improves with increasing rotational rate. In this region it has been found for vessels with an essentially smooth inner core that [A-5, 7, 8, 9]

$$Nu \sim Ta^n \quad (A.2)$$

where,

$$Nu = \frac{2\delta h}{k}, \text{ is the Nusselt Number,}$$

h = heat transfer coefficient

k = thermal conductivity

δ = gap width,

and n is on the order of 1 to 1/2. For air $n \approx .9$ from Ta_c to about $2Ta_c$, and $n \approx .5$ beyond $2Ta_c$ [A-5]. This transition may be due to higher harmonics which distort the vortex motions. (In his book, Schlichting [A-3], shows photographs of the vortex motion at Ta_c and $3.4 Ta_c$. At the later value there is a clear waviness, due to higher harmonics, to the vortex motion.) At very high rotational rates the fluid motion becomes more and more disordered - approaching turbulence, but still with a strong periodic component [A-10].

For fluids other than air, it has been reported that n is a function of the kinematic viscosity ν , with no explanation why this should be [A-5]. In general, however, it was found that $n \approx 1$ for $\nu > \nu_{\text{air}}$ and $n \approx 1/2$ for $\nu < \nu_{\text{air}}$. The data trends reproduced from [A-5] are shown in Figure A.3. One possible explanation for this data (see the original paper for the actual data) is that there are only two slopes; $n \approx 1$ when the vortex is formed, and $n \approx 1/2$ after higher harmonics appear, and that increasing ν has the effect of delaying the higher harmonics. If this is so, then a continuation of the data for the higher viscosity liquids should show a knee with a second slope of about 1/2. Such data maybe difficult to obtain, however, due to viscous heating effects. Similarly, the lower viscosity fluid (30% glycerol) may have experienced a transition to higher harmonics at a Taylor number very close to Ta_c , resulting in an overall slope near 1/2.*

*Of course other explanations of the data trends in Figure A.3 are possible. Obviously, if one is serious about this, much more work it needed to explain the kinematic viscosity effect on heat transfer.

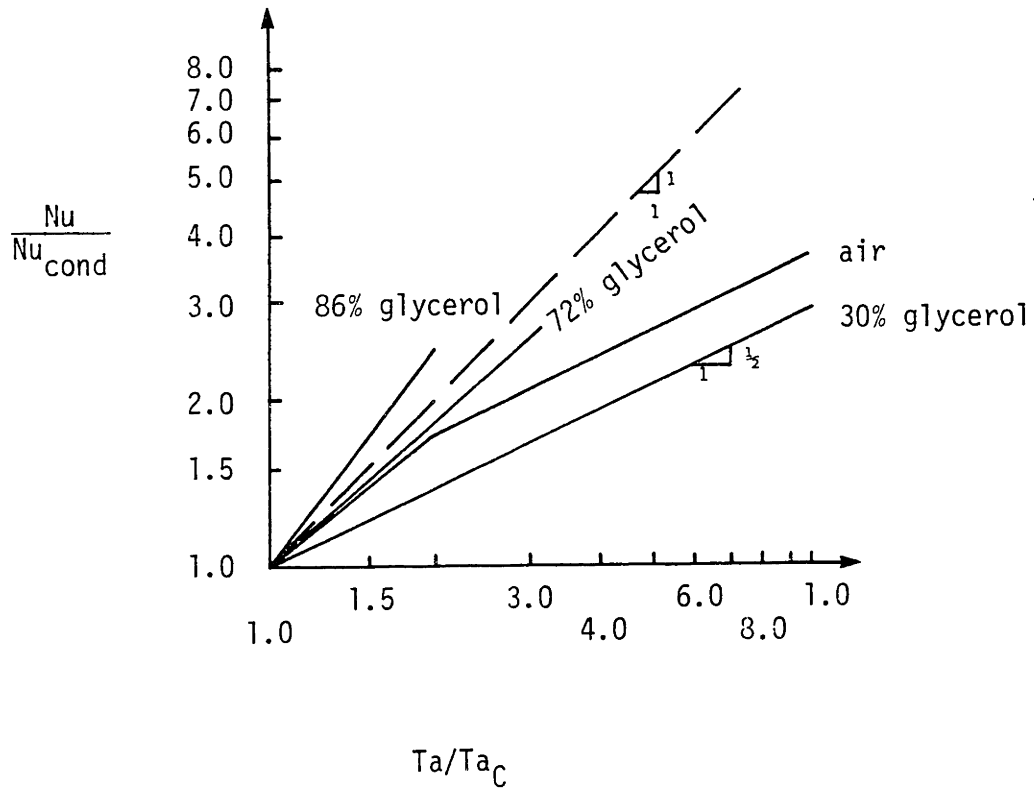


Fig. A.3 Comparison of heat transfer across-the-gap results for different fluids [A-5].

To gain some insight into this across-the-gap heat transfer situation, and learn how the grooved core vessel might compare with the data just presented, a simple mathematical model is developed in the next section.

A.3 Mathematical Model

This development, based upon the idealization which is shown schematically in Figure A.4, follows the work of Cole [A-11]. Our goal, is to determine the heat transfer across a circular gap that contains a vortex. The fluid in the gap has properties; density ρ , viscosity μ , heat capacity C_p , and thermal conductivity k . The circular gap is of radius R .

Consider a potential vortex in the circular groove of magnitude

$$\bar{v}_\theta = \frac{\Gamma}{2\pi r} \hat{e}_\theta.$$

where \hat{e}_θ is a unit vector in the θ direction, and Γ is a constant. Substitution into the energy equation, and elimination of unimportant terms yield

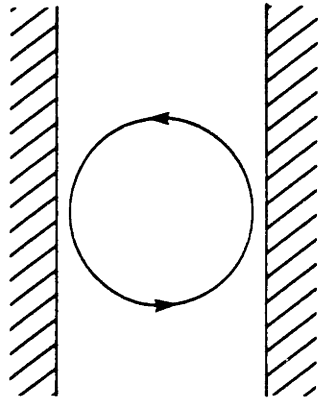
$$\frac{\Gamma}{2\pi r^2} \frac{\partial T}{\partial \theta} = \alpha \left\{ \frac{\partial^2 T}{\partial r^2} + \frac{1}{r} \frac{\partial T}{\partial r} + \frac{1}{r^2} \frac{\partial^2 T}{\partial \theta^2} \right\}.$$

where

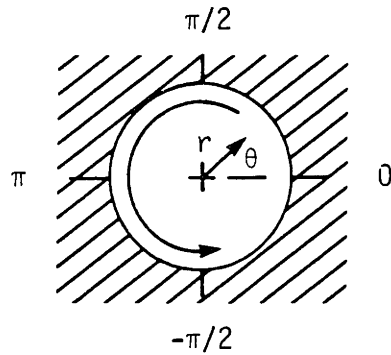
$$\alpha = k/\rho C_p.$$

This can be solved by separation of variables, i.e. $T(r,\theta) = f(r)g(\theta)$, and leads to two linear differential equations, one with constant coefficients, and one with variable coefficients. The general solution is

$$T(r,\theta) = \sum_{n=-\infty}^{n=+\infty} C_n r^{\sqrt{n^2 - \frac{i n \Gamma}{2\pi \alpha}}} e^{i n \theta}.$$



Vortex in annulus gap



Vortex in idealized circular gap

Fig. A.4 Real case, and idealized case for mathematical model.

where the constants C_n are to be determined by boundary conditions. A particularly convenient boundary condition to solve for is:

$$T = T_0 \cos \theta, \quad r = R = 1$$

We can match this with the special case ($n=1$), and obtain

$$T = T_0 r^{\sqrt{1+iPe}} e^{i\theta} \quad (\text{real part}).$$

Note that

$$\frac{\Gamma}{2\pi\alpha} = \frac{VR\rho}{\mu} \frac{Cp\mu}{k} = Pe = Re_{\text{vortex}} Pr,$$

where

$Pe = \text{Peclet No.}$, and $Pr = \text{Prandtl No.}$, and V is a characteristic velocity for the vortex.

Also since

$$h_{\theta} = \frac{k (\partial T / \partial r)_{r=1}}{2T_0}$$

and

$$h = \int_{-\frac{\pi}{2}}^{\frac{\pi}{2}} h_{\theta} d\theta$$

we can obtain Nu by taking only the real part of our result. So

$$Nu = \frac{2hR}{k} = 2 \sqrt{\frac{1 + \sqrt{1 + Pe^2}}{2}}$$

For $V=0$ we obtain the conduction result

$$Nu_{\text{cond}} = 2, \quad (\text{A.3})$$

and for $Pe \gg 1$, we obtain

$$\frac{Nu}{Nu_{cond}} = \frac{1}{\sqrt{2}} \sqrt{Re_{vortex} Pr} \quad (A.4)$$

Note that Cole obtained a similar result for solid body rotation in the circular groove.*

Now in order to match this result with the experimental observations of others, we need some relationship between Re_{vortex} and Ta . For a given geometry and fluid then, we are interested in how V_{vortex} varies with the rotational rate of the inner cylinder ω . Unfortunately, there is no easy way to make this estimate for the smooth cylinder case. Based upon our previous observation that $n \approx 1$ in equation (A.2) for some of the cases shown in Figure A.3, we might expect that

$$V_{vortex} \sim \omega^2 \quad (A.5)$$

But this remains to be confirmed for the smooth core case.

For the grooved core case, on the other hand, there is some evidence that equation (A.5) is correct. For example if we assume that the vortex in the grooved annulus are driven by an invicid pressure gradient, then

$$\frac{\partial p}{\partial r} \approx \rho \omega^2 r,$$

and if this is resisted by viscosity at the grooved wall

$$\nabla p \approx \mu \nabla^2 v$$

then a relationship like equation (A.5) is obtained. Also, by a finite difference method Rotz [A-12] obtained a similar result for viscous

*These results, given in equations (A.3) and (A.4), exhibit the same trends as often found in the literature. That is, in the absence of the vortex motion, heat transfer is by conduction across the gap. After the vortex is formed, heat transfer improves monotonically as a function of the "vigor" of the vortex motion. The condition $Pe \gg 1$ is easy to satisfy for almost all fluids except liquid metals.

liquids in a grooved core vessel. Therefore, it seems likely that equation (A.5) is reasonably correct for a range of liquids in the grooved core vessel. Furthermore, if the idealizations shown in Figure A.4 are approximately correct, i.e. the vortex fills the annular gap, then it is reasonable to expect, based on these velocity arguments, that

$$\text{Nu} \sim \text{Ta}^1 \quad (\text{A.6})$$

for across-the-gap heat transfer in a grooved core vessel. There remains, of course, the issue of the constant in equation (A.6). In general though, this result compares favorably with the results for the smooth core vessels and suggests that the grooved core vessel may perform well as a heat transfer device.

The actual mode of heat transfer we are interested in, as mentioned earlier, is not across-the-gap. So while this analysis may give some indication of the expected performance of a grooved core vessel as compared to a smooth core vessel, it can not be compared directly to the experimental results discussed in the next section.

A.4 Experimental Results

A device like the one shown in Figure 3.1 was designed and built here at M.I.T., and shipped to the Goodyear Tire and Rubber Co. for testing. The results reported here are for heating a solution of hexane and polybutadiene - and in separate runs - pure hexane in the annulus. Heating was accomplished from the core, with the outer cylinder insulated. The solution, or solvent, was pumped through the device during heating. This situation deviates substantially from the previous theoretical analysis. The major differences are;

1. since the fluid is being pumped through the annulus, there is now an axial flow component, as well as a rotational flow component,
2. heat transfer is not across the gap, but from the core to the fluid, and
3. the high rotational rates generated substantial viscous heating.

Heat transfer coefficients were determined by noting the inlet and outlet temperatures of the solution (or solvent) and the glycol through the core, and taking the log mean temperature difference. The heat of agitation was subtracted from the heat input at high rotational rates, so that the overall heat transfer coefficient U was calculated as follows

$$U = (Q_h - Q_a) / A \Delta T_{LM} \quad (A.7)$$

where

$Q_h = MC_p \Delta T$ is the observed heating of the solution

Q_a = the heat of agitation (see Figure A-8)

A = area of core

ΔT_{LM} = log mean temperature difference (see [A-13]).

The range of axial Reynolds numbers Re , and rotational Taylor's numbers are shown in Figure A.5. The heat transfer results are given in Figure A.6.

The effect of axial flow is to retard, and in the extreme to completely prevent the vortex instability [A-7]. This is illustrated by

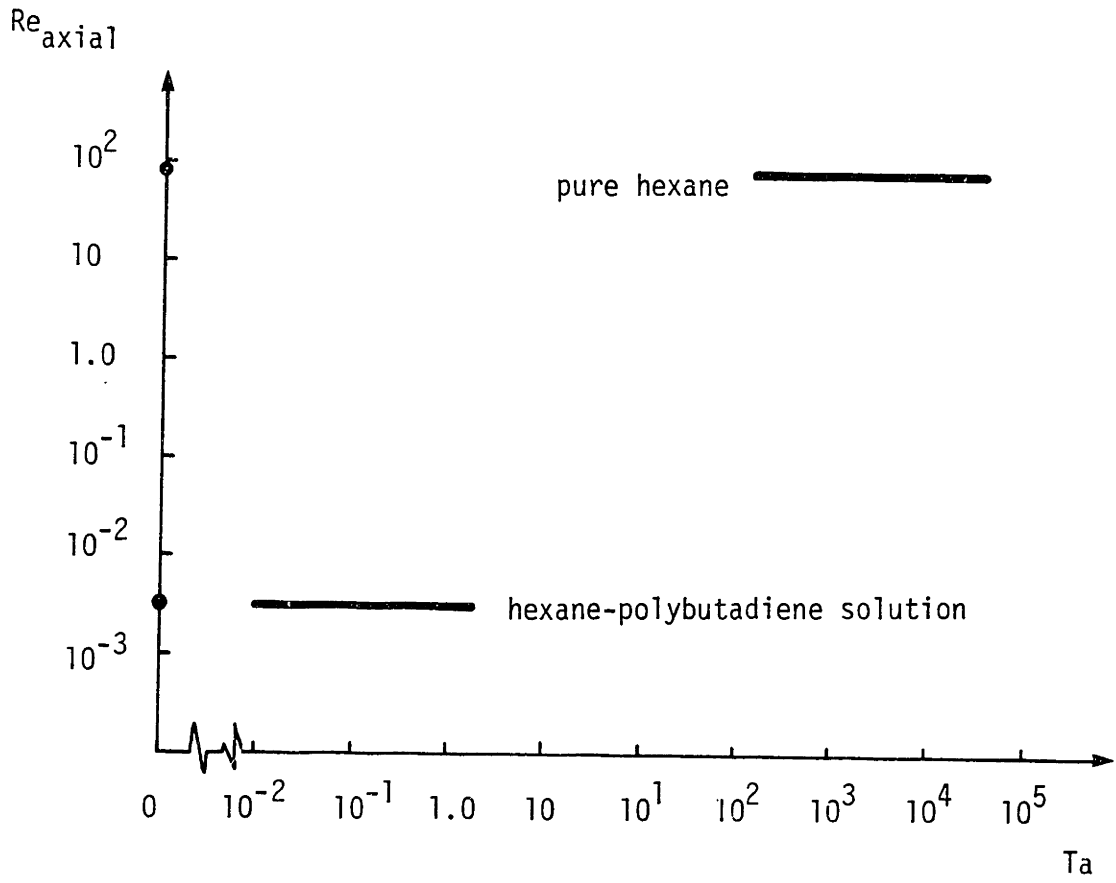


Fig. A.5 Range of Re_{axial} and Ta for experiments.

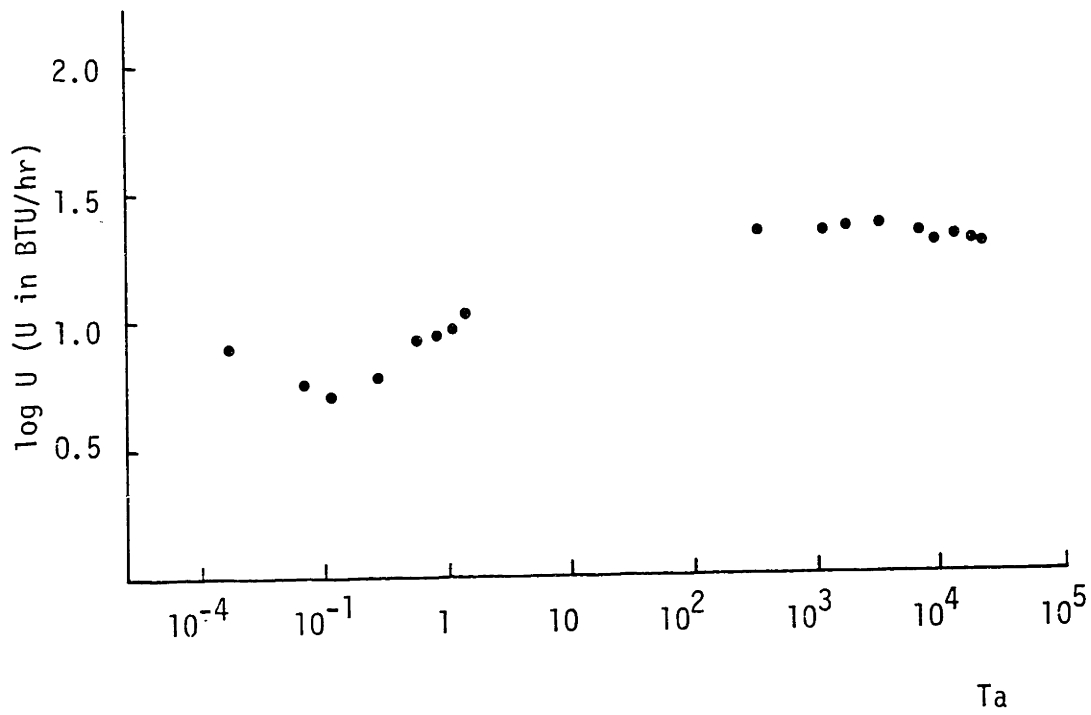


Fig. A.6 Heat transfer results for vortex reactor.

the heat transfer data for pure hexane in Figure A.6. Here U is independent of Ta , and the axial flow condition completely dominates-at a relatively small value of Re . Becker and Kaye [A-7] show that for an equivalent smooth core vessel, with an equivalent $Re = 92.5$, the vortex would be delayed until $Ta = 120$ but not obliterated as is the case with our grooved core vessel. It seems safe to speculate that the low viscosity hexane can not follow the contour of the core, which causes separated flow.

The data for the 13% solution, shown in Figure A.6 and again in Figure A.7 exhibits a trend which was not expected. Heat transfer was best with the core stationary (not shown in Figure A.7, the point would plot at $\log U = 1.11$) and at very high rotational rates (1000 RPM; $Ta = 1.8$). The later effect is what we sought and should be due to vortex pairs in the grooves. The first effect is due to a radial velocity component of the flow at both low Re_{axial} and low Ta .

That is, at $Re_{axial} = 5 \times 10^{-3}$, $Ta = 0$ it is probably true that the solution faithfully followed the contour of the core (shown in Figure 3.1). This gives rise to a nonzero radial velocity component which is in the direction of the temperature gradient. As a consequence heat transfer is quite good.

Now as the core is rotated, Ta increases, and a new component must be added to the fluid velocity vector in the annulus. This new component, the circumferential one, grows with increasing rotational rate, and eventually dominates all other components. This all takes place in the laminar region ($\omega < 100 \text{rpm}$) and results in reducing the

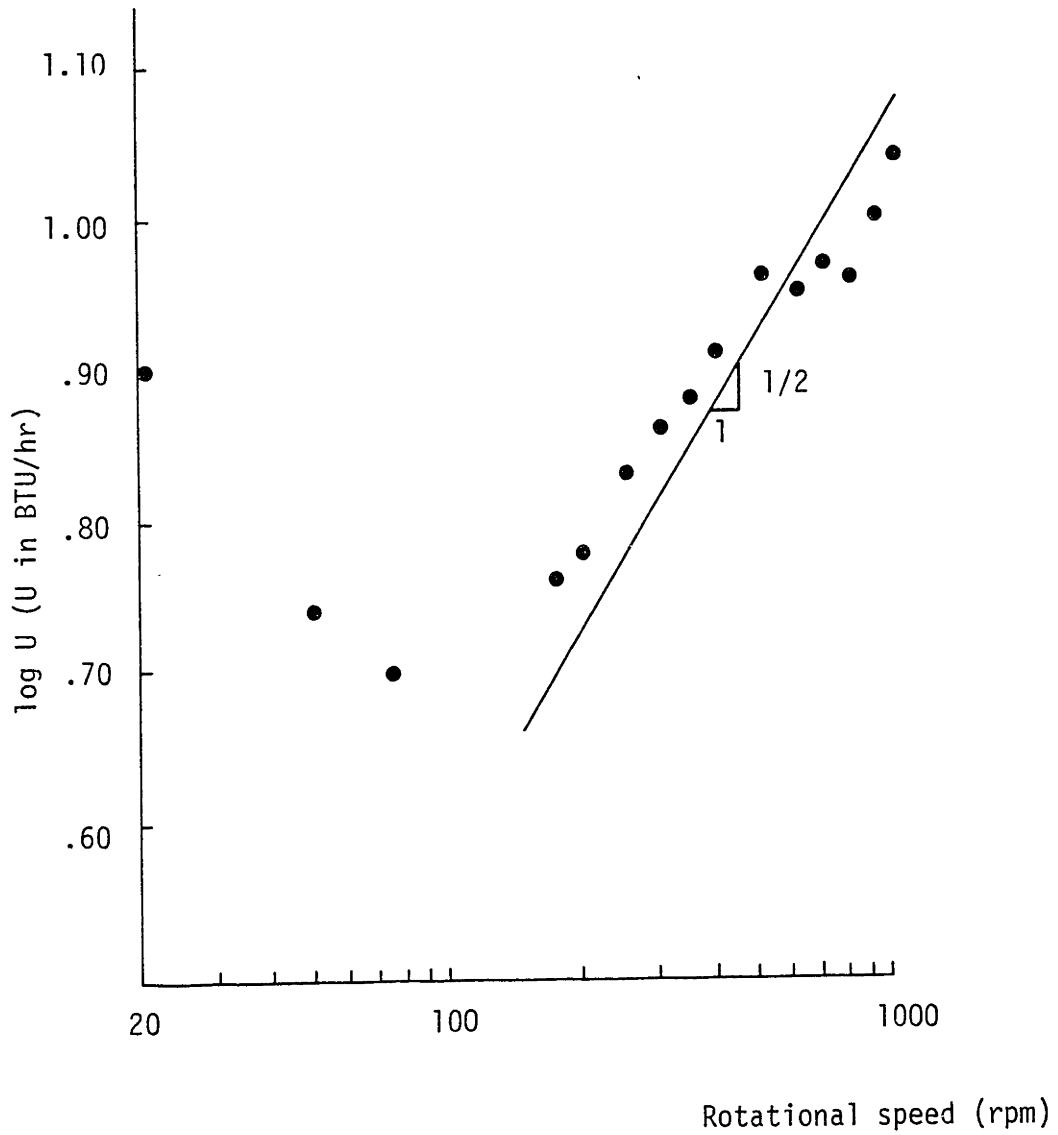


Fig. A.7 Heat transfer results for 13% Wt. PBD solution in vortex reactor.

heat transfer coefficient.

Now at still higher rotational rates the vortex pairs grow and begin to dominate the heat transfer behavior. As a consequence heat transfer now improves with increasing ω .

Note that the rather high rotational rates shown in Figure A.7 (200 to 1000 rpm) correspond to very low values of Ta , i.e. 0.4 to 1.8. For an equivalent smooth cylinder, using a modified criteria for finite narrow gaps given by Haas and Nissan [A-5], one would not expect vortices until $Ta \geq 60.6$. So the data in Figure A.7 indicates that grooving the inner cylinder significantly reduces the rotational rates required to produce vortices in the annulus.*

The slope of the line shown in Figure A.7 is 1/2 (note the scale difference for the two axes in the figure) suggesting that

$$Nu \sim Ta^{1/2}. \quad (A.8)$$

As already mentioned, it is not possible to compare this result directly with the across-the-gap model because of the many dissimilarities between the two cases. This rather weak power dependency, however, along with the rather high viscous heating effect shown in Figure A.8 make the proposed device quite unattractive for any cooling application.

*To confirm the existence of the vortices, we constructed a geometrically similar device with glass walls and observed the motion of neutrally bouyant particles. With the aid of a strobe light, vortices could be seen at Taylor numbers on the order of one.

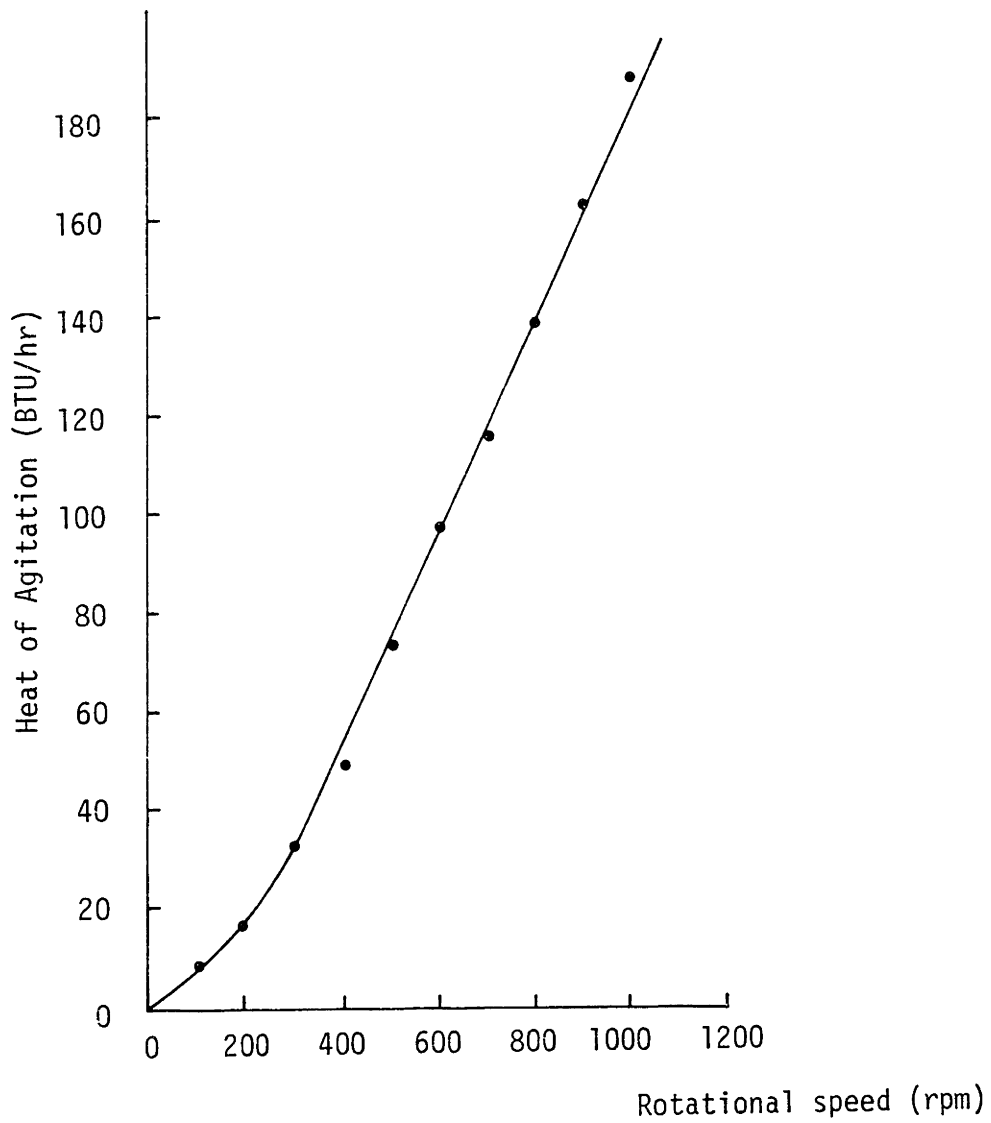


Fig. A.8 Viscous heating effect for vortex reactor (13% Wt. PBD solution).

In conclusion then, as far as the original intention of the grooved core device is concerned, this device suffers from the same problem all vessels of this type have. Namely, that viscous heating and heat transfer are coupled (as discussed in Chapter 3), so improving heat transfer by increasing the rotational rate as indicated in equation (A.8) will also result in significant viscous heating, as shown in Figure A.8. For heating applications, on the other hand, where the shear in the device does not degrade the fluid, this device should perform quite well.

REFERENCES

FOR APPENDIX A

- A-1 S.J. Chen "Heat Transfer and Thermal Homogenization of Viscous Flow in the Static Mixer Unit" Kenics Corp. KTEK-3, One Southside Road, Danvers, Mass. 01923 (1972)
- A-2 M.C. Potter and J.F. Foss, Fluid Mechanics Ronald Press N.Y. p.286 (1975)
- A-3 H. Schlichting, Boundary Layer Theory 6th ed. McGraw-Hill Book Co. N.Y. p.440 (1968)
- A-4 G.I. Taylor, "Stability of a Viscous Liquid contained between Two Rotating Cylinders", Phil. Trans. R. Soc. London, Series A 223 p.289 (1923)
- A-5 F.C. Haas and A.H. Nissan, "The Effects of Onset of Taylor Vortices on Heat Transfer" 1961 International Heat Transfer Conference, University of Colorado, Boulder ASME, N.Y. p. 643 (1961)
- A-6 C.R. Rotz and N.P. Suh, "New Techniques for Mixing Reacting Liquids, Part I. Mechanical Means to Improved Laminar Mixing", Polymer Engineering and Science, 16 10, (1976)
- A-7 K.M. Becker and J. Kaye, "Measurement of Diabatic Flow in a Annulus With an Inner Rotating Cylinder" TRANS. ASME, J. Heat Transfer p.97 (May 1962)
- A-8 C. Gazley, "Heat-Transfer Characteristics of the Rotational and Axial Flow Between Concentric Cylinders" TRANS. ASME p.79 (Jan. 1958)
- A-9 I.S. Bjorklund and W.M. Kays, "Heat Transfer Between Concentric Rotating Cylinders", TRANS. ASME J. Heat Transfer p.175 (Aug. 1959)
- A-10 J. Kaye and E.C. Elgar, "Modes of Adiabatic and Diabatic Fluid Flow in an Annulus with an Inner Rotating Cylinder", ASME Transactions 80 p.753 (1958)

- A-11 J.D. Cole "Note on the Effect of Circulation in Heat Transfer"
USAF Proj. Rand. R. Memo RM-1351 (24 Sept. 1954)
- A-12 C.A. Rotz, " A Generalized Approach to Increased Mixing
Efficiency for Viscous Liquids", S.M. thesis M.I.T. (1976)
- A-13 R.B. Bird, W.E. Steward, and E.N. Lightfoot, Transport
Phenomena, Wiley (1960)

APPENDIX B

FREE VOLUME THEORIES

In our discussion of the Flory-Huggins Theory in Chapter 4 it was pointed out that the main conceptual shortcoming of this theory was its implicit assumption that there is no volume change upon mixing, i.e. $\Delta V_M = 0$. This is contrary to known observations [B-1]. This problem manifests itself in our inability to properly estimate the temperature and concentration dependence of the interaction parameter g . Since this was written as (see equation 4.42)

$$g = \frac{z}{kT} [\Delta w_{12} - T \Delta s_{12}], \quad (\text{B.1})$$

our problem boils down to that of adequately describing certain thermodynamic mixing functions.

This problem has been tackled by Prigogine, Flory and Patterson [B-2, 3, 4] who started out by noting that the desired mixing functions only depend upon molecular configurational properties.

By configurational properties, we mean those thermodynamic properties that are controlled by the low frequency, high amplitude molecular motions that affect the volume. These include rotations and translations, and the low frequency torsional oscillations of chain molecules. High frequency bond stretching and other internal modes aren't important; they don't contribute to the mixing function [B-2]. These types of molecular motions can be effectively related to the

macroscopic thermodynamic properties we are interested in by statistical mechanics.

The starting point here is to determine the configurational partition function Q , which relates the kinetic and potential energies of molecules to the configurational thermodynamic variables. For example the configurational Helmholtz free energy F_{conf} can be related to Q as [B-2]

$$F_{\text{conf}} = -kT \ln Q \quad (\text{B.2})$$

where

$$Q = \frac{1}{N! h^{3N}} \int e^{-\frac{H}{kT}} d\bar{r}^N d\bar{p}^N \quad (\text{B.3})$$

and

$$H = \frac{\bar{p}^N \cdot \bar{p}^N}{2m} + U(\bar{r}^N) \quad (\text{B.4})$$

Here H is the Hamiltonian for a three dimensional system of N molecules, each with mass m and momentum \bar{p} . The difficulty in dealing with liquid systems, is determining an adequate expression for the potential interaction term $U(\bar{r}^N)$, which is assumed here to be a function of the N position variables \bar{r} i.e. $\bar{r}^N = \bar{r}_1 \bar{r}_2 \bar{r}_3 \dots \bar{r}_N$. For gases, for example, one can approximate $U = 0$, and obtain the ideal

gas laws using a relationship between pressure p and Q similar in nature to equation (B.2) [B-5].

For liquids, the potential interactions cannot be ignored. They can be handled in a general way, however, by recognizing that for certain classes of interactions (London-D forces for example) the potential well can be characterized by only two parameters. This is shown in Figure B.1. The important parameters are the depth of the well ϵ^* , a characteristic energy; and the characteristic interaction length r^* . With these two important parameters, and with appropriate approximations, estimates can be made for configurational thermodynamic functions.

The problem of polymer solutions, however, is complicated in two important ways; 1) mixture rules must be developed to characterize the potential function between unlike pairs [B-6], and 2) at least one additional parameter is needed to characterize the important structural differences between long chain polymers, and the smaller solvent molecules [B-7].

Prigogine has worked all of this out [B-2], and his end results can be best presented by employing certain dimensionless quantities called reduced quantities. For example the reduced temperature T^* is obtained by dividing the temperature T by a reduction temperature T_0 , characteristic for a particular molecule. The full definition is [B-2]

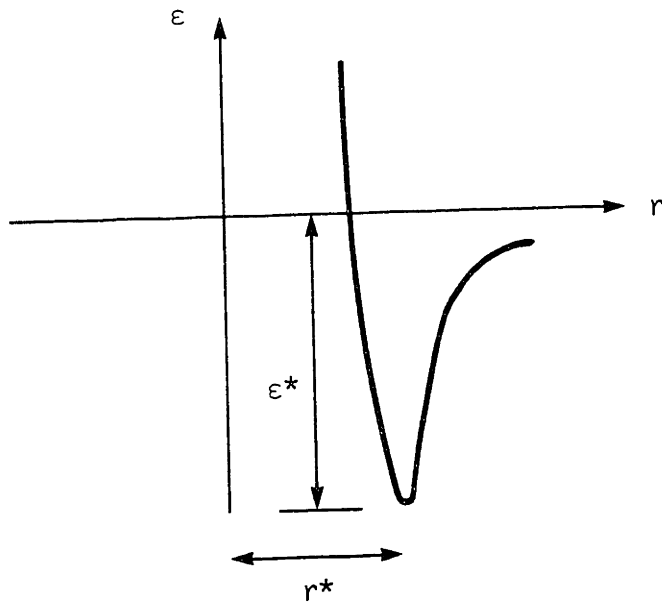


Fig. B.1 Potential interaction function.

$$T^* = \frac{T}{T_0} = \frac{3ckT}{qz\epsilon^*} \approx \frac{c}{q} \frac{kT}{\epsilon^*} \quad (\text{B.5})$$

where $\frac{c}{q}$ is the so called structural factor, and z is the lattice coordination number. In effect T^* is basically the ratio of the kinetic energy (kT) of a substance, depending on the number of degrees of freedom ($3c$), to it's cohesive energy ($qz\epsilon^*$), where there are qz external contacts for a polymer of r segments (note that \bar{r} is a position variable, r^* is a characteristic interaction length, and r is the number of segments in a polymer). For a monomer $q = 1$ and $3c = 3$. Other important reduced parameters are,

$$V^* = \frac{V}{Nr(r^*)^3} \quad \text{Volume}$$

$$U^* = \frac{U}{Nq\epsilon^*} \quad \text{Energy} \quad (\text{B.6})$$

$$G^* = \frac{G}{Nq\epsilon^*} \quad \text{Gibbs free energy}$$

where there are N molecules of a certain substance.

The great success story of Prigogine's development has been, that when V^* and T^* are plotted (at constant reduced pressure) for a great variety of liquids including monomers, solvents, and polymers up to infinite molecular weight, these all fall on one curve, yielding a single equation of state [B-8, 9]. Consequently, when plotted appropriately, vastly different substances can be identified as having

corresponding states. Furthermore, when combined with certain mixing rules, these plots can show mixing functions. This is shown in Figure B.2 and B.3. The difference between the mixing rule curve (dashed), and the corresponding states curve gives the mixing functions. For example, Figure 2-B shows that $\Delta V_M < 0$, where $\Delta V_M = \Delta V_M^* / Nr(r^*)^3$, and [4-B],

$$\Delta V_M^* = \left(V^* (\langle T^* \rangle) - [\phi_1 V^*(T_1^*) + \phi_2 V^*(T_2^*)] \right) \quad (B.7)$$

where

$$\langle T^* \rangle = \phi_1 T_1^* + \phi_2 T_2^* \quad (B.8)$$

Figure B.3 shows that $\Delta G_M(nc) > 0$, where $\Delta G_M(nc)$ is the noncombinational contribution to the Gibbs free energy of mixing. Both of these results agree, at least qualitatively, with what has been observed for polymer solutions.

Following from the work of Prigogine, Patterson then developed an expression for the interaction parameter g . Note that the magnitude of $\Delta G_M(nc)$ depends on the curvature of G^* as a function of T^* , and

$$\frac{d^2 G^*}{dT^{*2}} = - \frac{Cp^*}{T^*} \quad (B.9)$$

where Cp^* is the reduced configurational heat capacity [B-4]. This appears in Patterson's final expression which is converted in quantities for the solvent [B-10].

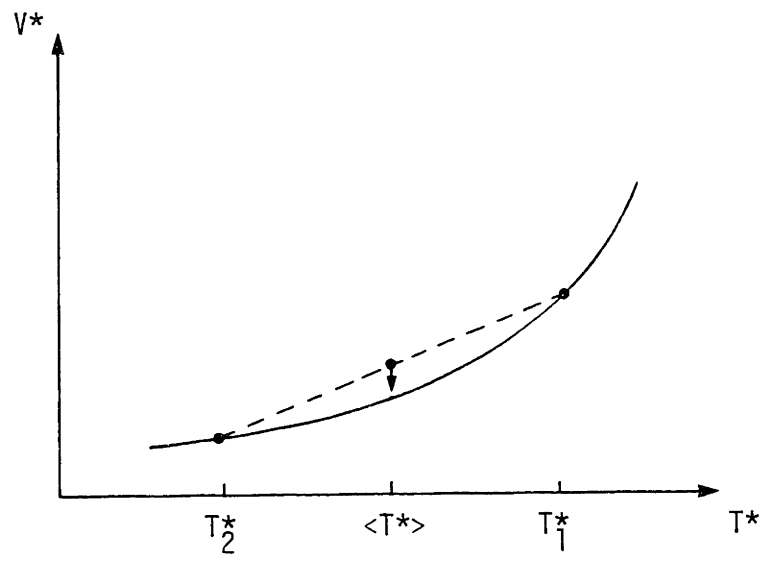


Fig. B.2 Reduced volume as a function of reduced temperature.

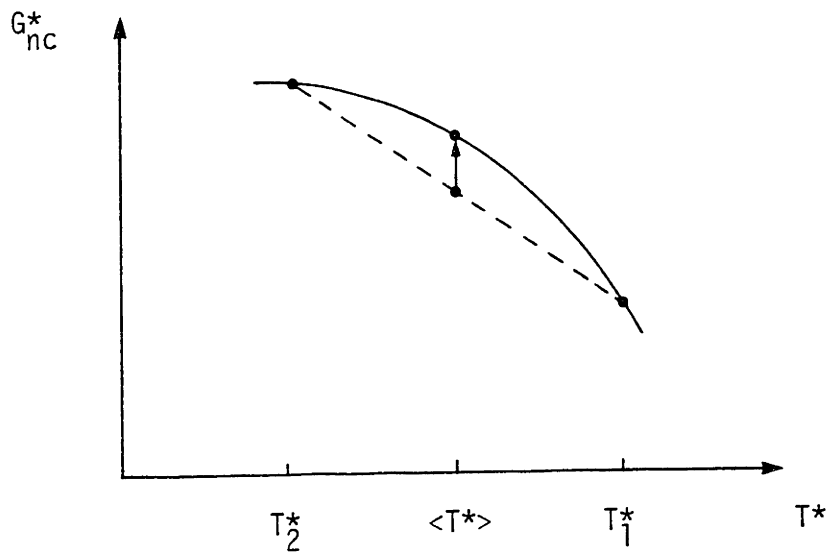


Fig. B.3 Reduced Gibbs free energy as a function of the reduced temperature.

$$g = (- U/RT) v^2 + (C_p/2R) \tau^2 \quad (\text{B.10})$$

This expression is for nonpolar systems, and uses the old concentration dependence as given by the Flory-Huggins Theory. The contribution that this equation provides is in the temperature dependence. The first term in equation (B.10) is analogous to Flory's enthalpic term. The second term is the new "structural" contribution arising from changes of free volume on mixing the dense polymer with the expanded solvent. v , and τ are temperature independent molecular parameters, related to ϵ_1^* , ϵ_2^* , r_1^* , r_2^* , $(C/q)_1$ and $(C/q)_2$. U and C_p are the configuration energy and it's derivative, the configurational heat capacity of the solvent. U is a negative quantity, equal to the negative of the energy of vaporization or to the negative of (heat of vaporization minus RT). Figure B.4 shows a plot of $-U$ for temperatures above 300°K for n-hexane. The negative of the slope of this curve gives the configurational heat capacity of the solvent, which goes to infinity at the critical temperature for the solvent. Thus equation (B.10) predicts that enthalpic contribution will decrease with temperature while the structural effect will increase, and that the high temperature phase transition will always occur before the critical temperature of the solvent. These trends are in agreement with observations [B-7].

For many solvents, $-U$ can be approximated by an empirical equation of the form

$$- U = C_0 \left(1 - \frac{T}{T_c}\right)^m \quad (\text{B.11})$$

where T_c = the critical temperature for the solvent (508°K for n-hexane) and C_0 and m are constants. Differentiating and substituting into (B.10) yields the temperature dependence explicitly as

$$g = \frac{C_0}{RT} \left[\left(1 - \frac{T}{T_c}\right)^m v^2 + \frac{T}{4T_c} \left(1 - \frac{T}{T_c}\right)^{m-1} \tau^2 \right] \quad (\text{B.12})$$

now in many cases $m \approx 1/2$, points for $m = .5$ (°), and $m = .526$ (+) are shown on Figure B.4, substituting $m = 1/2$ into equation (B.12) and expanding yields

$$g = \frac{C_0}{RT_c} \left\{ \frac{v^2}{(T/T_c)} + 1/2 \left(\frac{\tau^2}{2} - v^2\right) + \frac{1}{8} (\tau^2 - v^2) \left(\frac{T}{T_c}\right) + \frac{1}{16} \left(\frac{3}{2} \tau^2 - v^2\right) \left(\frac{T}{T_c}\right)^2 + \frac{5}{128} (2\tau^2 - v^2) \left(\frac{T}{T_c}\right)^3 + \dots \right\} \quad (\text{B.13})$$

The difficult part of Patterson's expression (B.10) is the determination of τ^2 and v^2 , but they are usually of order 1, and 1/2 respectively. So the second term in (B.13) can be positive, negative, or zero, but all other coefficients should be positive. Also, we are always dealing in the regime $\frac{T}{T_c} < 1$, so to a rough approximation

$$g = g_1 + \frac{g_2}{T} + g_3 T \quad (\text{B.14})$$

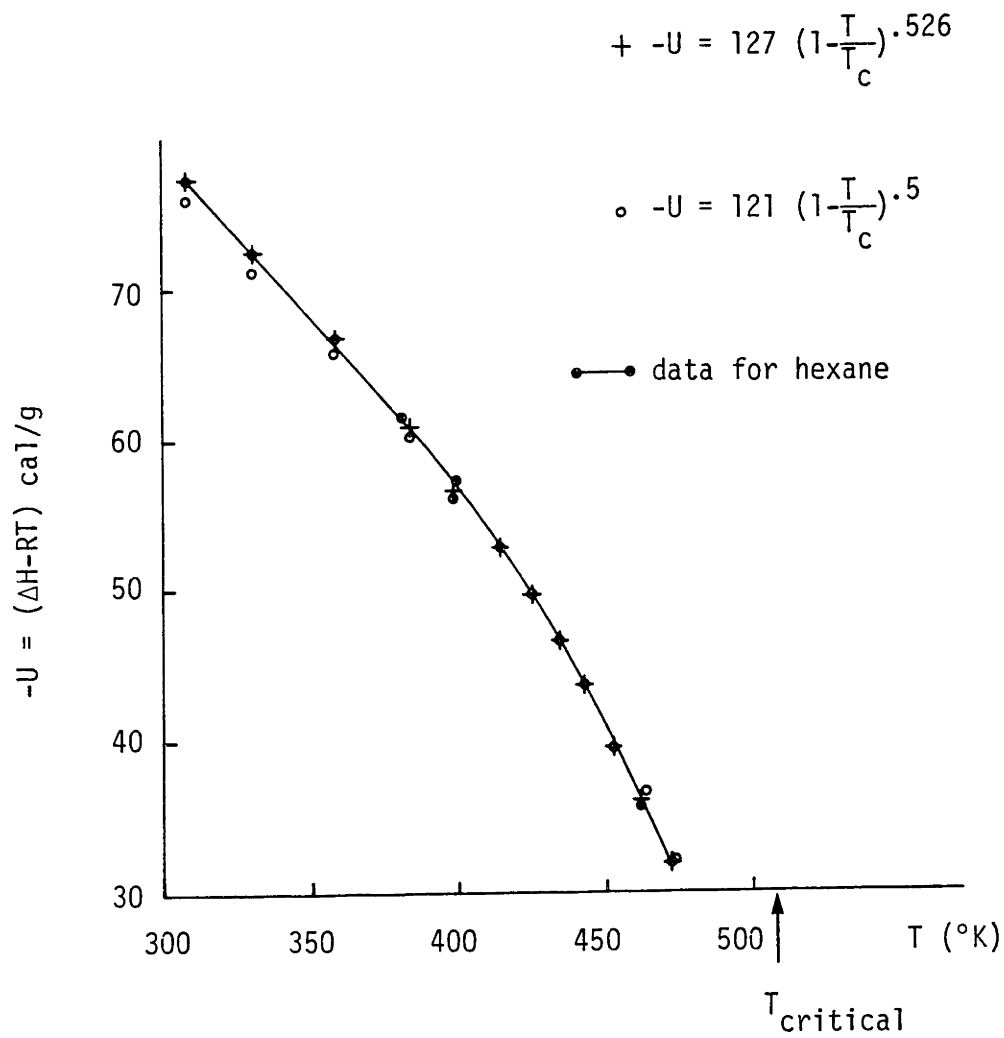


Fig. B.4 -U vs. T for hexane.

this agrees with equation (4.50) in Chapter 4 which was derived by a different manner. At temperatures near T_c , the full expression given in equation (B.12) should be used.

REFERENCES

TO APPENDIX B

- 1-B A. Tager, Physical Chemistry of Polymers, MIR Publishers, Moscow (1978)
- 2-B I. Prigogine, with A. Bellemans and V. Mathot, The Molecular Theory of Solutions, North-Holland Publishing Co. Amsterdam (1957)
- 3-B P.J. Flory, J.L. Ellenson, and B.E. Eichinger, "Thermodynamics of Mixing of n-Alkanes with Polyisobutylene", Macromolecules 1 p.279 (1968)
- 4-B D. Patterson, "Thermodynamics of Non-Dilute Polymer Solutions" Rubber Chemistry and Technology 40 p.1 (1967)
- 5-B F.C. Andrews, Equilibrium Statistical Mechanics, Wiley-Interscience, 2nd ed. (1975)
- 6-B N.G. Parsonage and L.A.K. Staveley, "Current Theories of Solutions of Non-Electrolytes", Quarterly Review - London 13, p.306 (1959)
- 7-B D. Patterson, "Review; Free Volume and Polymer Solubility. A Quantitative View", Macromolecules 2, 6 p.672 (1969)
- 8-B V.S. Nanda and R. Simha, "Equation of State and Related Properties of Polymer and Oligomer Liquids", J. of Physical Chemistry 68, 11 p. 3158 (1964)
- 9-B R. Simha and A.J. Havlik, "On the Equation of State of Oligomers and Polymer Liquids", J. of American Chemical Society 86, 2, p.197 (1964)
- 10-B D. Patterson, "Role of Free Volume Changes in Polymer Solution Thermodynamics", International Symposium on Macromolecular Chemistry, P.449, Prague (1965)

APPENDIX C

EXPERIMENTAL DETERMINATION OF THE COEXISTENCE CURVES

The coexistence curves shown in Figure 5.9 were determined by heating and centrifuging the solution. This procedure was particularly important for the 12.3% wt solution since it would not readily separate by gravity. In fact, even in a 1700 rpm centrifuge several minutes were required to produce complete settlement for this solution.

The settlement rate in the centrifuge could be observed by taking a series of strobe photographs like the one shown in Figure C.1, and noting the progress of the dilute phase - mixed phase interface. Results after heating the 12.3% wt. solution to 160°C are shown in Figure C.2. So settlement is complete after 6 minutes, and 90% complete after 2 min. These times are long compared to the 7.9% wt. solution which settled completely after 10 sec. in the centrifuge.

The long settlement time for the more concentrated solution caused some uncertainty in the temperature value. This is because the centrifuge could not be heated to the solution temperature. The temperature profiles for the solution in a heated (80°C) and unheated (25°C) centrifuge are shown in Figure C.3. Clearly the situation is improved by heating the centrifuge, but the solution temperature still drops 3% in the first 2 minutes (or 4°C if heated to 170°C). While this is not a problem for the 7.9% solution, it is significant for



Fig. C.1 Photograph of physical separation of phases in centrifuge. Tube on left shows interface between dilute phase and mixed phases.

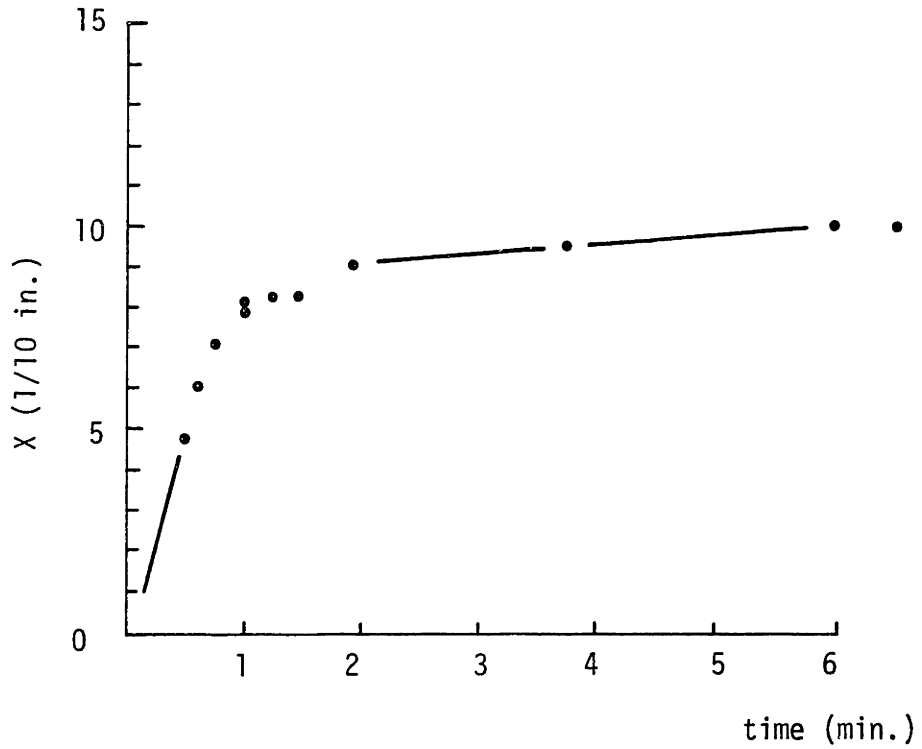


Fig. C.2 Time history of dilute phase - mixed phase interface for 12.3% Wt. solution, originally at 160°C, in centrifuge. $X = 0$ is dilute phase - vapor phase interface.

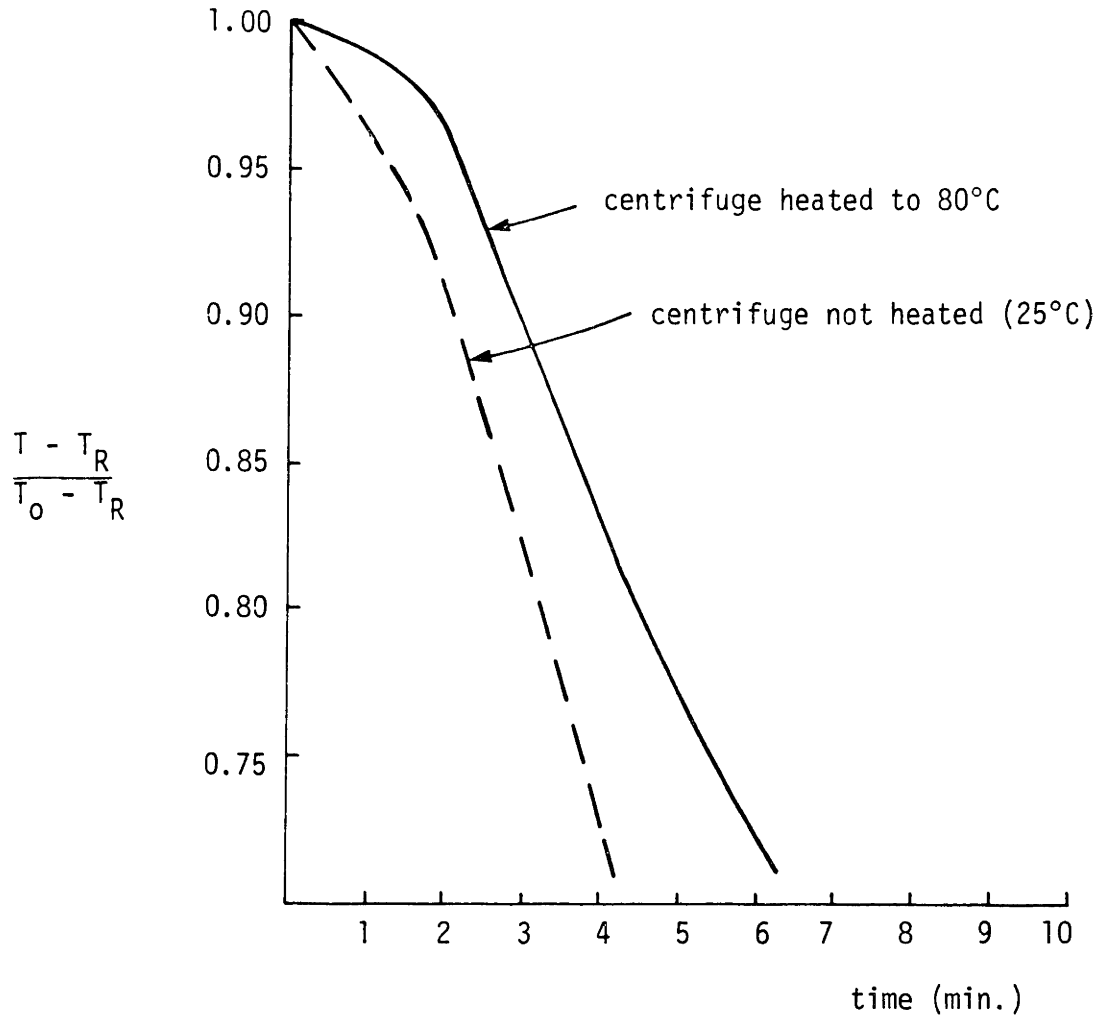


Fig. C.3 Temperature profiles for solution in centrifuge.
 T = temperature, T_R = room temperature (25°C),
 T_0 = original solution temperature.

the 12.3%. In fact, if we go all the way out to 6 minutes, the uncertainty on the temperature for the $C_0 = .123$ coexistence curve is + 0, - 28%. Things are not really that bad, however, when we realize that the cloud point curve, and the $C_0 = .079$ coexistence curve (again referring to Figure 5.9) are actually upper and lower bounds for the $C_0 = .123$ coexistence curve. Since these upper and lower bounds points are hard to sort out from one another it was felt that putting more effort into determining the coexistence curve for $C_0 = .123$ was not merited.*

The determination of the volume ratio β_v for the dilute phase volume V' and the concentrated phase volume V'' shown in Figure 5.11 was done in a similar manner. The 7.9% wt. solution was heated, centrifuged and then reheated to obtain the correct volumes. These values are compared with the coexistence curve values (which were determined by heating, centrifuging and measuring the resulting concentrations) by using the specific volume estimate given in Figure 5.10. That is

$$\beta_v = \frac{V'}{V''} = \frac{v'}{v''} \beta_w \quad (C.1)$$

$$\beta_w = \frac{W'}{W''} = \frac{C'' - C_0}{C_0 - C'} \quad (C.2)$$

*In fact, the three right hand lines drawn in Figure 5.9 are hard to justify on any other than conceptual grounds. What the data points are telling us, is that the variation in the cloud point values and the coexistence values is on the order of the experimental error ($\pm 1^\circ\text{C}$).

where the concentrations of the original solution, and the resulting dilute and concentrated solutions are C_0 , C' , and C'' respectively, and the mass of the resulting dilute phase and concentrated phase are W' and W'' , and their sum equals the original mass of C_0 , i.e. $W_0 = W' + W''$. Also the specific volumes of the dilute phase and concentrated phase are v' and v'' . As shown in Figure 5.11 the agreement between the two methods is pretty good.

The volume ratio for $C_0 = .123$ was determined from the coexistence curve, and the specific volume estimate. Note that by definition both curves go to zero ($\beta_v = 0$) at their cloud point.

Volume ratio data, and coexistence curves for broad molecular weight polymers have been reported for other polymer-solvent systems by Koningsveld [C-1].

REFERENCES

FOR APPENDIX C

- C-1 R. Koningsveld, "Partial Miscibility of Multi-component Polymer Solutions", *Advances in Colloid and Interface Science* 2, p.151 (1968)

APPENDIX D

RAPID EVAPORATION SEPARATION SCHEME

The discovery in this thesis that rapid entry into the spinodal decomposition regime can greatly enhance solvent evaporation (see Figure 7.7), and the result presented in Section 3.3, that implementation of a heat pump cycle can greatly reduce the energy of separation, suggest yet another scheme for separating solvents from polymers. The steps for this process are listed below.

1. Heat and pressurize the polymer solution.
2. Spray dry the solution so that it rapidly goes into the spinodal decomposition regime.
3. Collect the dried rubber. Here, as an optional step the rubber can be treated with some type of partitioning agent to prevent the rubber particles from agglomerating or massing together again. It has long been recognized in the rubber industry that the mixing of powdered rubbers rather than baled rubber would greatly reduce the energy required for that step [D-1].
4. Collect and pressurize the solvent vapors
5. Condense the solvent
6. Drop pressure
7. Clean and return the solvent for reuse.

This rapid evaporation separation scheme is shown in Figure D.1. Of course the scheme could be operated without the heat pump cycle, eliminating the compressor and valve. Not shown in Figure D.1 is the transfer of the heat of condensation to the spray drier.

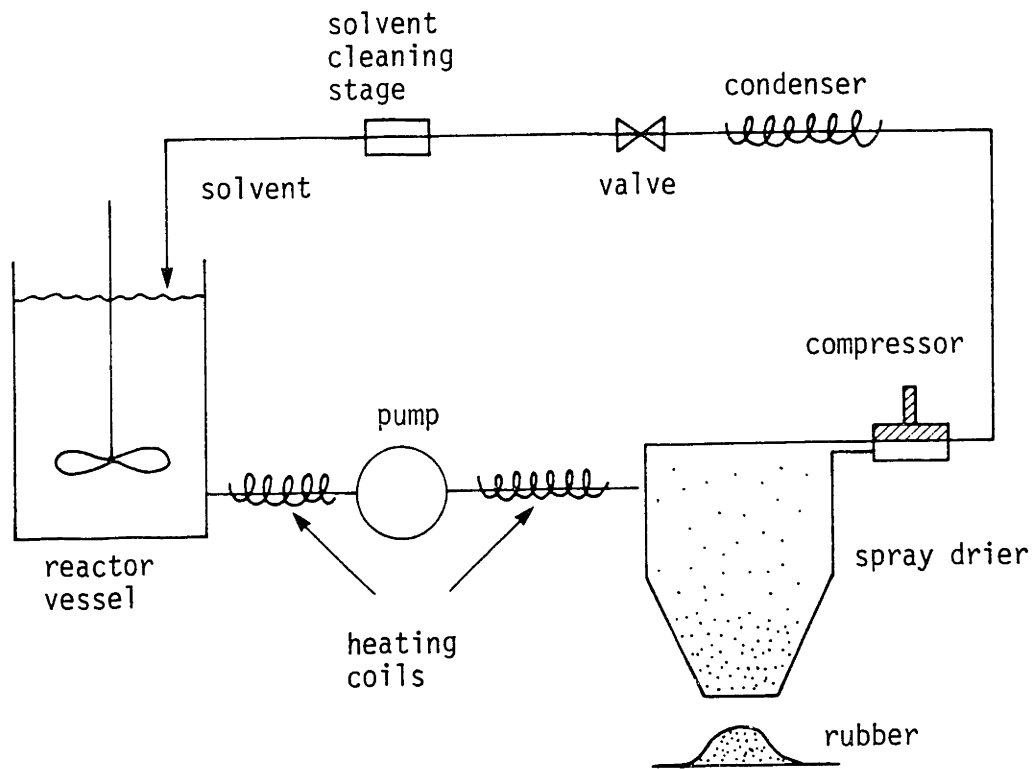


Fig. D.1 Rapid evaporation separation scheme

REFERENCES

FOR APPENDIX D

- D-1 R.G. Bauer et al, "The "Revolution in Rubber Processing: Soon or Never?"; in Science and Technology in Polymer Processing N.P. Suh and N.H. Sung Eds. M.I.T. Press (1979)

BIOGRAPHICAL NOTE

Timothy George Peter Gutowski

Tim Gutowski was born on January 2, 1946 in Chicago, Illinois to Mr. and Mrs. Chester G. Gutowski. He received his B.S. degree in Mathematics from the University of Wisconsin at Platteville in 1967. One year later he received his M.S. degree in Theoretical and Applied Mechanics from the University of Illinois at Champaign-Urbana. During 1969 he was associated with Wiss Janney and Elstner, a structures and dynamics consulting firm in Northbrook, Illinois. Later that year he joined the Peace Corps and served in Ecuador, South America for three years. During his stay in South America he worked on a colonization project and taught mechanical vibrations to college seniors at the Escuela Politecnica Nacional in Quito. Upon his return to the United States, he joined the acoustical consulting firm of Bolt, Beranek and Newman in Cambridge, Massachusetts. There, he was a senior consultant in acoustics and vibration control for 4-1/2 years. He returned to school, at the Massachusetts Institute of Technology, in 1977 to pursue a doctorate in Mechanical Engineering. Following graduation he will join the staff at M.I.T. as an assistant professor of Mechanical Engineering.